Evolution of Atmospheric Aerosols Along Trajectories Crossing the Los Angeles Basin

Thesis by
Lara Shane Hughes

In Partial Fulfillment of the Requirements
for the Degree of
Doctor of Philosophy

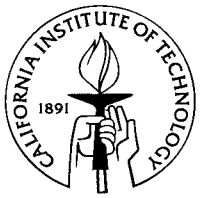

California Institute of Technology
Pasadena, California

2001

(Defended September 15, 2000)

Acknowledgements

There are many, many people who have helped to make this research possible.

First and foremost, I owe a huge debt of gratitude to Dr. Glen Cass, my research advisor. His guidance, patience, depth of knowledge, insight, and analytical abilities are a source of constant amazement to me, and have certainly made this research and this thesis possible. Thank you so much, Glen.

I would like to thank all of my friends and collaborators from the Prather group at the University of California - Riverside, whose work with the aerosol time-of-flight mass spectrometry instruments is integral to this research. We put in long hours of field study, data analysis, and life together, and I wish them all the best. Over the years, they have included Eric Gard, Chris Noble, Donny Liu, Phil Silva, David Fergenson, Deborah Gross, Markus Gälli, Brad Morrical, Sylvia Pastor, Keith Coffee, Sergio Guazzotti, Anne Johnson, Tas Dienes, and Professor Kim Prather.

Thanks to Jon Allen for co-planning, co-participating and commiserating in the large field studies of 1996 and 1997; for teaching me all I know of Matlab and LaTeX; and for words of encouragement when encouragement was needed.

Thanks to fellow Cass group members who made the field studies possible by contributing their time and effort to the cause. They included Christos Christoforou in the 1996 field study, Paul Mayo in the 1997 field study, and Lynn Salmon, Mike Kleeman, and Rob Johnson during both studies. In addition, thanks are due to Bob Cary at Sunset Labs, and Paul Mayo and Lynn Salmon at Caltech for carbon analyses; to Drs. Ilhan Olmez and Michael Ames at the MIT Nuclear Reactor Laboratory for neutron activation analyses; and to Lynn Salmon for some of the ion chromatography and colorimetry analyses.

Thanks to the sponsoring agencies which have funded this research over the years: Chevron, U.S. Environmental Protection Agency Center on Airborne Organics, the Center for Air Quality Analysis at Caltech, the California Air Resources Board (ATOFMS work), the Coordinating Research Council, Inc., and the USDOE

Office of Heavy Vehicle Technologies through the National Renewable Energy Laboratory.

Thanks are due to Joe Cassmassi and the staff of the South Coast Air Quality Management District for providing meteorological support during the field experiments and to Kevin Durkee of the SCAQMD and Lean Dolislager, Ash Lashgari, Nehzat Motallebi, and Clinton Taylor of the California Air Resources Board for answering questions and providing me with relevant meteorological and gas species concentration data collected by those agencies.

Loads of thanks to friends and family who have provided support and welcome distractions from the trials and tribulations of grad school, keeping me happy and (relatively) sane, including Sharon, Ericka, Laura (and Tim and Drewbie), Andy, Leah and Ben, all those in the Caltech a cappella, theater, and jazz band communities, "the band" in its several incarnations, and "Lisa's class."

And last, but not by any means least, thanks to Nat, who has made life better in innumerable ways, who makes me laugh, and who gives me strength and happiness. I look forward to becoming Dr. *Gertler* in the very near future.

Evolution of Atmospheric Aerosols Along Trajectories Crossing the Los Angeles Basin

by

Lara Shane Hughes

In Partial Fulfillment of the
Requirements for the Degree of
Doctor of Philosophy

Abstract

A primary concern in the regulation, control and monitoring of particulate air pollution is its detrimental effect on human health. One objective of this thesis is to determine the concentration and chemical composition of urban atmospheric fine (diameter < 2.2 μm) and ultrafine (diameter < 0.1 μm) particulate matter (PM). Laboratory research into ultrafine particles suggests that these particles may be especially damaging to health. Size-segregated fine PM was collected in Pasadena, California, using microorifice impactors. Ultrafine particle mass concentrations ranged from 0.88-1.58 $\mu g\ m^{-3}$, small in comparison to fine PM, but ultrafine particle number concentrations in the size range 0.017-0.1 μm particle diameter were relatively large at $1.3\times10^4 \pm 8.9\times10^3\ cm^{-3}$. This study provides the first detailed data published on urban ultrafine particle chemical composition including organics and elemental carbon, trace metals, and ionic species. Organic compounds were the largest component of ultrafine particle mass.

Development of effective particulate control policies requires a thorough understanding of the chemical and physical processes affecting primary particle emissions as they are transported downwind from emissions sources. Mathematical models which calculate the chemical evolution of airborne particles as they are affected by gas-to-particle conversion processes can provide the needed

insight when combined with experimental data on particle evolution at the single particle level. Three field studies were conducted in the Los Angeles area for the purpose of gathering the necessary experimental data by sampling single air parcels at multiple points along an air parcel trajectory. Cascade impactors, particle size distribution monitors, filter-based PM samplers, and aerosol time-of-flight mass spectrometry instruments capable of making single-particle size and composition measurements were employed at three urban monitoring sites chosen along typical wind trajectories. The three studies focused on different aspects of particle evolution: particle transformation during transport inland over urban areas from the ocean; evolution of particle populations dominated by motor vehicle emissions from Central Los Angeles; and formation of particulate ammonium nitrate during transport over large ammonia sources. Particle populations transported over the Los Angeles area showed depletion and chemical alteration of sea salt particles, addition of fine carbon-containing particles, and secondary aerosol nitrate formation. Measurements made at the single particle level show that particles of the same size can differ substantially in chemical composition and that single particle composition becomes more complex over time as particles are transformed through a chemically reactive atmosphere.

Contents

List of Figures

List of Tables

Chapter 1

Introduction

1.1 Motivation

Two of the adverse effects of the presence of high atmospheric particulate matter concentrations are reduction in visibility and deterioration of human health. Suspended particulate matter can scatter and absorb light, thereby decreasing visibility; the extent of scattering and absorption is dependent on the size and composition of the atmospheric particles. Particles in the diameter range 0.1–1.0 μm most effectively scatter light in the visible range, while particles containing black carbon most effectively absorb light. A particle's chemical composition also determines its hygroscopicity, and thus its water content and light-scattering ability.

Recent epidemiological studies have found statistically significant associations between elevated atmospheric particulate matter concentrations and the occurrence of such health indicators as chronic cough, bronchitis, decreased lung function, and cardiopulmonary-related mortality [1]. Again, the ability of particles to cause health complications is dependent on their size and/or chemical composition. Fine particles (diameter $\leq$ 2.5 μm) are able to penetrate more deeply into the lungs than larger particles. Acidic particles may have unique damaging effects on the lungs. As an illustration, a six-city epidemiological study found mortality rates to be associated with fine particulate matter and with par-

ticulate sulfate concentrations, but not with total suspended particulate matter concentrations [2].

The significance of particle size is evidenced by recent laboratory animal experiments which suggest that ultrafine particles (diameter $\leq$ 0.1 μm) have an enhanced ability to adversely affect the lungs [3–7]. The mechanism or mechanisms by which this damage is done have not yet been determined. One theory proposes that lung clearance mechanisms work far less effectively on particles of this size range; another theory hypothesizes that the relatively large surface area to volume ratio of ultrafine particles, combined with their ability to penetrate deep into the lungs, results in a very efficient transfer of any harmful chemical species present in the particles to the lung. To effectively study the possible health effects of atmospheric ultrafine particles in the laboratory, knowledge of the chemical composition of such particles in the ambient urban atmosphere is needed. These data on the ambient atmosphere would also demonstrate the extent of exposure of urban residents to ultrafine particles. No surveys of the chemical composition of urban ultrafine particles existed in the scientific literature at the outset of the research to be reported here.

The annual average PM_{10} and fine particulate matter concentrations in Southern California have declined significantly over the last few decades [8, 9]. Emission control programs applied to sulfur oxide sources and diesel and gasoline-powered motor vehicles have had noticeable effects in decreasing fine particle sulfate, black carbon, and organic carbon concentrations over the years [8]. Annual mean PM_{10} concentrations in the South Coast Air Basin (SoCAB) that surrounds Los Angeles decreased 36% between 1988 and 1995, and SoCAB $PM_{2.5}$ concentrations decreased about 50% between 1990 and 1995 [9]. Airborne particle concentrations in the SoCAB still regularly exceed air quality standards, despite these improvements. As recently as 1994–1996, 63.2% of sampled days exhibited a PM_{10} concentration greater than the 50 $\mu g\ m^{-3}$ 24-h California state air quality standard. The maximum PM_{10} and $PM_{2.5}$ concentrations in the SoCAB during the same period were 181 $\mu g\ m^{-3}$ and 115 $\mu g\ m^{-3}$ respectively, both sig-

nificantly above the National Ambient Air Quality Standards of 150 μg m^{-3} for PM_{10} and 65 μg m^{-3} for $PM_{2.5}$ [9].

In order to design effective control policies to reduce particulate matter concentrations further and address the public health and visibility concerns associated with high particulate matter concentrations, the effects of chemical and physical processes, including secondary particle formation, encountered by primary particle populations during transport downwind from emissions sources must be well understood. Lagrangian trajectory-based and Eulerian grid-based aerosol process models have been developed which calculate the evolution of the size and chemical composition of particles in the atmosphere as they are transported across an urban area in the presence of gas-to-particle conversion processes, but it is difficult to obtain experimental information about particle transformation during transport with which to evaluate the performance of such models. High resolution field experimental data on particle chemical composition as a function of particle size are needed in order to provide a basis for comparison of model predictions to reality.

Aerosol process model evaluation studies performed to date have involved comparison of model predictions versus the average composition of all particles in several size ranges. Models have been developed recently that can predict the composition and size of individual particles in the atmosphere [10], but to date there are no field experimental data against which such predictions can be compared. Recently aerosol time-of-flight mass spectrometry (ATOFMS) systems have been developed which can obtain data on the size and chemical components of single particles. These single particle measurements can potentially be compared with the single particle level results from air quality models, but the ATOFMS instruments have certain limitations. These instruments undercount the number of particles in the atmosphere by a factor that depends upon particle size. The ATOFMS instruments must be calibrated to determine their counting efficiency and to relate the number of particles seen by the instrument to the number of actual atmospheric particles. Chemical component quantification on a single

particle or bulk basis is also difficult, because the mass spectrometer is not uniformly sensitive to all ions. The chemical sensitivity is also affected by the type and size of the particle. For this reason, the behavior of the ATOFMS instruments with simple particles created in the laboratory is expected to be different than with potentially complex atmospheric particles. If ATOFMS instrument data on single atmospheric particles are to be compared against model predictions, the ATOFMS instruments need to be collocated with more conventional particle sampling instruments, i.e., impactors, filter-based samplers, and size distribution instruments. The conventional instrument results can be compared to the ATOFMS data for insight into the behavior of the ATOFMS instruments and development of the correction factors which will allow more quantitative interpretation of the single particle data for subsequent use as a model evaluation data set.

1.2 Research Objectives

There are two major objectives to be addressed by this thesis. The first is to acquire field experimental data that characterizes particle chemical evolution over time within individual air parcels both at the bulk and single particle level, organized in a form that is suited to future air quality model evaluation studies. Multiple-site particle sampling studies have been conducted previously in the SoCAB [11-14]. But the field studies described in this thesis are different from previous work because they are the first field experiments in which multiple air monitoring sites equipped with cascade impactors and aerosol time-of-flight mass spectrometry systems have been located along single air parcel trajectories and used to characterize an airshed according to size-segregated particle and single-particle chemical compositions. Such impactor-based and single-particle information is needed for evaluating the predictions of atmospheric aerosol processes models that track primary particle emissions as an externally-mixed population having particle-to-particle differences in chemical composition as they are transported downwind in the presence of chemical reaction, dilution, and

deposition at the earth's surface [15].

The second objective of this thesis is to determine for the first time the chemical composition of urban atmospheric ultrafine particles. As stated in the previous section, this information is necessary for progress in research into the possible adverse health effects caused by inhalation of these particles and the mechanisms by which the particles cause this damage.

1.3 Approach

The first objective of this work is to determine how particle populations evolve chemically during transport through the atmosphere. To do this, several trajectory-oriented field experiments were designed and conducted with the aim of sampling single air parcels successively at several sites as they were advected across Southern California. Chapter 2 begins with a literature review of previous trajectory-oriented studies, and goes on to describe the design and execution of a field experiment conducted in September–October, 1996, to more fully meet current needs for air quality characterization and model evaluation data. A set of instruments capable of measuring continuous particle size distribution, total suspended particulate matter concentration and chemical composition, bulk and size-segregated fine particle concentration and chemical composition, and continuous single-particle size and chemical composition, was located at each of three urban monitoring sites in the Los Angeles area. In addition, background air quality measurements were made offshore at Santa Catalina Island for one 24-h period. Average size distribution and chemical composition data for each site over the course of the study are presented and compared. Time series information on particle chemical composition for each urban site is presented in the form of relative numbers of particles measured with the aerosol time-of-flight mass spectrometer (ATOFMS) containing key marker peaks for particular chemical substances.

The air monitoring sites used in the 1996 field study were chosen such that

they were located along a seasonally typical air parcel path across the SoCAB. In Chapter 3, the data from the 1996 field study are interpreted within the framework of two air parcel trajectories which were determined to have passed over 3 or 4 monitoring sites in succession at times when particle sampling was being conducted. Comparison of data on particle size and chemical composition obtained at each site and time along these trajectories yields experimentally-based information about the effects of emissions, chemical reactions, deposition, and other physical and chemical processes on the particle populations as they are transported across the SoCAB.

Chapters 4 and 5 describe the results of two field studies conducted in August–November, 1997, in association with the Southern California Ozone Study - 1997 (SCOS97). These field studies used a battery of instruments at each monitoring site that was very similar to that used at each site during the 1996 trajectory study described in Chapters 2 and 3. Data on particle size distribution, PM_{10} and $PM_{1.9}$ concentration and chemical composition, and single-particle size and composition data were obtained.

The field study described in Chapter 4 was designed to examine the evolution of particles emitted from motor vehicle sources. The air monitoring sites were chosen specifically for this purpose: Central Los Angeles because it is surrounded by the highest density of motor traffic in Southern California and Azusa because it is frequently downwind of Central Los Angeles. Two air parcel trajectories passing first near Central Los Angeles and then Azusa during the sampling experiments are identified. Data are presented in time series for each site, showing relevant motor traffic-induced diurnal peaks. Measurements made along the air parcel trajectories allows observations to be made about the various chemical and physical processes acting upon this urban particle population during transport.

The field study covered in Chapter 5 investigated the evolution of particles within an environment conducive to particulate ammonium nitrate formation. For this purpose, monitoring instruments were operated at Diamond Bar, Mira

Loma, and Riverside, California, sites which are generally upwind of, within, and downwind of, respectively, the Chino dairying area, where livestock and agricultural land uses contribute to large ammonia emissions. Several air parcel trajectories passing near two of the three sites in succession during sampling are identified. Again, by comparison of the particle populations found at each end of these trajectories, observations can be made about the ammonium nitrate formation process and its effects on the particle population.

Though toxicological evidence suggests that the inhalation of particles in the ultrafine size range (diameter ≤ 0.1 μm) can be unhealthy, little is known of the chemical compositions of ultrafine particulate matter in an urban atmosphere. The second objective of this work is to determine for the first time the chemical composition of such particles. Chapter 6 describes size distribution and chemical composition measurements made of wintertime atmospheric ultrafine particulate matter in Pasadena, California. In this experiment, micro-orifice impactors, filter-based samplers, a differential mobility analyzer, condensation nucleus counter, and optical particle counter were used together to gather information about ambient ultrafine, fine and total particulate matter. This information on ultrafine particle chemical composition can be used to inform the design of laboratory research on the health problems that may be caused by inhalation of atmospheric ultrafine particles.

Chapter 2

1996 Los Angeles Basin Trajectory Study

2.1 Introduction

The size and composition of airborne particles evolve over time in the atmosphere as the direct primary emissions of new solid and liquid particles from emissions sources in a city are mixed with regional background aerosol present due to long-distance transport. Emitted particles and background aerosol are also transformed by interaction with gaseous air pollutants. For example, SO_2 oxidation leads to secondary sulfate accumulation on the pre-existing particles [16]. Organic vapors can react to produce low vapor pressure products which subsequently become distributed onto the aerosol [17]. Nitric acid vapor reacts in the atmosphere with ammonia to produce ammonium nitrate aerosol [18-21], and nitric acid can also react with sea salt particles to produce sodium nitrate particles [22].

The size and chemical composition distribution of the airborne particle mixture within an air basin depends on how these secondary reaction products are distributed across the underlying primary particle size distribution. To control

the effects of exposure to airborne particles, it is necessary to know how emissions control decisions will affect the concentration, size, and composition of the particles. Particles of different sizes have different effects on visibility [23–25] and differ greatly in terms of their deposition locations in the lung [26].

Interaction between the gas and particle phases occurs at the single particle level. Individual particle size and hygroscopicity, and thus chemical composition, determines whether or not a particle will activate when fog forms, thereby facilitating sulfate formation by liquid phase chemical reactions. Whether or not organic vapors can partition into a particle likewise depends on the organic chemical constituents of the single particle. Knowledge of single particle composition is needed to study these processes, but in the past, with a few exceptions (e.g., [27]), the available information on the chemical components of particles has existed largely in the form of bulk chemical composition data taken from filter samples, in which a large number of particles are mixed together during collection and subsequent chemical analysis.

Recent air quality modeling approaches are capable of describing gas/particle interactions at the single particle level in a complex urban atmosphere [15]. In another recent development, new aerosol time-of-flight mass spectrometry (ATOFMS) instruments can be used to measure the size and mass spectrum of single particles [27–37]. The purpose of this chapter is to describe the design and execution of an experiment which deploys these ATOFMS systems alongside more conventional reference method instruments to observe and record single particle characteristics that can later be compared to air quality models that predict particle size and composition at the single-particle level.

Three air monitoring stations were established in mid-September, 1996, and operated on select days through early October, 1996, along a seasonally typical air parcel pathway crossing the Los Angeles Basin. A temporary fourth station was established at an offshore island upwind of these three sampling sites to measure background particle concentration, chemical composition, and size distribution. Data on single particle size and chemical characteristics were collected

continuously at each urban air monitoring station by aerosol time-of-flight mass spectrometry instruments [27, 28]. Particle size distributions were also measured continuously by electrical aerosol analyzers and laser optical particle counters. On certain days size-segregated, fine, and total suspended particulate matter samples of 4-h duration were collected for comprehensive chemical analysis at each site, using a low-volume filter-based sampling system and a pair of micro-orifice impactors (MOIs) at each site.

These measurements serve many purposes. First they provide a description of particulate matter characteristics as a function of particle size, chemical composition, and time in the Los Angeles Basin, which is the subject of the present chapter. The data later will be used to study the evolution of individual air parcels in a Lagrangian framework as they pass over successive air monitoring sites (see Chapter 3). In future work, the number distribution, mass distribution, and size-resolved chemical composition data taken by the conventional reference air sampling instruments will be used to calibrate the counting efficiencies and chemical sensitivities of the ATOFMS instruments under field sampling conditions in order to render the ATOFMS data into a quantitative description of particle size and composition. Ultimately, these data are intended for use as a model evaluation data set for air quality models that predict the size distribution and chemical composition of individual particles in the atmosphere [15, 22]

2.2 Related Studies

The South Coast Air Basin (SoCAB) surrounding Los Angeles, California, has been the focus of extensive studies of urban photochemical smog formation. Experiments employing multiple sampling sites to simultaneously examine atmospheric aerosols at locations across the basin have been conducted since the early 1970's. The California Aerosol Characterization Experiment (ACHEX) [11] yielded data on particle size distributions and chemical composition measurements at up to five sites in the SoCAB between September 1972 and October 1973. Lund-

gren impactor samples and bulk aerosol filter samples were analyzed by neutron activation analysis (NAA), X-ray fluorescence analysis (XRF), X-ray photoelectron spectroscopy for chemical analysis (ESCA), and various chemical methods to determine non-carbonate carbon, sulfate, nitrate, and trace element concentrations. Electrical aerosol analyzers (EAAs) and optical particle counters (OPCs) provided detailed information on particle size distributions.

In 1982, ionic aerosol species and gas-phase HNO_3, NH_3, O_3, NO, and NO_x were simultaneously measured with 2-h time resolution over 48 hours at ten SoCAB sites to provide a database from which to evaluate the predictions of both Lagrangian trajectory and Eulerian grid-based air quality models for aerosol nitrate formation [13, 21, 38, 39]. Analysis of these data showed that inorganic nitrate was distributed between the gas and particle phases in approximate agreement with predictions for the thermodynamic equilibrium between the gas and particle phases [40], and that particulate nitrate formation could be predicted based on NO_x, NH_3, and organic vapor emissions from local air pollution sources [21, 38, 39].

In the summer and fall of 1987, the Southern California Air Quality Study (SCAQS) was conducted with the objectives of observing particle characteristics and providing data for the evaluation of air quality models for the formation and transport of photochemical oxidants and particulate matter. Collection of particulate matter filter samples having 4-h to 7-h time resolution occurred at nine sites throughout the SoCAB. Aerosol samples were analyzed for carbon, inorganic ions, and elemental composition. Concurrent measurements of gas phase HNO_3, NH_3, SO_2, O_3, NO, NO_x, and CO were made, along with detailed speciation of volatile organic compounds [12, 41–44]. At Claremont, California, and occasionally elsewhere, measurements of particle size distributions were made with electronic size distribution monitors, and cascade impactors were used to collect data on particle chemical composition as a function of particle size [41, 42, 44]. The extensive database gathered from the SCAQS experiments has been used to evaluate the predictions of a variety of models for secondary aerosol formation, transport,

and deposition in the Los Angeles area [15, 17, 45–52], as well as models for light scattering and visibility reduction in the atmosphere [25, 53]. The SCAQS experiments did not include measurements of individual semi-volatile vapor-phase and particle-phase organic compounds. Data on semi-volatile vapor-phase organic compounds are necessary in order to study secondary organic aerosol formation and gas/particle partitioning. Therefore, during the summer of 1993, simultaneous short-term time series measurements of particle-phase, gas-phase, and semi-volatile organic compounds were made at four urban air monitoring sites and at an offshore island in the Los Angeles area [14, 54–56]. Inorganic ions and organic and elemental carbon components of the aerosol were measured as well, along with gas-phase HNO_3, HCl, NH_3, SO_2, O_3, NO, NO_2, and CO concentrations.

The field study described in the present paper differs from previous efforts because it provides the first field experiment in which multiple air monitoring sites equipped with ATOFMS systems have been used to characterize an airshed based on real-time single particle-level size and chemical composition data. The purpose of the present paper is to describe the basic experiment, to present the data on bulk aerosol properties, and to introduce examples of the raw data on single particle composition collected by the ATOFMS systems. The siting of the air monitoring stations is designed to lie along typical air parcel trajectories, and in later analyses single air masses will be studied as they pass over several sites successively, thereby providing unique insights into chemical processes and transformations. Eventually, the data can be used to evaluate the predictions of an existing atmospheric aerosol processes model that predicts both the size and composition distribution of the aerosol as well as particle-to-particle differences for particles of the same size by separately tracking the individual primary particles emitted from different sources as they become coated by or integrated with secondary aerosol conversion products over time [15].

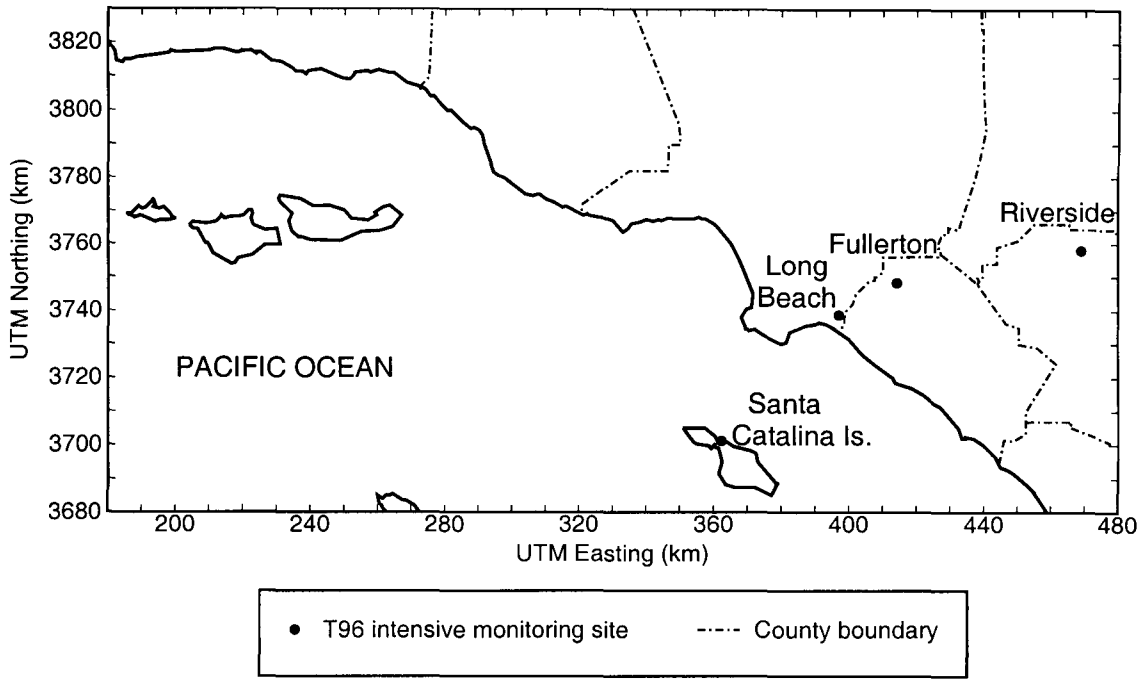

Figure 2.1: Air monitoring sites used during September–October, 1996, field study.

2.3 Experimental Methods

Sampling of size-segregated, fine, and total suspended ambient particles for subsequent chemical analysis and measurement of airborne particle size distributions were conducted over the course of two weeks in late September and early October, 1996. Instruments were stationed at three sites in the urban Los Angeles, California, area: Long Beach, Fullerton, and Riverside (see Figure 2.1). In addition, the upwind background aerosol size distribution and chemical composition was characterized at Santa Catalina Island.

An electrical aerosol analyzer was operated daily at each of the three urban sampling sites; laser optical particle counters were placed at Long Beach and Riverside. In addition to these conventional sampling methods, an ATOFMS was operated continuously at each of the three urban sites. This set of instruments was used to obtain continuous measurements of particle number distribution and single particle chemical composition.

On the basis of weather predictions indicating probable inland air transport,

four days (September 23 and 24, 1996, and October 1 and 2, 1996) were chosen for more extensive sampling. Intensive experiments were conducted over pairs of consecutive days to accommodate the previously observed travel time of air parcels across the basin [21]. On these four days, the low-volume filter samplers, impactors, and VOC canisters at each site were used for one 4-h period each day (the "intensive operating period," or IOP). Two additional days (September 25 and 26, 1996) were chosen for intensive sampling at Riverside only, because conditions there were very hazy and nitrate concentrations were observed to be particularly high on those days.

Background concentration samples were taken for one 24-h period, starting at 1300 PDT September 21, 1996, near Two Harbors on Santa Catalina Island, 35 km upwind of the mainland. Three cascade impactors (two MOUDIs with Teflon substrates and one MOI with aluminum foil substrates), a modified low-volume filter sampler, and a continuous UV photometric ozone monitor (Dasibi Environmental Corp., Model 1003-AH), but no ATOFMS, were used at this location.

The experiment was designed to permit a later search for "single air parcels" that pass consecutively over several air monitoring sites as they are transported across the basin. Previous experience with experiments designed to achieve this objective [21] suggested the following time schedule: intensive sampling was conducted in Long Beach at 0700–1100 PDT, in Fullerton at 1100–1500 PDT, and in Riverside at 1500–1900 PDT. By combining the September 21–22 background measurements at Santa Catalina Island with the September 23–24 intensive experiments and the September 25–26 experiments at Riverside, a six-day consecutive period of observations exists as air parcels are advected across the air basin. The relationship between instruments and sampling schedules is illustrated in Figure 2.2.

An electrical aerosol analyzer (EAA, TSI Inc., Model 3030) was used at each site to measure particle number concentrations in the size range $0.017 < D_p < 0.250$ μm. The EAA at Fullerton was equipped with an electrometer having an improved amplifier for increased sensitivity. Each EAA was interfaced with a per-

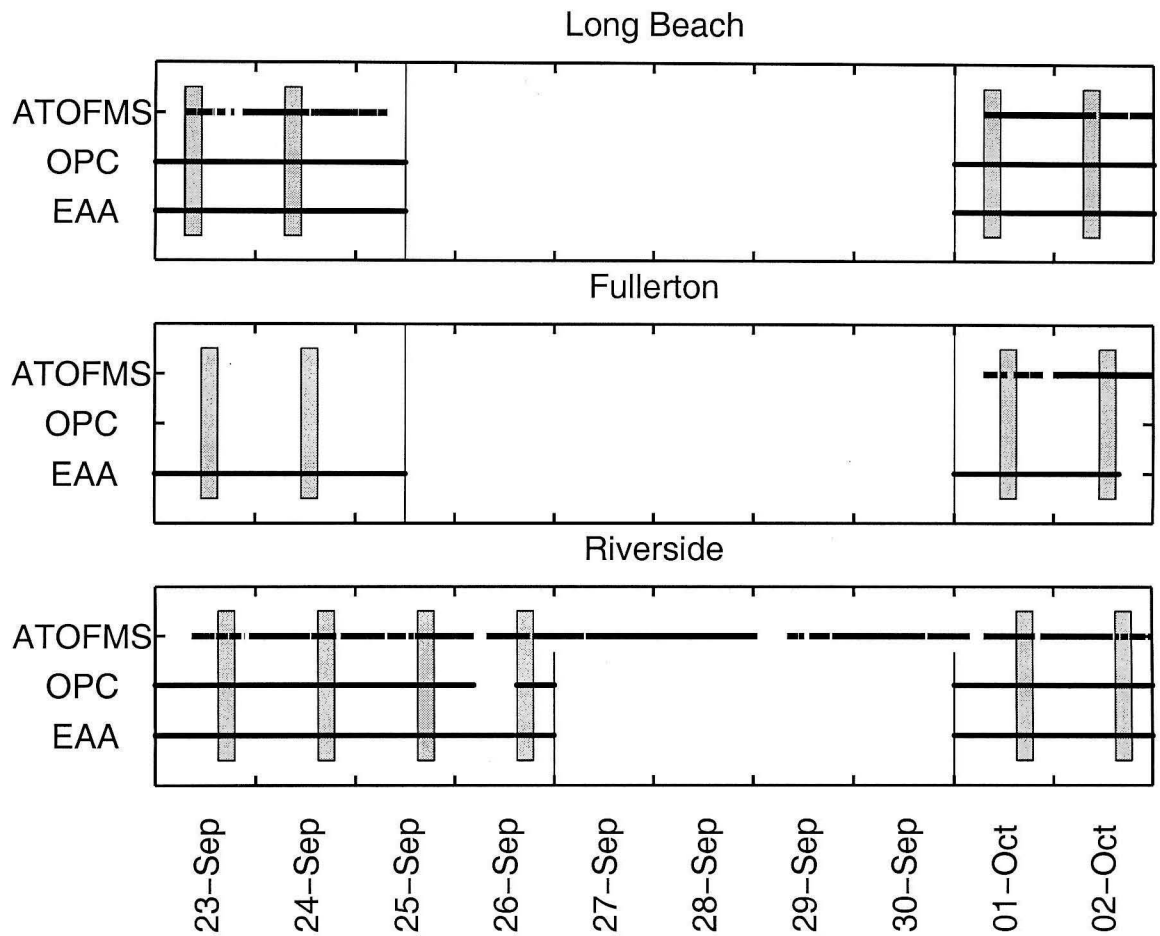

Figure 2.2: Times of operation (in PDT) of ATOFMS instruments, OPCs, EAAs, and other instruments at each site during the study. Shaded boxes indicate the intensive operating periods; total and fine particle filter samples, size-segregated impactor samples, and VOC canister samples were taken only during these 4-h periods of intensive operation.

sonal computer which enabled the acquisition of a particle number distribution over this size range approximately once every 7 minutes.

Laser optical particle counters (OPC, Particle Measuring Systems, Model ASASP-X) were used at two of the three sites (Long Beach and Riverside) to corroborate the size distribution data from the EAA over the size range where the two instruments overlap and to extend size distribution measurements to larger particle sizes. This instrument recorded particle number distributions in 31 channels over the size range $0.09 < D_p < 2.6$ μm every 5 seconds. Size distributions from the OPC were corrected as suggested by Hering [57] to take into account the difference in the refractive index between the polystyrene latex (PSL) spheres used to calibrate the instrument and typical Los Angeles area atmospheric aerosols.

Three ATOFMS instruments were used; the Long Beach and Fullerton sites each had transportable ATOFMS systems [28], and a laboratory-bound ATOFMS [27] sampled in Riverside. Despite design differences between the transportable and laboratory-bound systems, the three ATOFMS instruments can be calibrated to yield essentially equivalent results through intercomparisons with the impactor and OPC data from this study [58]. The ATOFMS instruments operated continuously, collecting number distribution data in the aerodynamic particle size range $0.2 < D_a < 5$ μm, and obtaining mass spectra for a subset of the input particle population.

Each air monitoring site was equipped with a pair of cascade impactors. One 10-stage rotating Micro-orifice Uniform Deposit Impactor (MOUDI, MSP Corp., Model 100) [59] and one 10-stage non-rotating Micro-orifice Impactor (MOI, MSP Corp., Model 110) [59] were operated simultaneously to measure fine particulate mass and chemical composition as a function of particle size. A Teflon-coated cyclone separator was placed upstream of each impactor in order to capture coarse particles ($D_a > 1.8$ μm) that might otherwise enter the impactor and distort the mass distribution measurements by bouncing from their appropriate collection stages. Particles reported here were collected on stages 5–10 of the impactors over the size range $0.056 < D_a < 1.8$ μm; the upper stages of the impactor were

loaded with impaction substrates, but were not analyzed. The non-rotating impactor was loaded with aluminum foil substrates (MSP Corp.), while the rotating impactor was loaded with Teflon substrates (Teflo, Gelman Science). No grease or oil was used on the substrates in order to avoid adding a source of organic contamination.

In addition to the above instruments, total (no size separation) and fine (D_a < 1.8 μm) airborne particle samples were collected using a low volume filter-based sampling system (see Figure 2.3). Total particulate matter was collected on one open-faced quartz fiber filter (Pallflex, 2500 QAO) and on two parallel open-faced Teflon filters (Gelman Sciences, Teflo, 2.0 μm pore size) at the flow rates shown in Figure 2.3. The two open-faced Teflon filters removed particles from the air, and the airstream then passed through several chemically impregnated back-up filters designed for collection of certain reactive gases. A pair of oxalic acid impregnated glass fiber filters (Gelman Type AE, 47mm diameter), filters "G" in Figure 2.3, collected gas-phase ammonia, to be detected as ammonium ion. A pair of K_2CO_3 impregnated quartz fiber filters (Pallflex, 2500 QAO, 47mm diameter), filters "H" in Figure 2.3, collected gas-phase SO_2, to be detected as sulfate ion. For fine particle samples, ambient air was passed through an acid-washed Pyrex glass inlet line to a Teflon-coated AIHL-design cyclone separator [60] at a nominal flow rate of 26 lpm before particle collection on a set of parallel filters: one quartz fiber filter (Pallflex, 2500 QAO, 47mm diameter), two Teflon filters (Gelman Sciences, Teflo, 2.0 μm pore size, 47mm diameter), and one pre-washed nylon filter (Gelman Sciences, Nylasorb, 47mm diameter). The flow rates sampled by these filters are shown in Figure 2.3. An additional nylon filter, located downstream of an MgO-coated diffusion denuder, was used in conjunction with the nylon filter downstream of the cyclone alone to measure gas phase nitric acid and fine particle nitrate by the denuder difference method. The air flow rate through each filter or set of filters was measured before and after each 4-h sampling period with a calibrated rotameter. While these *filter samples* did not offer the size-specific information available from the impaction substrate

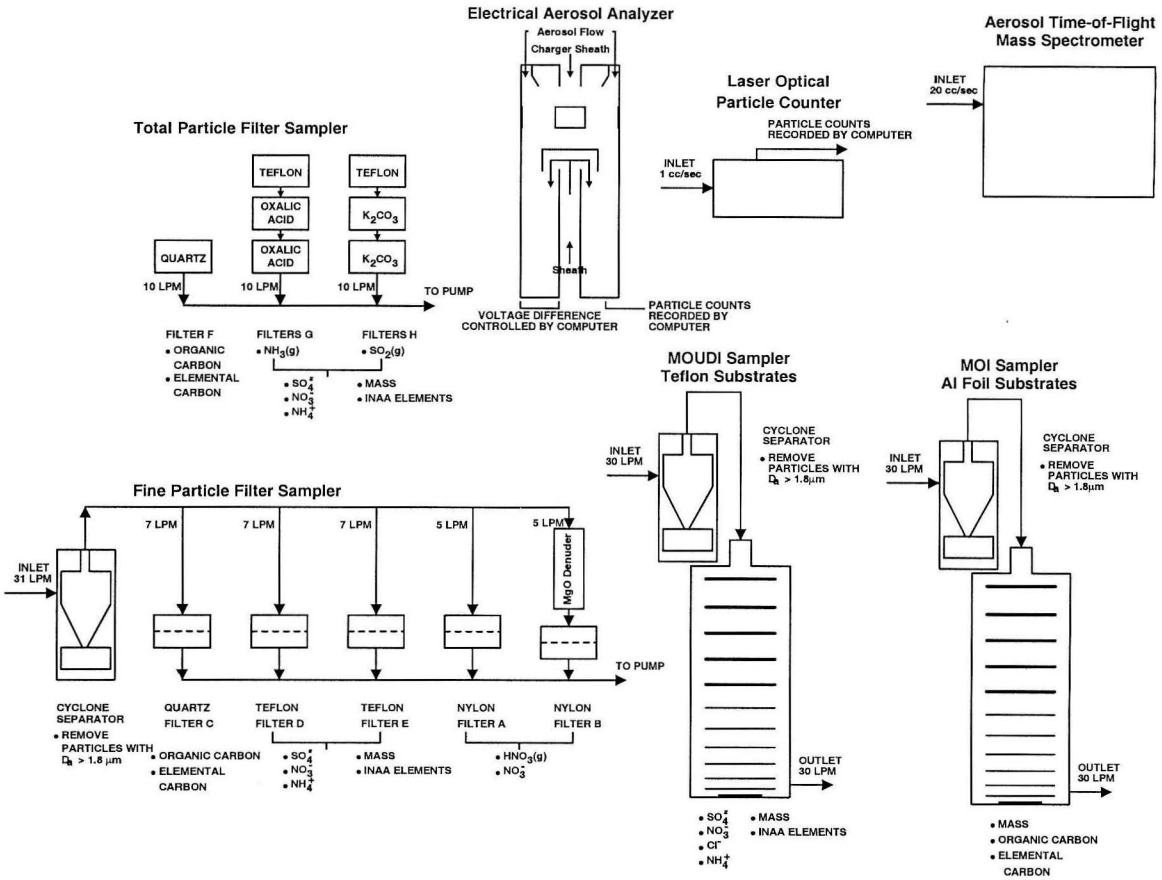

Figure 2.3: Schematic diagram of the particulate matter sampling systems used in this study.

samples, they served as an important check on the entire quantity of fine particle material in the atmosphere. These samples have the advantage of a greater available mass, thereby facilitating the chemical analysis procedures.

Mass concentration determinations were made from all foil and Teflon impaction substrates and Teflon filters and afterfilters, by repeated weighing before and after sample collection on a Mettler Model M-55-A mechanical microbalance maintained in a temperature- and humidity-controlled environment (21.0 ± 0.5°C, 37 ± 3% RH). Foil substrates were pre-cleaned of any organic contaminants by baking for 40–50 h at 550°C, and all quartz fiber filters were pre-cleaned by baking for at least 10 h at 550°C.

All impactor substrates and filters were cut in half before chemical analysis to allow the use of multiple chemical analysis methods. The samples collected

on aluminum foil substrates and quartz fiber filters were analyzed for elemental and organic carbon using the thermal-optical carbon analysis method of Huntzicker et al. [61] as modified by Cary [62]. One half of each sample collected on a Teflon substrate underwent analysis by ion chromatography (Dionex Corp, Model 2020i) for the anions NO_3^-, $SO_4^=$, and Cl^- [63], and the extract was also analyzed by an indophenol colorimetric procedure for NH_4^+ [64] using an Alpkem rapid flow analyzer (Model RFA-300). The second half of each Teflon impactor substrate was subjected to neutron activation analysis for detection of trace elements [65]. Gas phase ammonia collected on oxalic acid-impregnated glass fiber filters was measured as ammonium ion using the indophenol colorimetric procedure cited above on the Alpkem rapid flow analyzer (Model RFA-300). Gas phase SO_2 collected on K_2CO_3-impregnated quartz fiber filters was detected as sulfate ion by ion chromatography. Nylon filters upstream and downstream of a MgO-coated diffusion denuder permitted determination of gas phase nitric acid and fine particle nitrate by the denuder difference method using the ion chromatographic analysis procedures described by Solomon et al. [66]. Detection limits for $SO_4^=$, NO_3^-, NH_4^+, and TC (total carbon) were 0.62, 0.53, 0.36, and 0.78 μg per sample, corresponding to 0.17, 0.15, 0.10, and 0.43 $\mu g\ m^{-3}$ for an impactor stage, for example.

Continuous gas-phase measurements were made of selected air pollutants at Long Beach and Riverside. O_3 (Dasibi Environmental Corp., Model 1003-AH at Long Beach, Model 1003-PC at Riverside) and NO/NO_2 (ThermoElectron Corp., Model 14B/E) measurements were made at both Long Beach and Riverside. In addition, O_3, NO, NO_2, and CO data were obtained from nearby South Coast Air Quality Management District (SCAQMD) air monitoring stations.

Electropolished stainless steel canister samplers were used at Long Beach and Riverside to capture volatile organic compounds. The 6-L canisters were shipped and deployed into the field under high vacuum. 4-h integrated samples were collected in the canisters through PFA Teflon sample lines purged with ambient air, after which the canisters were resealed. Total non-methane organic com-

pounds in the gas phase were measured by cryogenic preconcentration and direct flame ionization detection according to EPA Method TO12 [67]. Individual organic compounds from the stainless steel canister samples were analyzed by gas chromatography/flame ionization detection.

2.4 Results and Discussion

2.4.1 Meteorology

In order to describe pollutant transport conditions over the September 21-October 3, 1996, sampling period, wind fields were constructed according to the method of Goodin et al. [68]. Meteorological data used as inputs to these calculations included hourly averaged wind speed and direction at 29 meteorological stations maintained by the South Coast Air Quality Management District.

Figures 2.4a and 2.4b illustrate the wind patterns characteristic of the period September 21-30, 1996. Figure 2.4a shows the calculated wind field in the study area at 0600 PDT on September 24, 1996. Wind speeds were very low. Overnight stagnation occurred across the air basin every night for 15-18 hours, beginning at 1900-2200 PDT in the evening and ending at 1200-1500 PDT the following day. Figure 2.4b shows the calculated wind field on the afternoon of the same day at 1300 PDT. Stagnation had ended, and the wind was blowing onshore from the ocean, in the general direction from southwest to northeast, providing the desired transport across the three urban air monitoring sites. The wind patterns changed during the second intensive period of operation, October 1-2, 1996. Figure 2.4c shows the calculated wind field in the area at 0600 PDT on October 1, 1996. Instead of the overnight stagnation seen the previous week, flow occurred up the coast from the southeast overnight. Figure 2.4d shows the calculated wind field on the same day at 1300 PDT. In the afternoon, the typical onshore sea breeze flow from the southwest toward the northeast was observed. The result of this set of wind patterns was that during the October 1-2 period, air parcels

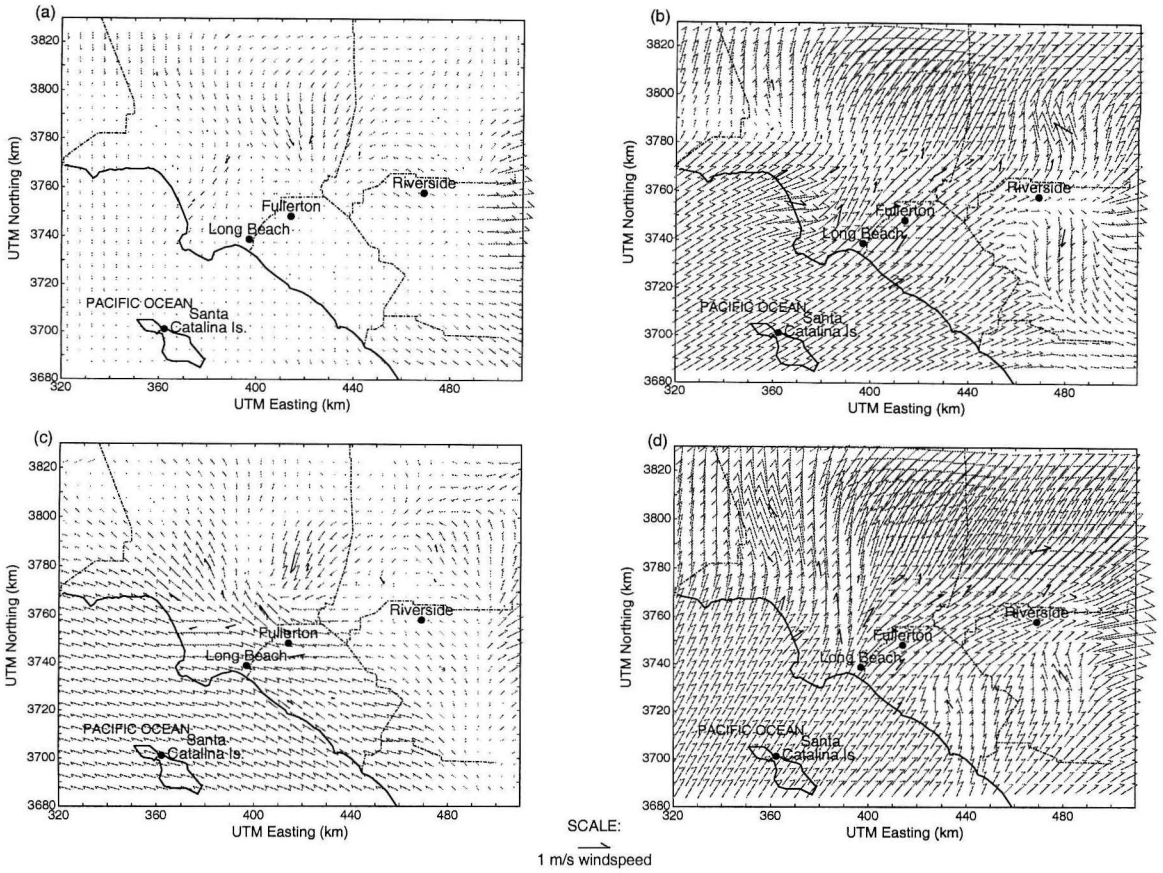

Figure 2.4: Surface windfields over the study area at a) 0600 PDT on September 23, 1996; b) 1300 PDT on September 23, 1996; c) 0600 PDT on October 1, 1996; d) 1300 PDT on October 1, 1996.

traveled along a zig-zag trajectory, first parallel to the coast, then inland, before being sampled at the air monitoring sites, and did not pass over the three urban sites sequentially as had been hoped.

Weather conditions throughout the sampling period were mild and devoid of precipitation. No significant fog was reported onshore on days of intensive sampling. We did observe a fog bank offshore to the west of the Santa Monica Bay coastline during portions of the Santa Catalina Island background experiments (though not between that island and the mainland). Conditions at Long Beach in the morning during the intensive sampling periods were overcast with little to no breeze, temperatures ranging from 19 to 25°C, and humidity ranging from 45 to 75%. Fullerton during the late morning to early afternoon intensive sampling

periods experienced patchy clouds, temperatures ranging from 19 to 27°C, and relative humidity ranging from 35 to 65%. Conditions at Riverside during the late afternoon intensive sampling periods included temperatures ranging from 17 to 32°C, and relative humidities ranging from 20 to 65%. At Riverside in the afternoon, skies were clear of clouds, but on most days a haze due to photochemical smog was present. Maximum wind speeds were about 3 m s^{-1}.

2.4.2 Ozone

Continuous measurements of ozone concentrations were made alongside the sampling equipment at Santa Catalina Island, Long Beach, and Riverside. In addition, data on hourly average ozone concentrations at air monitoring stations near Fullerton and Riverside were made available by the SCAQMD. Results are shown in Figure 2.5. The ozone peak occurred at about 1500 PDT every day at all three urban locations. In addition, a secondary peak often occurred overnight at Long Beach, at 0100–0600 PDT. Ozone concentrations measured at the background site at Santa Catalina Island on September 21–22, 1996, were essentially constant both day and night at close to 57 ppb. It is interesting to note that the regional ozone background concentration, which averaged 57 ppb, is generally closer to the maximum inland concentrations than to the minimum inland concentrations during this period; the ozone depletion below the background levels seen overnight is likely due to O_3 scavenging by NO at night. With upwind regional background O_3 levels at 57 ppb, only modest O_3 increases above background are needed to reach the new U.S. national ambient air quality standard for ozone which was set in 1997 at 0.08 ppm O_3 not to be exceeded over an 8-h averaging period on more than four days per year, averaged over three years [69].

2.4.3 Particle Size Distribution

Continuous particle size distribution measurements were made at Long Beach and Riverside throughout the study using OPCs. When these data are combined

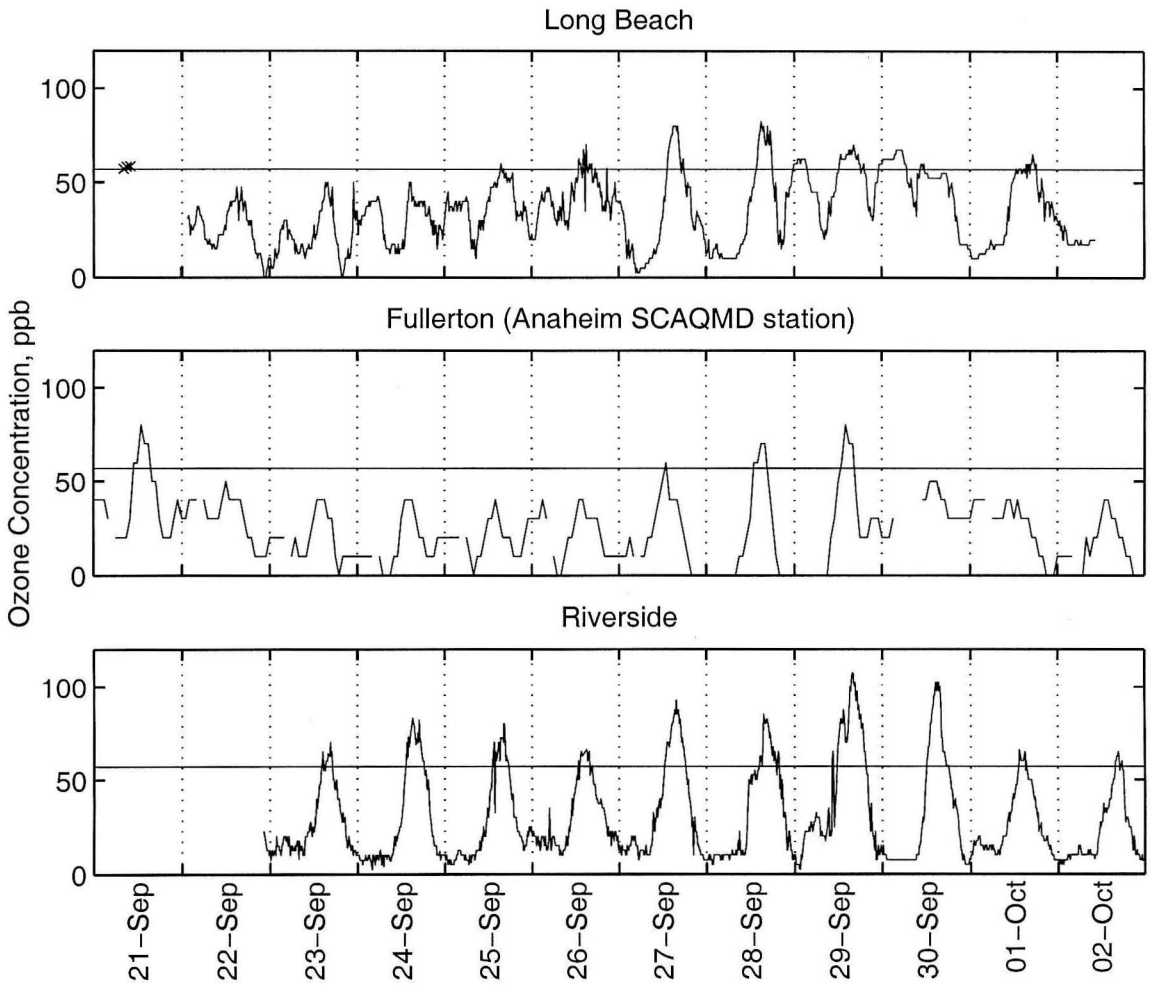

Figure 2.5: Ozone concentrations at all four sampling sites during the study. Solid horizontal line drawn at 57 ppb O_3 is supplied for reference purposes and indicates the average ozone concentration observed at the Santa Catalina Island background site based on measurements made on September 21–22, 1996. The "x" symbols on the Long Beach graph indicate the actual ozone concentrations measured at Santa Catalina Island, which did not vary greatly between daytime and nighttime samples.

with data from the EAAs at those sites, continuous particle size distributions are obtained over the diameter range $0.017 < D_p < 3.0$ μm. Particle number distributions averaged over all hours of the study are shown in Figure 2.6ab. These number distributions have been converted to mass distributions assuming a particle density of 1.3 g cm^{-3} and averaged over all the study days in 4-h periods to demonstrate the diurnal differences in average particle mass distributions at Long Beach and Riverside (see Figure 2.6c–h). Throughout the study, the particle mass distribution at Riverside is largely unimodal in the submicron particle size range. The peak in the particle mass distribution at Riverside occurs at somewhat larger particle sizes (0.5 μm) than at Long Beach. This is in contrast to much of the data taken a decade earlier during the SCAQS experiments which showed two modes in the particle mass distribution in the particle diameter range between $0.1 < D_p < 1.0$ μm, one at about 0.7 μm particle diameter, and another at about 0.2 μm particle diameter (see for example Eldering et al. [25]). The mode at 0.2 μm diameter during the SCAQS experiments, which is absent at Riverside in the present experiment, was attributed to the primary particle emissions from diesel engines and other primary aerosol carbon sources [15]. The relative reduction in the size of the 0.2 μm mode in the mass distribution in the present experiment suggests soot emission reductions over the past decade; more extensive sampling would be needed to confirm this hypothesis, but it agrees with the decreasing trend in fine elemental carbon concentrations observed in the Los Angeles area since 1982 [8], the dominant source of which is diesel engine exhaust [70].

2.4.4 Fine Particle Chemical Composition

The size distribution of the ambient aerosol chemical composition averaged over all cascade impactor data taken at the background site and at the three urban sites, is shown in Figure 2.7. The background aerosol at Santa Catalina Island is almost entirely composed of inorganic substances. The urban sites show addi-

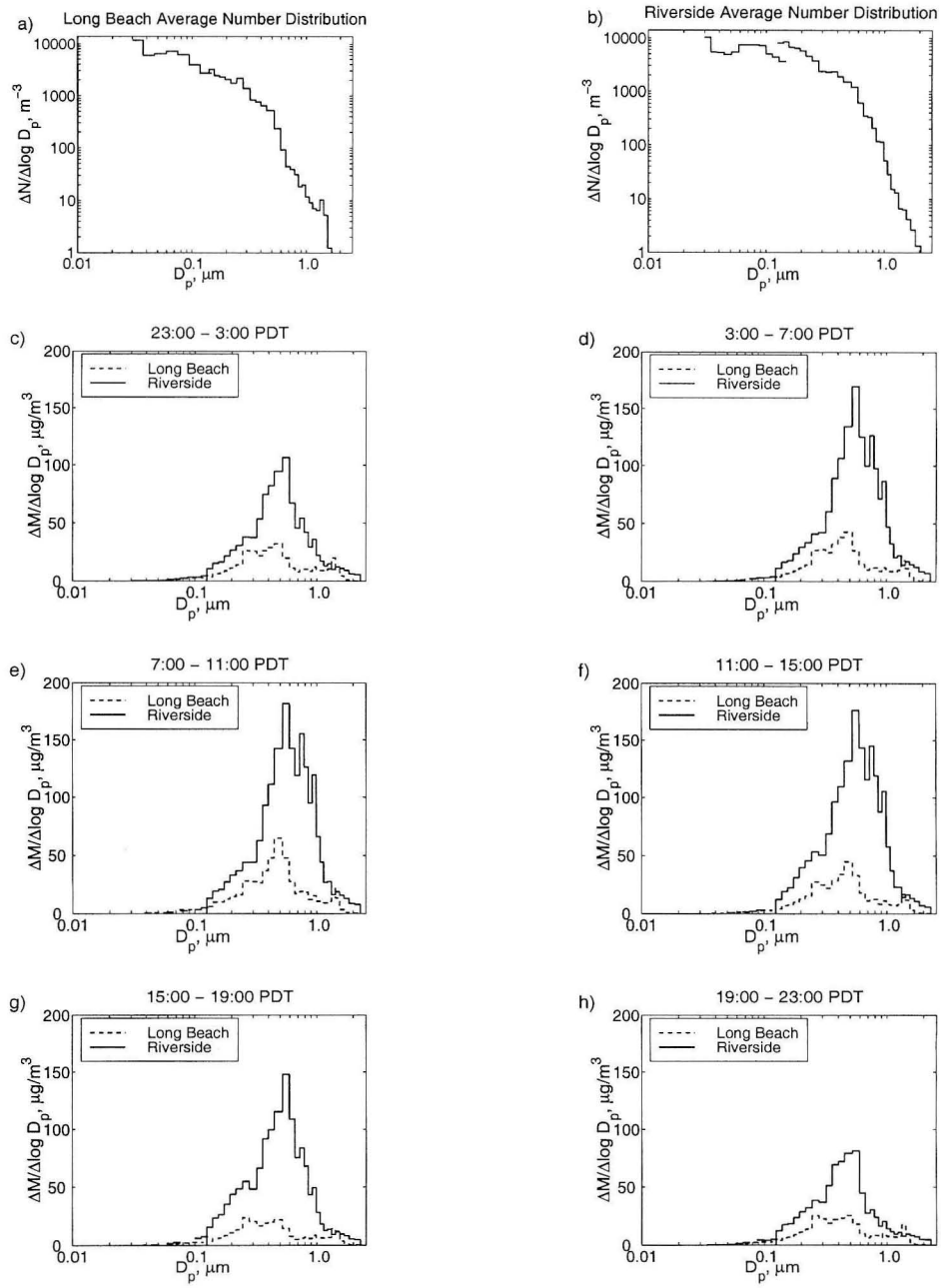

Figure 2.6: Particle number distributions measured by the EAAs and OPCs at a) Long Beach and b) Riverside, averaged over the course of the entire study. Particle mass distributions at Long Beach and Riverside averaged over the time intervals c) 2300–0300 PDT, d) 0300–0700 PDT, e) 0700–1100 PDT, f) 1100–1500 PDT, g) 1500–1900 PDT, and h) 1900–2300 PDT.

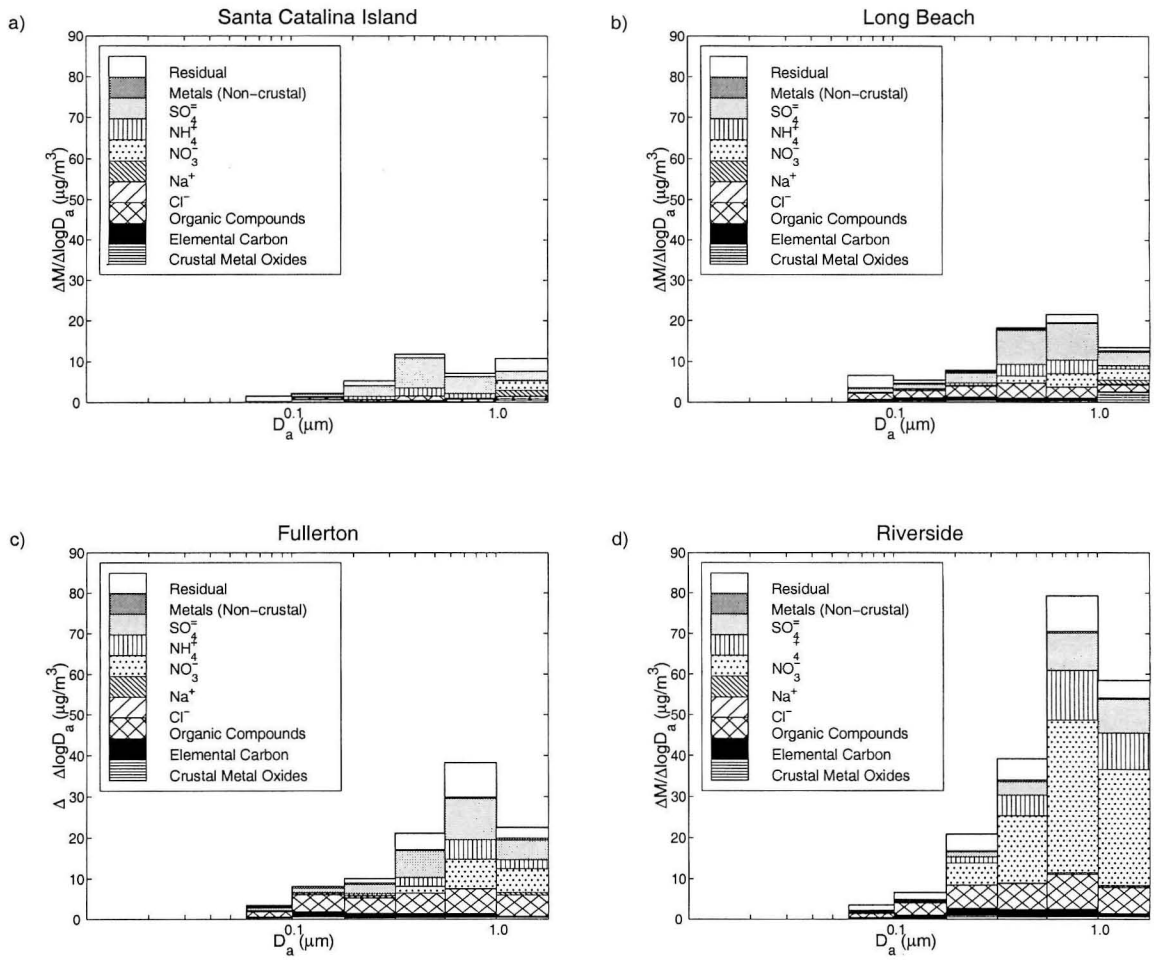

Figure 2.7: Size-dependent chemical composition of airborne particles in Southern California averaged over all cascade impactor samples taken at each sampling site over the course of the study. Samples are taken at different times of the day at each site (see text).

tions of carbonaceous compounds to the background aerosol. The Riverside site is distinguished by large amounts of ammonium and nitrate in the aerosol, as has been seen previously [13, 71-73]. Fine sulfate concentrations measured at Long Beach and Riverside during the present study are lower than the September-October monthly average sulfate concentrations measured near these places in 1982 and 1993 [8].

Different numbers of impactor samples were taken at the different sites, and on different days (see Figure 2.3). In the next chapter, sets of these impactor samples taken on specific days, as well as fine particle, total suspended particle, and gas-phase pollutant data representing passage of the same air mass over successive sampling sites will be presented such that a Lagrangian rather than Eulerian view of particle evolution can be obtained [74].

2.4.5 Single Particle Chemical Composition

The aerosol time-of-flight mass spectrometry instruments located at Long Beach, Fullerton, and Riverside are capable of drawing a continuous stream of particles from the atmosphere and determining both the size and chemical constituents of the individual particles present, one particle at a time. The particles are accelerated through a converging nozzle, after which three skimmers collimate the stream and diverging particles are pumped away. Remaining particles pass into the vacuum chamber of the instrument. As a particle passes through two laser beams consecutively, its terminal velocity (which is dependent on particle aerodynamic diameter) is measured, and from that velocity the particle size is determined. Knowing the speed of the particle, a timing circuit is set to trigger a high-power desorption laser which intercepts the particle. The ions generated by laser desorption of species from the particle are swept into the mass spectrometer, where spectra indicating the elemental and molecular composition of the particle are generated. The ATOFMS instruments sampled continuously throughout the periods shown in Figure 2.2. Depending on the instrument considered

(transportable vs. laboratory ATOFMS) mass spectra were acquired for 6–14% of the particles detected by the ATOFMS instruments, for a total of more than 319,000 individual particle spectra.

Examples of the mass spectra of characteristically different particles are shown in Figure 2.8. Figure 2.8a shows the positive ion mass spectrum of a sea salt particle of aerodynamic diameter 1.77 μm. The particle contains Na^+, K^+, and Ca^+ as the major positive ion constituents, along with smaller amounts of $Na_3SO_4^+$, indicative of sodium sulfate. In Figure 2.8b, the spectrum of an ammonium nitrate-containing particle of diameter 0.37 μm is shown. The key ions NH_4^+ and NO^+ that indicate ammonium and nitrate, respectively, are accompanied by C^+ and C_3H^+, suggesting that this particle possibly is composed of a secondary ammonium nitrate coating over a primary carbon particle core in a way that qualitatively matches many of the particles predicted by the air quality model of Kleeman et al. [15]. Figure 2.8c shows a 0.42 μm diameter particle that is composed of hydrocarbons and little else. Figure 2.8d depicts an elemental carbon-containing particle, indicated by fragments with integer numbers of carbon atoms, but little or no hydrogen. As in Figure 2.8b, the presence of ammonium nitrate indicator ions in the spectrum of this particle may represent a secondary ammonium nitrate coating.

The hundreds of thousands of individual particles that were characterized by the three ATOFMS instruments can be sorted into categories and used to display the time series of particles having specific chemical attributes. Examples of several such time series are presented in Figure 2.9. The threshold level for considering that a specific ion is present within a particle is that its peak area must constitute at least 0.5% of the total peak area of the spectrum. Figure 2.9a shows the time series of sodium-containing particles. Sodium is one marker for sea salt-derived particles, though it is also found at times in smaller combustion particles. Not surprisingly, the sodium-containing particle concentrations are highest at the coastal Long Beach site. The number concentration of particles containing carbon is highest at Riverside, reflecting accumulation of the primary

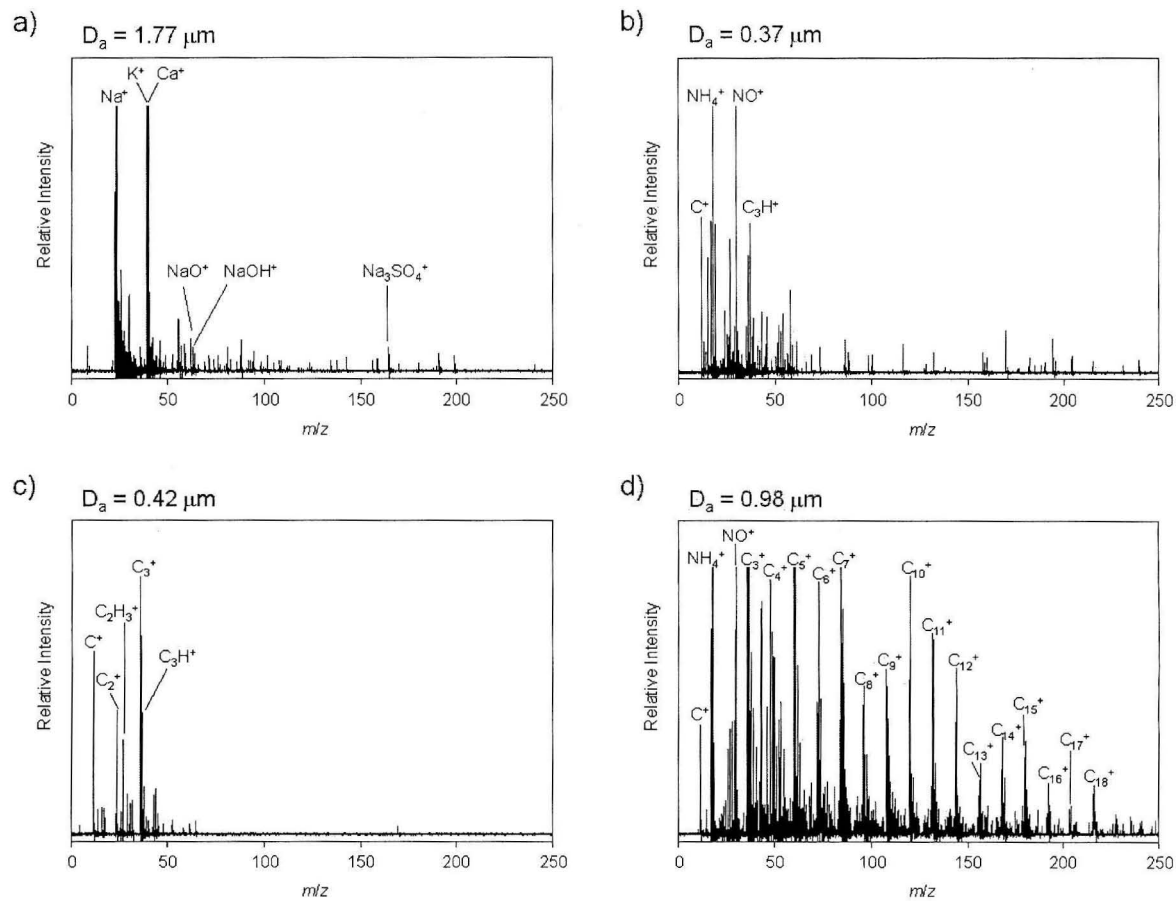

Figure 2.8: Sample mass spectra of particles sampled by ATOFMS instruments during this study. a) sea salt particle; b) ammonium nitrate-containing particle with organic carbon inclusions; c) organic carbon particle; d) predominantly elemental carbon particle with some ammonium nitrate content.

emissions from urban activities during air mass transit across the air basin, as is seen in Figure 2.9b. The time series of particle counts for particles containing ammonium and nitrate are shown in Figures 2.9c and 2.9d. The time series appear to be nearly identical, and indeed the ammonium and nitrate are generally found within the same individual particles. Very close examination of the ammonium- and nitrate-containing particle counts shows that nitrate-containing particles exceed ammonium containing particles at Riverside on some occasions, for example during the times on September 23–25 when sodium-containing particle counts are elevated at Riverside. Examination of single particle spectra show sodium nitrate particles, i.e., reacted sea salt, to be present at Riverside at those times.

The ATOFMS systems offer time series data on the occurrence of particles containing specific chemical species with temporal resolution on the order of minutes [75]. These instruments display particle counting characteristics that are more likely to detect particles at the larger end of the fine particle size range. The counting efficiency of the ATOFMS instruments as a function of particle size during this study has been determined by Allen et al. [58] through comparison with particle size distributions obtained from the cascade impactors and optical particle counters. The method and results of that comparison are detailed in reference [58], which shows how to reconcile the data from the matched sets of conventional instruments and the two ATOFMS designs operated at the air monitoring sites. At present, translation of relative peak heights or peak areas per spectrum for the various chemical species into absolute quantities of each chemical substance in a particle remains to be completed. Sensitivity factors that connect the relative abundance of some ions to their relative peak areas have been determined in the laboratory [76]. The questions of particle counting efficiency and chemical sensitivity will be addressed further in future work both through additional laboratory experiments and through calibration of the ATOFMS systems according to the chemical composition data as a function of particle size collected by the cascade impactors during the present experiments.

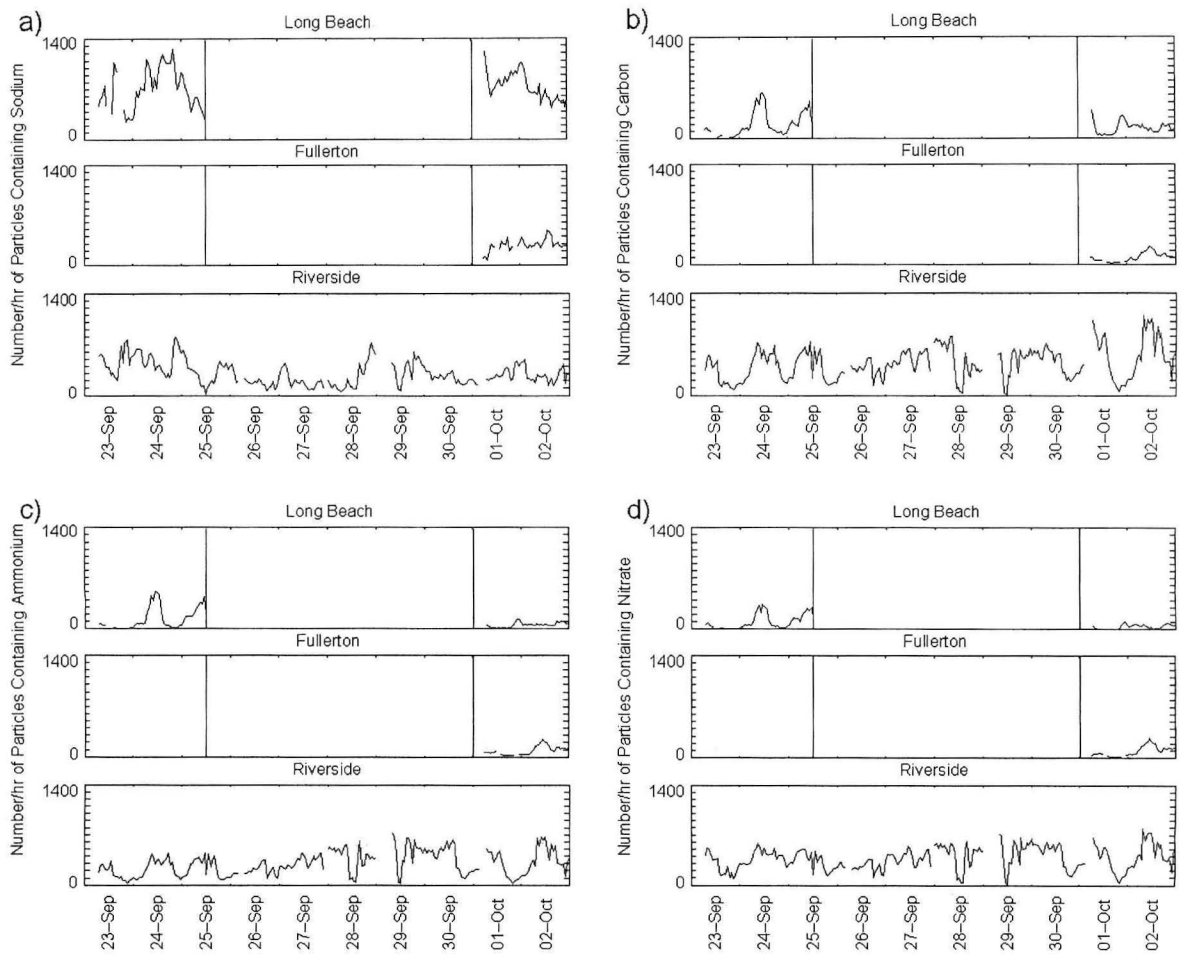

Figure 2.9: Time series showing relative number concentrations of a) sodium-containing particles, a marker for sea salt; b) carbon-containing particles; c) ammonium-containing particles; d) nitrate-containing particles among those particles for which spectra were collected. These data have not been adjusted to reflect the counting efficiency of the ATOFMS instruments [58].

Chapter 3

Evolution of Atmospheric Particles Along Trajectories Crossing the Los Angeles Basin: Santa Catalina Island – Long Beach – Fullerton – Riverside

3.1 Introduction

The development of air quality models which assist communities in designing effective air quality control strategies depends on an understanding of the chemical and physical transformation processes that occur in the atmosphere. The study of such processes, however, is complicated by the movement of air masses; it is difficult to tell from data taken at fixed locations how and why particle evolution occurs. The ideal field study situation in many cases would be to move the air monitoring instruments, keeping them always within a single air parcel as it moves along a trajectory dictated by wind direction and speed in order to observe aerosol transformations as they happen. Unfortunately, the complexity of

aerosol instruments and their power requirements often make such experiments impractical. Even instrumented aircraft have difficulty remaining aloft within the same air mass for several consecutive days. For that reason, few measurements exist showing how particle size distributions and chemical compositions evolve in the urban atmosphere over a several day period within a single air parcel in the presence of atmospheric chemical reactions, dilution, and deposition.

In late September and early October of 1996, a field experiment was conducted in Southern California in which four air monitoring stations were located along a typical air parcel trajectory in an attempt to observe particle evolution within the same air mass as it passes over each of the four stations in succession [77]. This experiment was described in the previous chapter. Particle size distribution, fine and total particle chemical composition, and size-segregated chemical composition measurements were taken sequentially at all four sites, at times intended to coincide with typical air mass motion, while continuous measurements of single-particle chemical composition were also made by aerosol time-of-flight mass spectrometry at three of the sites.

The purpose of this chapter is to examine the resulting database for events in which air parcels meet the criterion of successive passes over two or more monitoring sites, and through this analysis to develop a clear experimentally-based picture of how particles and gases within the same air mass change over time during transit across the Los Angeles Basin.

3.2 Background

Studies of secondary particle formation processes have been carried out on a number of occasions in Southern California by initializing a Lagrangian trajectory model with background pollutant concentration data taken upwind of the Los Angeles area and then comparing model predictions to pollutant measurements made on the downwind side of the city.

In one of the first of these studies, Roberts [78] examined SO_2(g) to particu-

late $SO_4^=$ conversion rates along air parcel trajectories stretching from the Pacific Coast inland to Pasadena, California. From changes in the ratio of SO_2 to total airborne sulfur between the major SO_2 source areas at the coast versus measurements made at the downwind receptor site at Pasadena, it was calculated that SO_2 oxidation rates varied from 1–15% per hour, depending on the event studied.

The formation of NH_4NO_3 aerosol within air parcels crossing the Los Angeles area was studied by Russell et al. [20]. A photochemical trajectory model was used to predict total ammonium nitrate concentrations within air parcels arriving at El Monte, California, at various times on June 28, 1974, and the results were compared to field measurements taken at that site on that day by Reynolds et al. [79]. Model predictions agreed well with measured particulate nitrate ion, ammonium ion, gas-phase ammonia, and ozone concentrations. A later version of this model [21] was used to examine air parcel trajectories that traversed Southern California during a two-day field study conducted in 1982 in which gas- and particle-phase nitrogen species, including NO, NO_2, HNO_3, NH_3(g), particulate NO_3^-, and particulate NH_4^+ were measured at ten locations with 2-h and 4-h time resolution [13]. In this case an air parcel trajectory was identified which passed over or near three monitoring sites in succession: Long Beach, Anaheim, and Rubidoux (a far-inland site near Riverside). This represents the only previous instance to date in which aerosol nitrate formation within the same air parcel has been observed at multiple points in time. These data are of particular value as a model verification tool, as the contents of the air parcel are well known at several locations along the trajectory and initial conditions are well established.

Pandis et al. [80] examined sulfate production in the presence of an urban fog using several trajectory models applied to the database from the 1987 Southern California Air Quality Study (SCAQS) [12]. These calculations sought to explain the elevated sulfate levels detected at inland sites downwind of an overnight fog that occurred at the Long Beach monitoring site. A model simulating only gas-phase chemical reactions was able to accurately predict aerosol sulfate concentrations within air parcels that had not passed through the fog, but sulfate con-

centrations within those air parcels which had passed through fog were underpredicted if only gas-phase chemical reactions were considered. A model which represented both gas- and aqueous-phase chemistry was able to account for the increased aerosol sulfate concentrations in air exposed to fog, shedding light on the heterogeneous chemical processes. In closely related work, sulfate and nitrate formation by heterogeneous processes along trajectories passing through stratus clouds have been studied by Seigneur and Wegrecki [81], modeling gas- and aqueous-phase data collected within clouds by Richards et al. [82, 83]. The calculations included treatments of diffusion and vertical transport in addition to cloud chemistry, and good agreement was obtained with measured cloud species concentrations. Major nitrate formation pathways were found to be aqueous reduction of NO_3 radicals and heterogeneous hydrolysis of N_2O_5; major sulfate formation pathways were calculated to be aqueous oxidation of SO_2 by H_2O_2, O_2, and OH radicals.

Secondary organic aerosol formation along trajectories crossing Southern California was studied by Pandis et al. [17]. A photochemical trajectory model was applied to a summertime smog episode that occurred in Claremont, California, on August 28, 1987. Calculations showed that approximately 18% of the organic aerosol burden at Claremont could be attributed to gas-to-particle conversion in the atmosphere.

Other recent studies combine these trajectory models for sulfate, nitrate, and secondary organic aerosol formation with emissions data on the size distribution of primary particle emissions from sources in order to render comprehensive predictions of the changes that occur in the size and chemical composition distribution of the atmospheric particle mixture [10, 15, 52, 53, 84]. Models have been created both for internally mixed aerosols, in which all particles of the same size are assumed to have exactly the same composition [52, 53, 84], and for externally mixed aerosols that reflect the differences in initial particle chemical composition at different sources [10, 15]. Predictions have been compared to cascade impactor measurements of ionic species, carbonaceous species, and

mass size distributions taken in Claremont by Wall et al. [41] and by Zhang et al. [24].

In all cases except the study by Russell and Cass [13], only the particle characteristics at the end points of the trajectories studied have been known experimentally in any detail, and particle evolution along the trajectories has generally been inferred by calculations rather than actual observations. One purpose of the present research is to replace these inferences about the intermediate evolution of the particle size and composition distribution with actual measured values that can later be used for stringent tests of air quality model performance.

3.3 Experimental Methods

As part of the present study, ambient air samples were collected on seven days over the course of two weeks in late September and early October, 1996 [77]. Instruments were stationed at three urban sites in the Los Angeles, California, area, chosen to lie along a seasonally typical air parcel trajectory: Long Beach, Fullerton, and Riverside. In addition, off-shore upwind background concentration data were taken at Santa Catalina Island (see Figure 2.1).

An electrical aerosol analyzer (EAA, TSI model 3030) and an aerosol time-of-flight mass spectrometry (ATOFMS) instrument [27, 28] were operated continuously at each of the three urban sampling sites. Laser optical particle counters (OPCs, Particle Measuring Systems model ASASP-X) were operated continuously at the Long Beach and Riverside sites. The high resolution particle size distribution data taken by the electrical aerosol analyzers and optical particle counters are presented in references [58, 77]. A pair of micro-orifice cascade impactors (MSP Corp., model 100) and a low-volume filter-based fine and total suspended particle sampler [77] were operated at each urban site for a 4-h period of time on each day of the two 2-day periods of intensive sampling. Additional impactor and filter-based measurements were made at Santa Catalina Island, upwind of the other sites, on the days preceding the first intensive experiment, and at Riverside,

at the downwind end of the air mass transport corridor, on the two days following the first intensive experiment, thus extending the first experiment to six days covering the period September 21-26, 1996. The second intensive experiment took place on October 1-2, 1996.

Background concentrations were measured for one 24-h period, starting at 1300 PDT September 21, 1996, at the University of Southern California's Philip K. Wrigley Marine Science Center near Two Harbors on Santa Catalina Island, 35 km upwind of the mainland. Three cascade impactors, two MOUDIs (MSP Corp., model 100) [59] with Teflon substrates and one MOI (MSP Corp., model 100) with aluminum foil substrates were used at this location, along with a modified low-volume filter sampler, and a Dasibi (Model 1003) ozone monitor.

The experimental apparatus and chemical analysis procedures are fully described in the previous chapter. Impactor and filter samples were analyzed gravimetrically and by ion chromatography, colorimetry, thermal evolution and combustion analysis, and neutron activation analysis to measure the size distribution and ionic species, carbonaceous species, and trace elements distribution of the airborne particles over the period of these experiments. NO and NO_2 concentrations were measured continuously at the monitoring sites in Long Beach and Riverside (ThermoElectron Corp., Model 14B/E); these data were supplemented by hourly NO and NO_2 data from nearby South Coast Air Quality Management District (SCAQMD) air monitoring sites. HNO_3 and NH_3 were measured with 4-h time resolution during intensive operating periods. HNO_3 was determined using the denuder difference method, and NH_3 was collected on an oxalic acid-impregnated filter downstream of a Teflon pre-filter.

Total particulate mass, nitrate and ammonium ion measurements made using Teflon filters were corrected for volatilization loss of fine particulate NH_4NO_3 during sampling. The volatilization loss of NO_3^- from each Teflon filter sample was determined by comparison to the fine particle NO_3^- collected simultaneously on a Nylon filter located downstream of a MgO-coated diffusion denuder. The quantity of NO_3^- ion lost during sampling from the Teflon filter samples taken

during this experiment averaged 4.8 $\mu g\ m^{-3}$ (range 0.11 to 12.7 $\mu g\ m^{-3}$). Correction for the volatilization loss was accomplished by adding a stoichiometrically equivalent amount of both NH_4^+ and NO_3^- to the values measured on all fine and total particle Teflon filter samples in an amount equal to the difference between the NO_3^- collection on the denuded Nylon versus Teflon filters. $NH_3(g)$ concentrations measured by collection on oxalic acid-impregnated filters downstream of Teflon particle pre-filters likewise were corrected to subtract that portion of the $NH_3(g)$ collected that was due to volatilization of NH_4NO_3 from the upstream Teflon pre-filter.

NO, NO_2, and HNO_3 were not measured at Santa Catalina Island. PAN was not measured at any site during this study and is not included in the material balances presented later in this paper. Those PAN concentrations that have been measured in the Los Angeles area in recent years have been low, even during smog episodes; PAN measurements taken in late summer 1993 averaged only 0.92±0.94 ppb in Long Beach, 1.06±1.27 ppb in Central Los Angeles, and 1.76±1.33 ppb in Azusa during a severe photochemical smog episode [54].

Four days (September 23 and 24, 1996, and October 1 and 2, 1996) were chosen for extensive sampling at the urban monitoring sites on the basis of weather predictions indicating probable inland air transport. Pairs of days were chosen for intensive experiments to accommodate the anticipated travel time of air parcels across the air basin [21]. On these four days, the low-volume filter samplers and impactors at each site were used for one 4-h period each day (the "intensive operating period," or IOP). Intensive sampling was conducted at Riverside only on September 25 and 26, 1996, to observe the progression of air parcels sampled upwind on previous days.

The experiment was designed to permit a later search for "single air parcels" passing consecutively over several of our monitoring sites as they travel across the basin. Previous experience with experiments designed to achieve this objective [21] suggested the following time schedule: intensive sampling was conducted in Long Beach at 0700–1100 PDT, in Fullerton at 1100–1500 PDT, and

in Riverside at 1500–1900 PDT. Sampling times and dates are summarized in Table 3.1.

Air parcel trajectories crossing Southern California during the September 21–October 3, 1996, sampling period were calculated by backward integration through wind fields constructed according to the method of Goodin et al. [68]. Meteorological data used as input to the trajectory calculations included hourly averaged wind speed and direction at 29 meteorological stations maintained by the South Coast Air Quality Management District.

Figures 3.1a, b, and c illustrate characteristic air parcel trajectories occurring during the study. Each circle along the trajectories pictured in Figure 3.1 represents one hour of elapsed time. The air parcel trajectories ending in Riverside at 1500 PDT on September 24 and on September 25, 1996, are shown in Figures 3.1a and b, respectively. A similar on-shore wind pattern was seen throughout the period September 21–30, 1996. During that period, overnight stagnation occurred across the air basin every night for 15–18 hours, beginning at about 1900–2200 PDT in the evening and ending at about 1200–1500 PDT the following day. Figure 3.1c shows the calculated air parcel trajectories ending at the Fullerton and Riverside air monitoring sites at 1500 PDT on October 2, 1996. Instead of the overnight stagnation seen the previous week, air flowed up the coast from the southeast overnight. Air parcels during that second phase of the experiment did not travel along a direct eastward inland route which would cause them to pass over more than one of the three established urban monitoring sites, and for that reason the October 1–2, 1996, intensive experiment will not be discussed further here.

Of the days which included data from all three urban sites, the closest match to the desired transport conditions occurred over the period September 21–24, 1996 (Trajectory 1), shown in Figure 3.1a. Back calculation of the trajectories from Riverside indicates that the air that arrived in Riverside over the period 1500–1900 PDT September 24, 1996, originated near Santa Catalina Island during the September 21–22 background concentration measurement experiments,

	Santa Catalina Island	Long Beach	Fullerton	Riverside
Sept. 21-22, 1996	1300-1300 PDT[a]			
Sept. 23, 1996		0700-1100 PDT	1100-1500 PDT	1500-1900 PDT
Sept. 24, 1996		0700-1100 PDT	1100-1500 PDT	1500-1900 PDT
Sept. 25, 1996				1500-1900 PDT
Sept. 26, 1996				1500-1900 PDT
Oct. 1, 1996		0700-1100 PDT	1100-1500 PDT	1500-1900 PDT
Oct. 2, 1996		0700-1100 PDT	1100-1500 PDT	1500-1900 PDT

[a] PDT = Pacific Daylight Time

Table 3.1: Intensive sampling time periods.

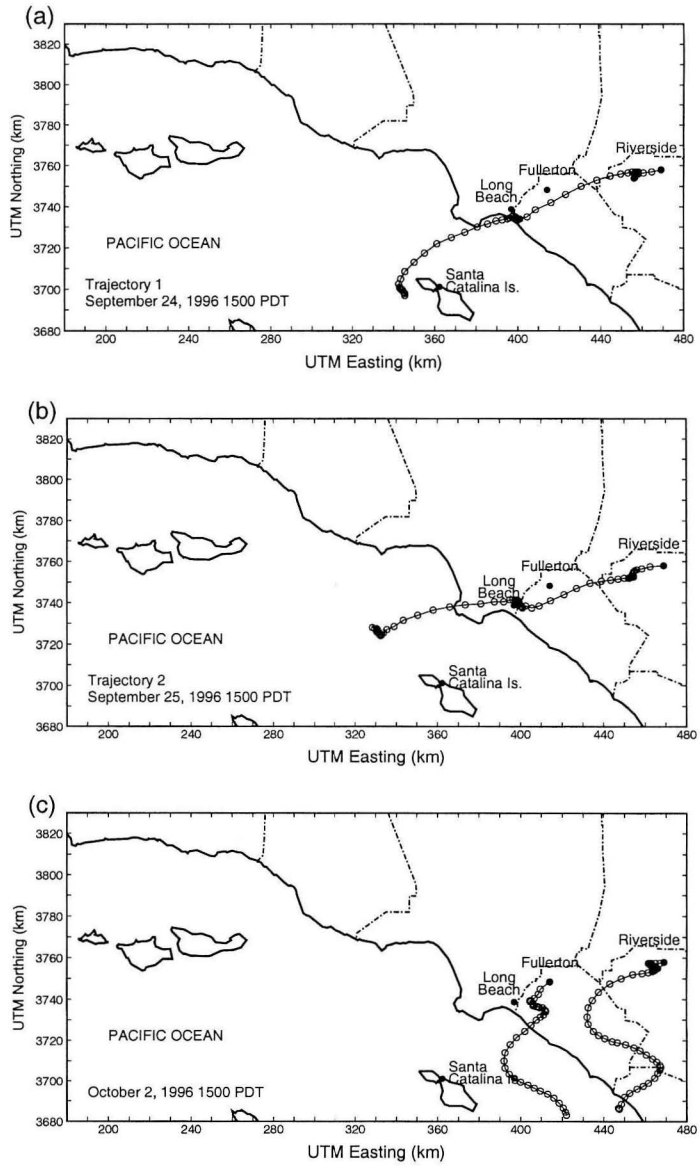

Figure 3.1: a) Air parcel Trajectory 1 reaching Riverside at 1500 hours PDT on September 24, 1996. The trajectory passes near all three urban sampling sites and the background sampling site. Pattern is typical of the trajectories seen in the first week of sampling, September 23–30, 1996. b) Air parcel Trajectory 2 reaching Riverside at 1500 hours PDT on September 25, 1996. c) Air parcel trajectories reaching Fullerton and Riverside at 1500 hours PDT on October 2, 1996. Both air parcels traveled roughly northward and did not stagnate overnight on the night of September 30–October 1. Pattern is typical of the trajectories seen during the second week of sampling, October 1–3, 1996.

stagnated in and near the Long Beach monitoring site over the night and throughout the morning of September 23, 1996 (IOP 0700–1100 PDT), and passed through Fullerton at 1400–1700 PDT September 23, 1996 (IOP 1100–1500 PDT). Similar transport conditions continued during the period September 24–25, 1996 (Trajectory 2), producing another air parcel trajectory, shown in Figure 3.1b, which passed near each monitoring site in succession. The air mass that arrived in Riverside during intensive sampling at 1500–1900 PDT on September 25, 1996, passed through Fullerton at 1430–1900 PDT September 24, 1996 (IOP 1100–1500 PDT), and stagnated in and near the Long Beach monitoring site over the night and throughout the morning of September 24, 1996 (IOP 0700–1100 PDT).

The remainder of this chapter will examine the evolution of the air masses as they travel along these two trajectories, passing over each of three or four sampling sites in succession.

3.4 Results and Discussion

3.4.1 Nitrogen Species Along Air Parcel Trajectories

Material balances on the nitrogen-containing pollutants measured sequentially along the two air parcel trajectories studied have been constructed, as shown in Figure 3.2. All concentrations are shown in terms of μg m^{-3} of nitrogen. Figure 3.2a shows the nitrogen species mass balance along the September 21–24, 1996, trajectory; Figure 3.2b shows the same data for the September 24–25, 1996, trajectory.

The total aerosol ammonium plus nitrate concentration begins at a very low value of 1.8 μg N m^{-3} over the ocean at Santa Catalina Island. While HNO_3 was not measured at Santa Catalina Island during this study, previous work shows that HNO_3 concentrations over the ocean upwind of Los Angeles at San Nicolas Island (see Figure 2.1) are very low, averaging about 10% of fine aerosol nitrate concentrations [66]. As the Trajectory 1 air parcel stagnates near Long Beach in

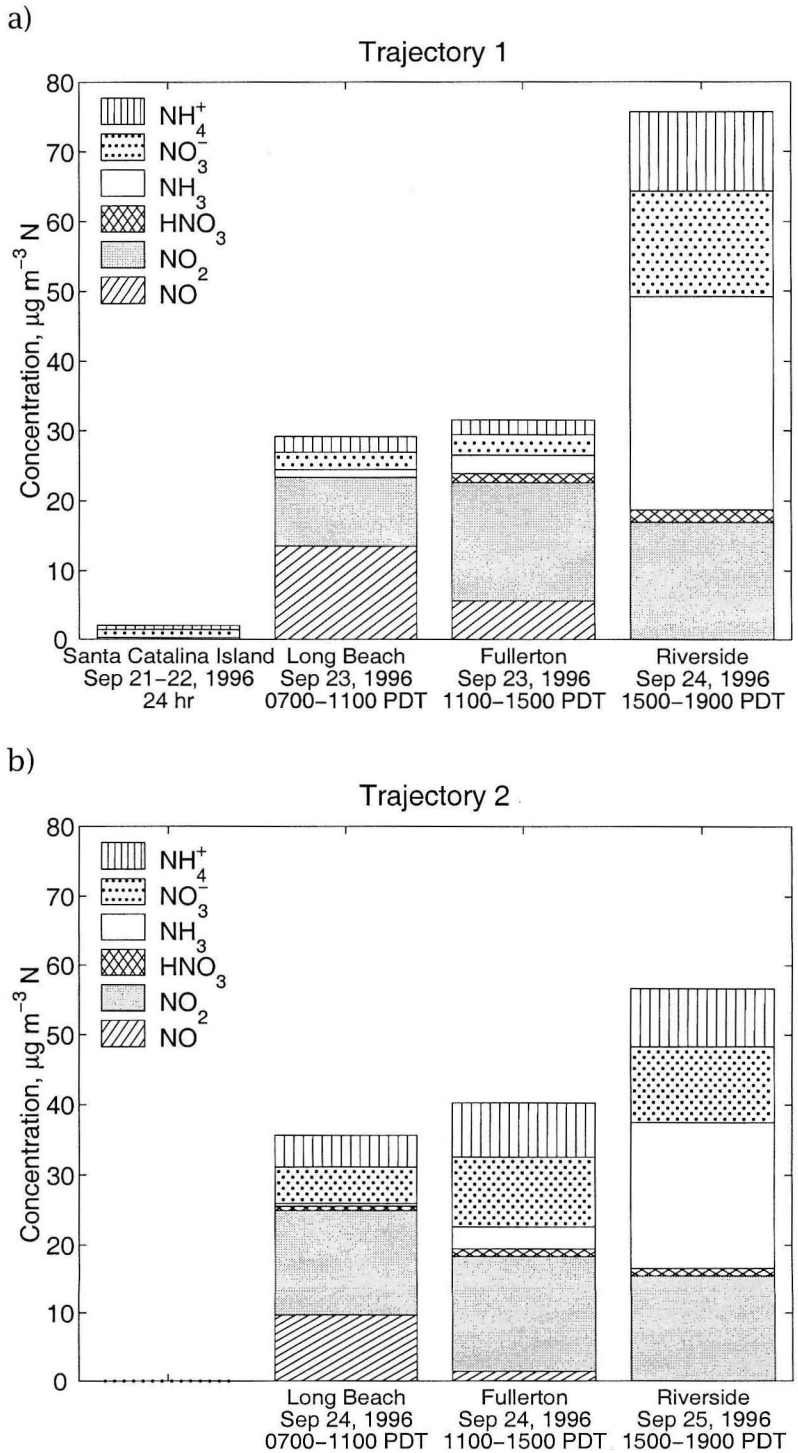

Figure 3.2: a) Nitrogen species balances along Trajectory 1, September 21–24, 1996. NO, NO_2, and HNO_3 were not measured at Santa Catalina Island. b) Nitrogen species balances along Trajectory 2, September 24–25, 1996.

the morning hours of September 23, substantial quantities of NO, and to a lesser extent NO_2, accumulate within the air mass studied due to combustion source emissions within the urban area. The ammonium plus nitrate nitrogen concentration in the particle phase more than doubles to a total of 4.7 μg N m^{-3} at Long Beach. Gas phase nitric acid levels at Long Beach remain negligible; instead, nitric acid formed is apparently quickly transferred to the particle phase or removed by dry deposition. The Trajectory 2 air mass measured in Long Beach likewise shows elevated quantities of NO, NO_2, and particulate ammonium and nitrate, in the presence of a negligible HNO_3 concentration.

Over the course of a few hours transit from Long Beach to Fullerton, NO conversion to form more NO_2 is observed, accompanied by small but noticeable increases in nitric acid vapor and increased gaseous ammonia concentrations. Higher HNO_3 and NH_3 concentrations can be maintained in the gas phase at Fullerton in the midday period, as ambient temperatures are higher there than at Long Beach during the earlier hours of the day (see [40, 85]). In the Trajectory 1 air mass, particulate ammonium and nitrate concentrations at Fullerton remain about the same as were observed earlier at the Long Beach site, indicating that dilution and dry deposition have compensated for emissions and pollutant transformation between Long Beach and Fullerton. In the Trajectory 2 air mass, particulate ammonium and nitrate concentrations at Fullerton are nearly double those at Long Beach.

After passing Fullerton, the air parcels studied pass over western San Bernadino County and then stagnate in western Riverside County overnight. By the following afternoon, as each air parcel finally reaches Riverside, essentially all NO has been converted to NO_2, and approximately half of the oxides of nitrogen in each air parcel exist as inorganic nitrates (HNO_3 plus aerosol NO_3^-) formed from the further oxidation of NO_2.

Even more remarkably, as each of the two air parcels studied reaches Riverside, about half of the measured reactive nitrogen exists as NH_3 gas plus aerosol NH_4^+. This large amount of ammonia plus ammonium ion accumulated in the

air parcel as it passed over the agricultural areas in western San Bernadino and Riverside Counties. Emissions inventories and air quality modeling studies identify 54 types of ammonia emissions sources in the Los Angeles area, some of the largest of which are dairy farms, other livestock waste decomposition, and fertilizer use in these agricultural areas [10, 20, 21, 39]. As NH_3 emissions into the air parcels increase, both the NH_3 and the inorganic nitrate formed from NO_2 oxidation react to form particle phase NH_4NO_3. HNO_3 concentrations are depleted due to aerosol NH_4NO_3 production, dilution, and dry deposition, while a substantial excess of NH_3 gas still exists in each air parcel at the end of the second day of transport across the air basin despite the foregoing dilution, transformation, and removal processes.

3.4.2 TSP and Fine Particulate Matter Along Air Parcel Trajectories

Material balances on the bulk chemical composition of total suspended particulate matter (TSP) concentrations and fine particle (particle diameter $D_a \leq 1.8\mu m$) concentrations constructed from chemical analysis of filter samples are shown in Figures 3.3 and 3.4, respectively. Material balances on the Trajectory 1 air mass are presented in Figures 3.3a and 3.4a; material balances on the Trajectory 2 air mass are presented in Figures 3.3b and 3.4b. In compiling the mass balances in this study, organic compound concentrations are estimated by multiplying organic carbon concentrations by a factor of 1.4 to account for the mass of H, O, N, and S in the organic compounds [71]. Metals are presented at the equivalent mass concentrations of their common oxides. "Residual" concentrations indicate the gravimetrically-determined mass fractions that are not accounted for by identified chemical components. A portion of this unidentified material undoubtedly includes silicate minerals and calcium-containing mineral matter which were not measured by neutron activation analysis in this experiment. An ion balance was constructed on the ionic species present in each of the filter samples. The data

show that ion balances on average close to within ±15% for fine particle samples and within ±21% for TSP samples. The measurements made at Riverside generally show an excess of identified anions over identified cations.

Airborne particle mass concentrations within both trajectory air parcels increase during transport across the air basin, with the highest particle levels present at Riverside. Sulfate ion concentrations of about 5.8 $\mu g\ m^{-3}$ observed upwind of the urban area at Santa Catalina Island do not increase greatly as the Trajectory 1 air parcel passes over the first two urban sites. Even though there is a large amount of fuel combustion in Los Angeles, especially in the Long Beach harbor industrial and petroleum refining area, local sulfur oxide emissions have been driven to very low levels through the use of gaseous fuels and strict controls on industrial processes [86, 87]. Similarly, the sulfate ion concentration does not increase with distance traveled across the basin as the Trajectory 2 air parcel passes over the three urban monitoring sites. This confirms that there are few primary sulfate sources in the area today and that little SO_2 to sulfate conversion occurred in the atmosphere during these experiments. Sodium concentrations within both trajectory air parcels decline slightly while traveling inland from the coast, an indication that sea salt is the only significant sodium source.

Mineral dust (TSP crustal metal oxides), elemental carbon, and organic compound concentrations increase in the Trajectory 1 air parcel during transport across the air basin. The increases are modest between Long Beach and Fullerton, and much larger between Fullerton and Riverside, reflecting the longer travel times and greater emissions between Fullerton and Riverside and the generally drier and dustier soil conditions in the Riverside area when compared to the near coastal plain. Most dramatically, ammonium plus nitrate concentrations in the fine particle fraction of the aerosol reached $42.0 \pm 3.7 \mu g\ m^{-3}$ at Riverside on September 24, which is over 15 times higher than the fine particle ammonium plus nitrate concentrations measured in Fullerton the day before. The high ammonium and nitrate concentrations at the end of Trajectory 1 *in Riverside* are accompanied by $12.6 \pm 4.1\ \mu g\ m^{-3}$ of fine particle organic compounds, yielding

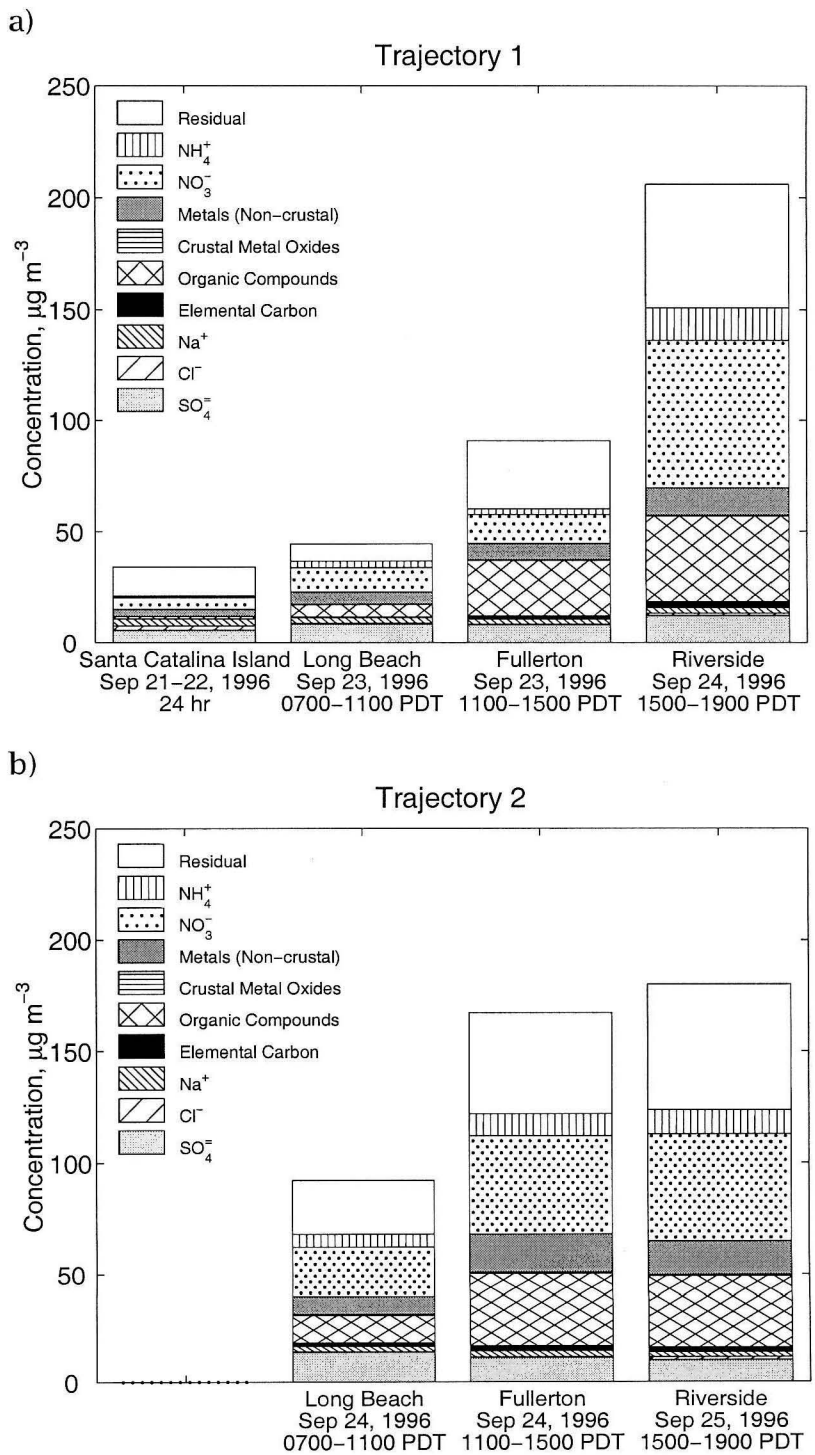

Figure 3.3: a) Total suspended particulate concentrations and chemical compositions along Trajectory 1, September 21–24, 1996, and b) along Trajectory 2, September 24–25, 1996.

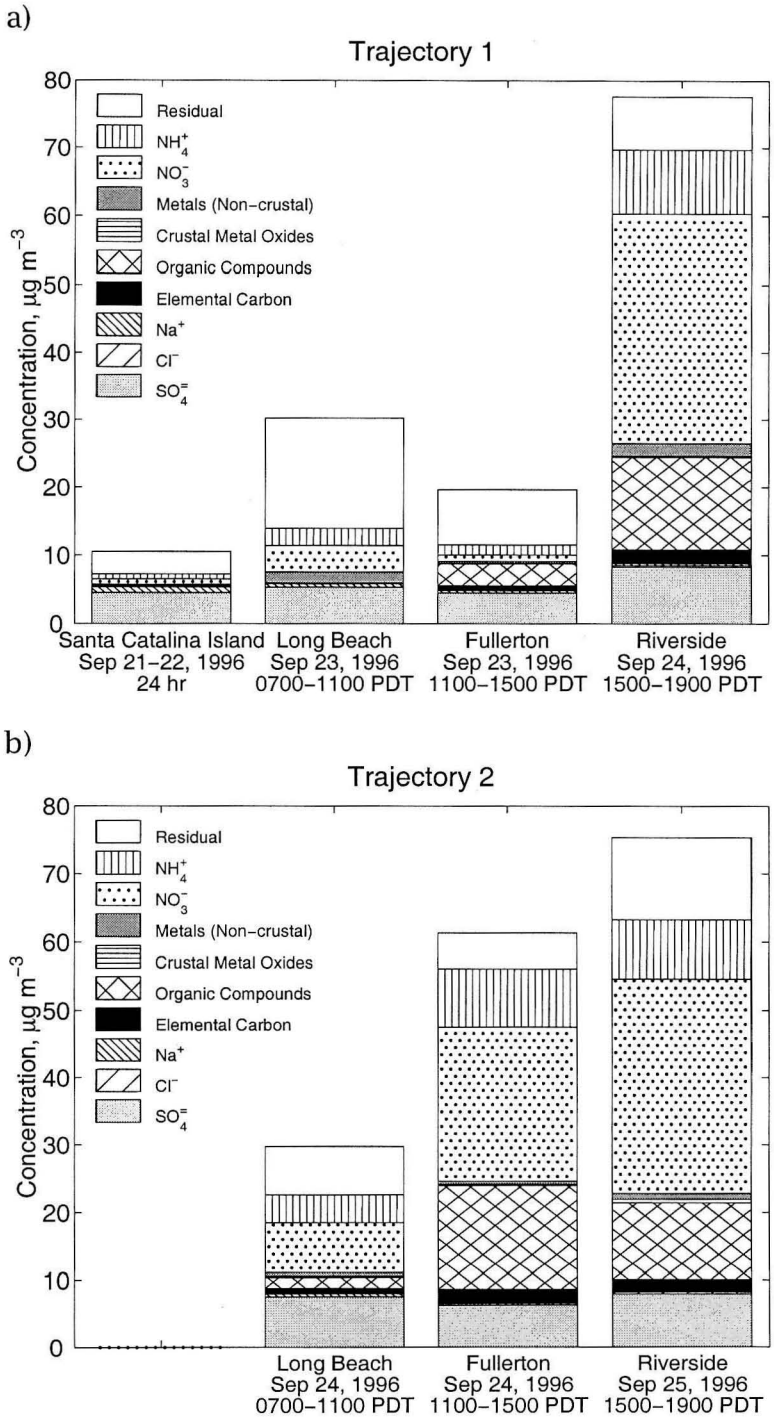

Figure 3.4: Fine particle matter ($D_a < 1.8\ \mu g\ m^{-3}$) concentrations and chemical compositions a) along Trajectory 1, September 21–24, 1996, and b) along Trajectory 2, September 24–25, 1996.

overall fine particle concentrations of 77.6±5.8 $\mu g\ m^{-3}$. TSP concentrations exceeded 200 $\mu g\ m^{-3}$ at Riverside at the end of air parcel Trajectory 1.

In contrast to events that occurred the previous day along Trajectory 1, mineral dust, organic compounds, and particulate ammonium plus nitrate concentrations within the Trajectory 2 air parcel increased significantly during transit between Long Beach and Fullerton. The largest part of the mass increase occurred due to ammonium nitrate production. Fine particle ammonium and nitrate increased by nearly a factor of three between Long Beach and Fullerton on September 24. The nitrogen balance in Figure 3.2 shows an earlier conversion of NO to NO_2 during the Trajectory 2 event when compared to the Trajectory 1 event, which may be responsible for the more rapid production of aerosol nitrate along Trajectory 2. Production of ammonium nitrate during travel between Long Beach and Fullerton requires ammonia emissions into the air parcel. Small but numerous ammonia sources exist on the western side of the air basin [10, 20, 21, 39], including recently documented emissions from motor vehicle traffic [88]. The fine particle ammonium and nitrate concentrations within the Trajectory 2 air mass continue to increase across the basin, reaching 40.5±3.5 $\mu g\ m^{-3}$ at Riverside on September 25, which accounts for more than half of the overall fine particle concentration of 75.3±4.8 $\mu g\ m^{-3}$ at the end of Trajectory 2.

3.4.3 Size-Segregated Fine Particulate Matter Along Air Parcel Trajectories

The size-dependent chemical composition of the fine fraction of the aerosol during each intensive sampling period was determined through analysis of cascade impactor samples. The size-segregated chemical compositions during the four observations taken along the Trajectory 1 air parcel path of September 21–24, 1996, are shown in Figure 3.5; the size-segregated chemical compositions of the samples taken along the Trajectory 2 air parcel path of September 24–25, 1996, are shown in Figure 3.6. Comparison of fine particle filter samples to the sum-

mation of the impactor stages shows agreement on average to within ±10% for EC, $SO_4^=$, and NH_4^+, within ±15% for NO_3^-, and within ±25% for organic carbon. The impactor samples are higher than the filters for EC and sulfate and lower than the filters for organic carbon and the more volatile NH_4^+ and NO_3^-, thus suggesting some NH_4NO_3 evaporation from the impactors. Generally, the integrated impactor results and the fine filter results for a single sampling event are statistically indistinguishable from each other, given the analytical uncertainties.

The Trajectory 1 air parcel shows a large increase in aerosol mass concentration and a shift in the particle size distribution to larger sizes during transport from Fullerton to Riverside. This can occur due to preferential growth of secondary aerosol ammonium nitrate on the hygroscopic non-sea-salt background aerosol particles that are present initially with a peak concentration at the larger end of the accumulation mode [89]. Changes in particle size within the Trajectory 2 air parcel are explained in detail by Kleeman, et al. [10, 89].

Chemical differences between the particles at Long Beach versus Santa Catalina Island include an increase in organic carbon, elemental carbon, and aerosol nitrate in submicron-size particles at Long Beach. The Long Beach aerosol also shows increases in such trace elements as Zn, Al, and Fe when compared to Santa Catalina Island. Several other observations can be made which show evidence of chemical transformations occurring in the course of transport across the air basin. The Na concentration and size distribution is very similar at both Santa Catalina Island and Long Beach, which would be expected since the primary source of Na at both locations is the same (i.e., sea salt). Aerosol chloride concentrations at Long Beach on September 23 are much lower than at Santa Catalina Island, and the majority of the aerosol NO_3^- at Long Beach is seen in Figure 3.5b to be associated with the largest impactor bin that also contains the bulk of the aerosol Na. All of this is consistent with air quality models that predict Cl^- displacement by NO_3^- due to atmospheric chemical reaction in the particle phase, as has been confirmed previously by analysis of single particle composition data taken during this experiment at Long Beach [22]. If HNO_3 reacts with

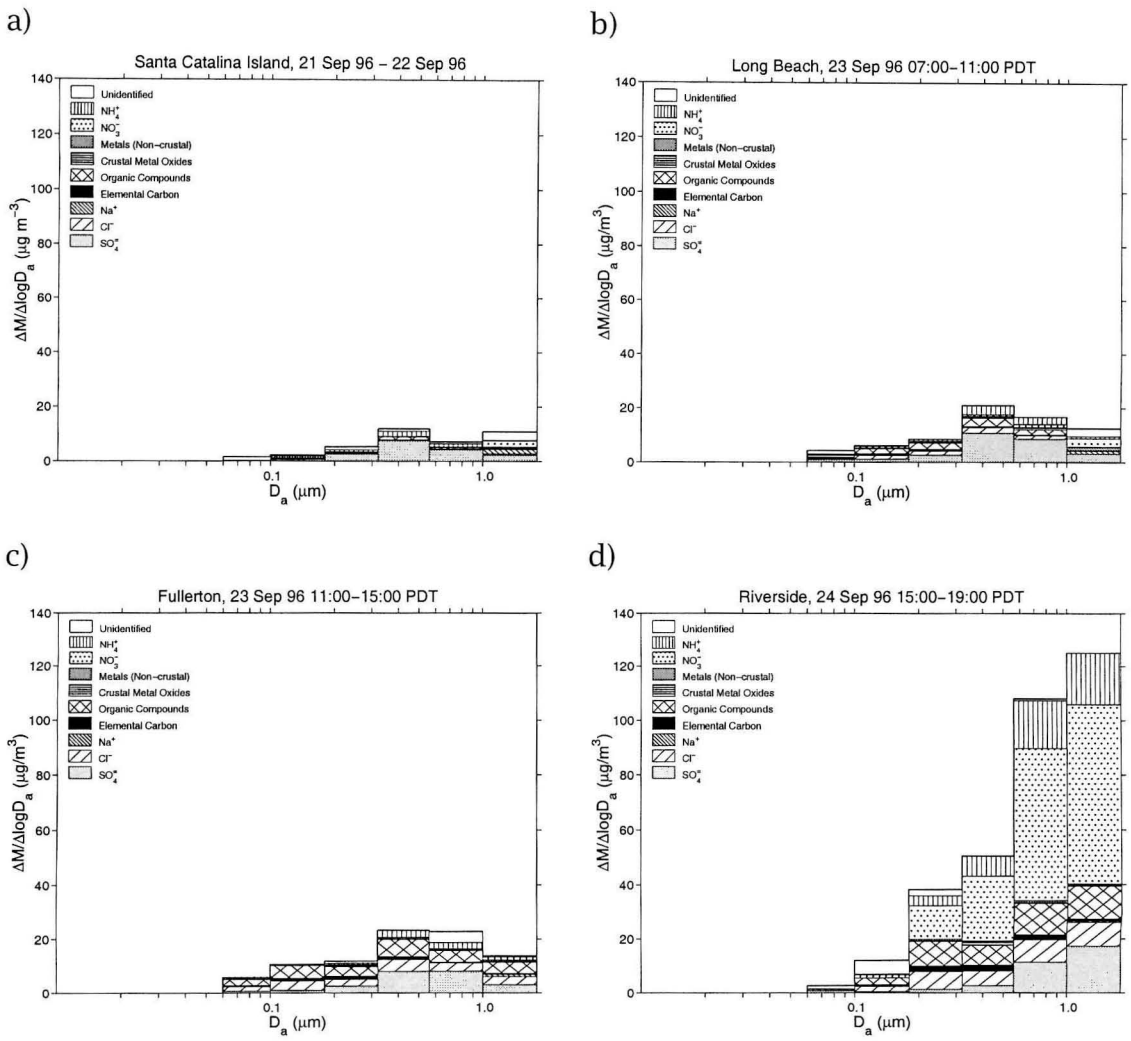

Figure 3.5: Size-dependent chemical compositions along Trajectory 1, September 21–24, 1996. a) Santa Catalina Island, September 21–22, 1996, b) Long Beach, September 23, 1996, 0700–1100 hours PDT, c) Fullerton, September 23, 1996, 1100–1500 hours PDT, d) Riverside, September 24, 1996, 1500–1900 hours PDT. Particle sizes are given as aerodynamic diameters.

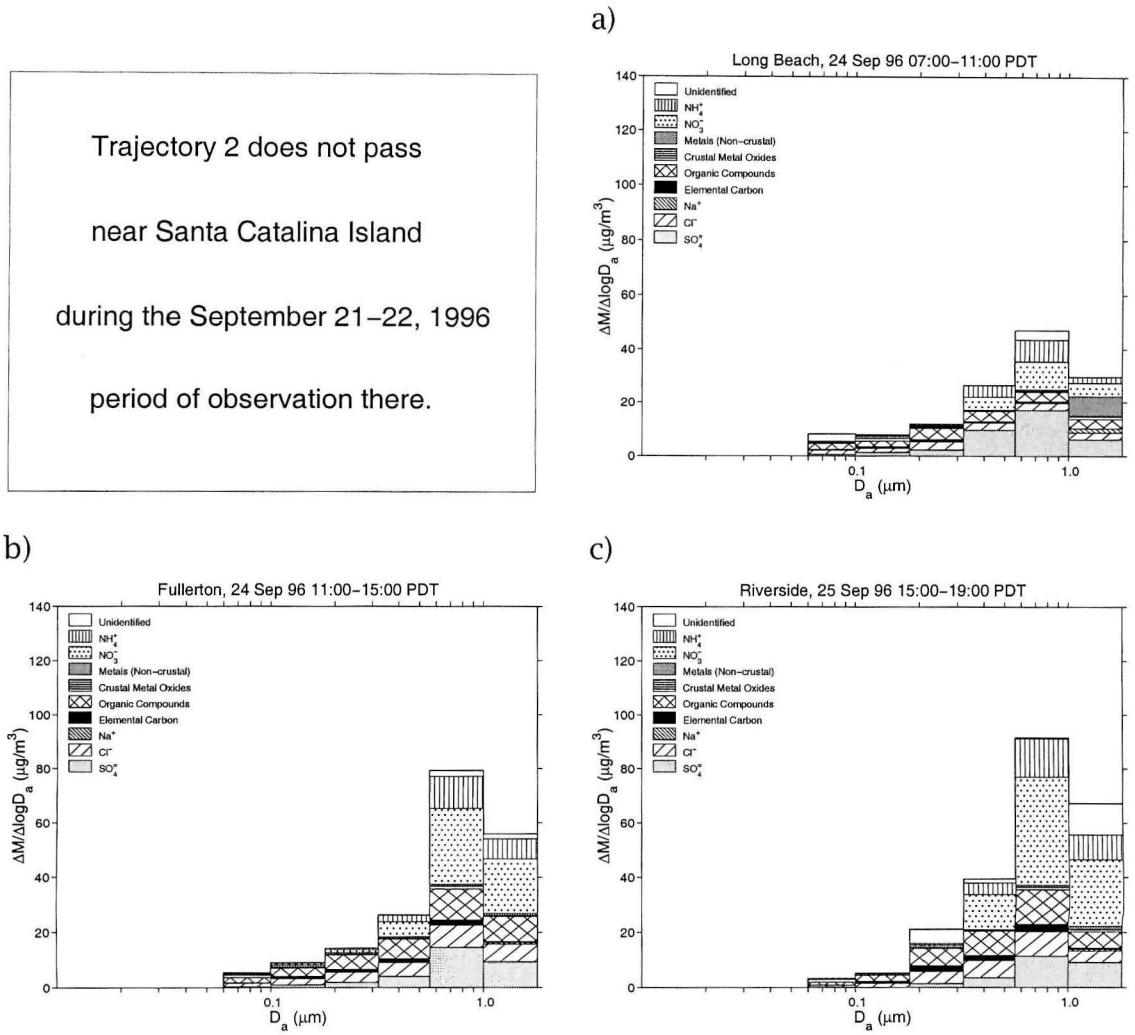

Figure 3.6: Size-dependent chemical compositions along Trajectory 2, September 24–25, 1996. a) Long Beach, September 24, 1996, 0700–1100 hours PDT, b) Fullerton, September 24, 1996, 1100–1500 hours PDT, c) Riverside, September 25, 1996, 1500–1900 hours PDT. Particle sizes are given as aerodynamic diameters.

NaCl, then HCl is liberated from the particle phase and accumulates in the gas phase [90]. Though aerosol-phase Cl^- virtually disappears from the air parcel by the time that it is sampled in Fullerton, aerosol Cl^- concentrations comparable to those seen at Santa Catalina Island are observed further along the trajectory in Riverside. (Cl^- concentrations are of a scale too small to be seen in Figures 3.5 and 3.6.) The renewed presence of Cl^- in aerosol form suggests that elevated levels of NH_3(g) in Riverside (see Figure 3.2) may react with high concentrations of gaseous HCl to produce particulate NH_4Cl [90]. The equilibrium dissociation constant for ammonium chloride is very sensitive to temperature and relative humidity. Over the range of temperature and relative humidity conditions measured during the intensive sampling period on September 24 at Riverside, 24°C and 61% RH to 35°C and 33% RH, the concentration product $[HCl][NH_3]$ at equilibrium with solid phase ammonium chloride falls in the approximate range 56–725 ppb^2, according to the data of Pio and Harrison [91]. Over the range of temperature and relative humidity conditions measured during the intensive sampling period on September 25 at Riverside, 21.5°C and 67.5% RH to 32°C and 37.5% RH, the equilibrium concentration product $[HCl][NH_3]$ falls in the range 31–368 ppb^2.

HCl was not measured in this study; NH_3 was measured with 4-h time resolution during the intensive sampling period. Measured NH_3 concentrations on the two days indicate that for solid-phase NH_4Cl to be in equilibrium with gas-phase concentrations at some time within the intensive sampling period, HCl concentrations would need to reach at minimum about 1.17 ppb and 0.96 ppb on September 24 and 25, respectively. Measurements in Riverside (Rubidoux) in September and October of 1986 found daily average HCl concentrations of 0.25–1.0 ppb [90], suggesting that conditions necessary for the presence of some solid phase NH_4Cl in equilibrium with gas phase NH_3 and HCl could reasonably have been present during the intensive sampling periods of September 24 and 25.

3.4.4 Evolution Along Air Parcel Trajectories at the Single-Particle Level

The aerosol time-of-flight mass spectrometry (ATOFMS) instruments operated continuously in positive ion mode at the Long Beach and Riverside sampling sites provide measurements of the chemical composition and size of individual aerosol particles at the beginning and end of the two air parcel trajectories studied here. At the time this study was carried out, the ATOFMS instruments could produce either a positive ion spectrum or negative ion spectrum for each particle hit by the mass spectrometry ablation laser. The choice was made to collect positive ion data throughout this study, and so the negative ion markers for sulfate ion species were not available. Modifications to the transportable ATOFMS instruments since the close of this study have added dual ion detection capability, and future studies will have both a positive ion spectrum and negative ion spectrum for each hit particle (see Chapters 4 and 5).

The mass spectra of the individual particles analyzed during the 4-h impactor sampling periods at the start and end of each trajectory were gathered together and compared to describe the changes that occur at the single particle level as air masses move across the air basin. Figure 3.7 illustrates the type of comparisons that can be made at the single particle level. Figure 3.7a shows the mass spectrum of a clean sea salt particle of 1.74 μm aerodynamic diameter sampled at Long Beach on the morning of the first day of Trajectory 1. The spectrum is characterized by large sodium (Na^+, NaO^+, and Na_2OH^+) peaks with the strong presence of that sodium as NaCl (see Na_2Cl^+ fragment peaks) and minor amounts of sodium nitrate ($NaNO_3^+$ marker fragment) and sodium sulfate ($Na_3SO_4^+$ fragment). Calcium and potassium also are present in sea salt and are easily seen in the mass spectrum of the clean sea salt particle. Figure 3.7b illustrates the changes that such a particle undergoes during transport from Long Beach to Riverside over approximately a one and a half day period. The dirty sea salt particle at Riverside is still identified by its very large sodium marker content. This aged sea salt particle

has been completely stripped of its chloride content by atmospheric chemical reactions involving the oxides of nitrogen to form sodium nitrate (see loss of mass 81 and 83 Na_2Cl^+ peaks accompanied by increase in the magnitude of the $Na_2NO_3^+$ peak). This can occur by the heterogeneous reaction of sea salt with vapor phase HNO_3 to form particulate $NaNO_3$ while releasing HCl gas [22, 90]; there are a number of other routes by which such conversion can occur as well [92–95]. Further, the "dirty" sea salt particle arriving at Riverside has accumulated gas-to-particle conversion products in the form of ammonium (NH_4^+) and nitrate (NO^+ marker) additions plus a coating of organic carbon compounds (C^+ marker, as well as yet unidentified mass fragments at the locations of the arrows in Figure 7b that are often seen in the mass spectra of organic aerosol particles). The dirty sea salt particle shows almost exactly the combination of species predicted by Kleeman and Cass [10] through air quality modeling calculations for an aged sea salt particle of 1.61 μm diameter transported across the Los Angeles Basin and arriving at Claremont, California, in August of 1987 (sodium with lesser amounts of ammonium combined with nitrate; complete chloride removal; traces of organics and sulfates, plus other elements, e.g., K, Ca, etc.).

Changes in the aerosol population as air masses are transported across the Los Angeles basin can be summarized based on analysis of the thousands of separate particles sampled by the ATOFMS systems during the 4-h periods at the start (Long Beach) and at the end (Riverside) of Trajectories 1 and 2. Statistically large numbers of particles were sampled over the size range 0.32–3.5 μm aerodynamic diameter at Riverside and over the range 0.56–3.5 μm at Long Beach. Particles at the larger end of this size range are most easily detected and sampled by the ATOFMS systems. In order to correct for this decline in particle detection efficiency with decreasing particle size, the counting efficiencies of the ATOFMS systems were determined by comparison with simultaneous measurements of the atmospheric particle number distribution and mass distribution made during this experiment by laser optical particle counters and micro-orifice impactors as described by Allen et al. [58]. Using the resulting detection efficiency curves, each

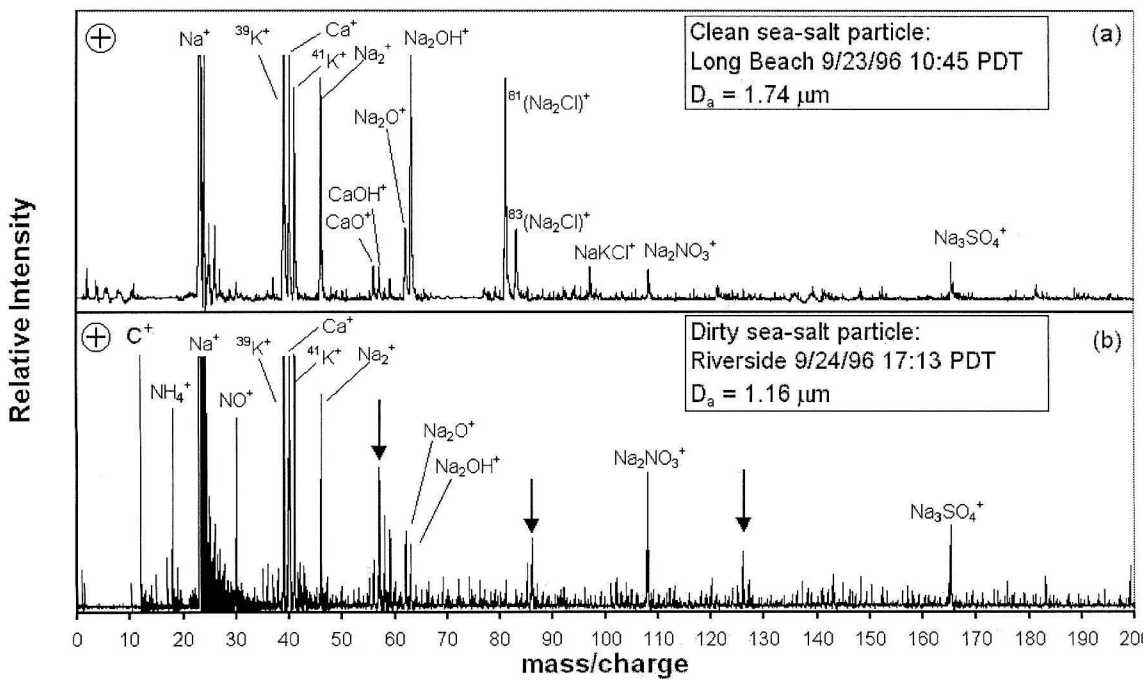

Figure 3.7: a) Representative ATOFMS instrument spectrum of a "clean" sea salt particle observed in Long Beach. b) Representative ATOFMS instrument spectrum of a "dirty" sea salt particle arriving in Riverside that has been transformed by gas-to-particle conversion processes.

particle for which a mass spectrum was obtained was "duplicated" in proportion to the degree to which particles of that size are undercounted by the ATOFMS systems. This process results in a collection of particles present at the start and end of each trajectory whose number concentration as a function of size matches that of the atmosphere at the time of sampling; each particle has a chemical composition represented by its mass spectrum.

The major chemical substances present in each particle were then summarized based on the presence of key indicator ions in the ATOFMS mass spectra. These key indicator ions are mass 18 for ammonium (detected as NH_4^+); mass between 22 and 23.5 for sodium (detected as Na^+); mass 30 (NO^+) or mass 108 ($Na_2NO_3^+$) for nitrate ion; mass 12 (C^+), 36 (C_3^+), or 37 (C_3H^+) for carbon; and masses 27 (Al^+) and 56 (Fe^+/CaO^+) or mass 7 (Li^+) as indicative of mineral dust particles. Occasionally a particle that produces H^+ counts (between masses 0.5 and 2.5) that go off scale (greater than 10,000 arbitrary units) is identified as a dust particle based on similar and unique behavior seen during source tests applied to local soil samples. A peak that corresponds to one of these key ions is judged to be present in the mass spectrum of a particle if peak height and peak area equal or exceed 10 and 15 arbitrary units respectively for the laboratory-based instrument at Riverside, or 15 and 30 arbitrary units respectively for the transportable instrument at Long Beach (the instrument designs are slightly different; these criteria provide comparable detection thresholds). To exclude consideration of trace amounts of a substance, the key ions are considered when classifying a particle only if their peak area exceeds 0.5% of the total peak area of the particle's mass spectrum. When the target masses listed above give unusually large signal, the base area of the peak for masses 23, 27, and 56 is broadened to the ranges 22–24, 25–29, and 54–58 mass units as long as the peak area is greater than or equal to 2500 arbitrary units. The range for mass 7 is broadened to 5–9 mass units as long as the peak area is greater than or equal to 200 arbitrary units. Since a positive ion indicative of the sulfate content of ammonium sulfate particles is not available, sulfate-containing aerosols cannot be enumerated in this

study. Particle spectra were classified according to the presence or absence of only these five key indicator ion groups; particles may contain other substances which were not specifically considered in this analysis. Particles were separated into particle size intervals that correspond to those of the impactor bins, and all particles having the same combination of key indicator ions within each size interval were grouped together. The results of this grouping of particles by type and size are pictured in Figure 3.8.

Figure 3.8 provides a color-coded display that shows for the first time a counting efficiency-corrected description of the extent of external mixing of major chemical substances in the atmospheric aerosol as a function of particle size. In addition, the figure demonstrates how the particle population changes due to dilution, deposition, emissions of new particles, and gas-to-particle conversion processes as the same air parcel moves across the Los Angeles urban area. Each of the squares in Figure 3.8 contains 100 colored dots, and each dot represents 1% of the number of particles in the atmosphere within the indicated size range. A dot having only a single color represents a comparatively simple particle type containing predominantly one of the key marker substances: blue for sodium-containing, red for nitrate-containing, orange for carbon-containing, or gray for mineral dust-containing particles. A dot with stripes of more than one color represents a group of more complex particles whose spectra contain more than one of the key marker substances. The color coding is a qualitative indicator of the composition of these complex particles; no statement is made about the mass fraction of each substance within the particles of that group. In particular, since the sensitivity of the ATOFMS for Na^+ is 71 times greater than for NH_4^+ [76], it is possible for a particle that contains mostly sea salt with a small quantity of ammonium nitrate to produce a mass spectrum with such a small NH_4^+ peak that it would be recorded as a sodium-only particle. Therefore the reader should not interpret the solid blue and orange dots as denoting only pure sea salt or carbon particles, respectively, but rather particles *that produced* spectra dominated by sodium and carbon peaks; there could be small quantities of

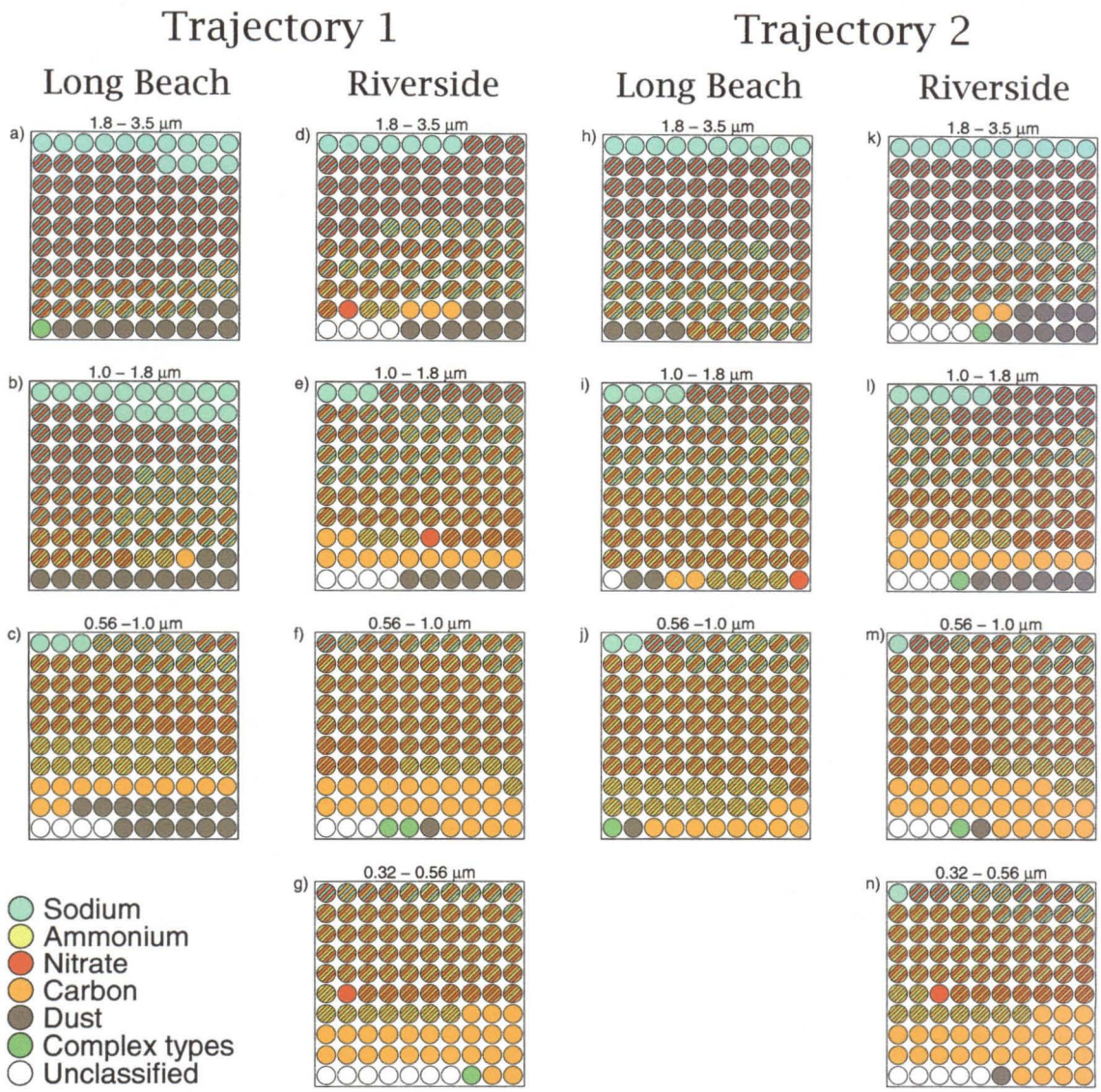

Figure 3.8: The chemical compositions of size-segregated particle populations at the start and end of Trajectories 1 and 2 as measured by the ATOFMS instruments. Each dot represents one percent of the particle population within the indicated aerodynamic particle diameter range. a–c) Particle populations at the beginning of Trajectory 1, Long Beach, September 23, 1996, 0700–1100 PDT. d–g) Particle populations at the end of Trajectory 1, Riverside, September 24, 1996, 1500–1900 PDT. h–j) Particle populations at the beginning of Trajectory 2, Long Beach, September 24, 1996, 0700–1100 PDT. k–n) Particle populations at the end of Trajectory 2, Riverside, September 25, 1996, 1500–1900 PDT.

gas-to-particle conversion products present on those particles at concentrations below the quantification limits used here. A blue and red striped dot represents a group of sodium nitrate-containing particles (e.g., wholly or partly reacted sea salt aerosol). A yellow and red striped dot represents a population of ammonium nitrate-containing particles. Dots that contain only orange (carbon) and yellow (ammonium) stripes could well indicate a group of particles with both carbon and ammonium sulfate, as the sulfate content of the particle would not be detected in this experiment. All combinations of key indicator ions that are present in greater than 0.5% of the particles in a given size range (a value which rounds up to a whole dot) are shown by appropriate stripe patterns in Figure 3.8. Particle types that individually account for less than 0.5% of the particle population in a given size range are grouped together and represented by a green dot or dots.

Some atmospheric particles are simple representatives of the direct emissions from a primary particle source type. Carbon-containing particles are emitted from many primary pollution sources, and an unreacted sea salt particle would be classified solely as a sodium-containing particle under this classification scheme. As these primary particle types interact with gas-phase air pollutants during transport across the air basin, the primary particles begin to incorporate secondary reaction products and become more complex. For example, sea salt particles can react with the oxides of nitrogen in the atmosphere to produce sodium nitrate aerosol which would be described as sodium-containing and nitrate-containing particles (blue and red striped dot). Primary carbon particles could acquire a coating of secondary ammonium nitrate, becoming a mixed carbon/ammonium/nitrate aerosol (orange, yellow, and red striped dot).

The left column of Figure 3.8 represents the overall population of particles sampled in the morning of September 23 at Long Beach at the start of Trajectory 1. In the largest particle size range examined, 14% of the particles present at Long Beach produced spectra with quantifiable amounts of sodium or sodium chloride markers (blue only) but not sodium nitrate, indicating largely unreacted sea salt particles. Sodium nitrate was present in most of the remaining particles

sampled in the largest size range studied, indicating that a partial conversion of sodium chloride to sodium nitrate was underway at this time at Long Beach. Trajectory analysis shows that the air parcel sampled at Long Beach during the period 0700–1100 PDT on September 23 had been over land or over the very busy Long Beach Harbor area since about 1600 PDT on September 22 (see Figure 3.1a). Carbon, ammonium, and mineral dust also are detected in a small percentage of the 1.8–3.5 μm diameter particles at Long Beach.

Moving toward the smallest particles examined at Long Beach in the 0.56–1.0 μm aerodynamic diameter range, the abundance of largely unreacted sodium-containing particles falls to 3% and the carbon-containing particle population increases dramatically. Seventy-nine percent of these smaller particles produce spectra containing at least some organic and/or elemental carbon markers, possibly due to fresh primary emissions from combustion sources in Long Beach. Most of the remaining submicron particles at Long Beach contain spectra showing mixtures of carbon and other substances, including carbon with reacted or unreacted marine aerosol (12%) and carbon with ammonium nitrate (34%). Although we believe that ammonium sulfate particles are present in this air mass on the basis of impactor sampling at Santa Catalina Island and Long Beach, these particles are not quantified in Figure 3.8. Negative ion mass spectra contain markers for ammonium sulfate that could be used in future studies; however, the data set for the present experiment contained only positive ion mass spectra. Ammonium ion could be detected, but no positive ion markers for sulfate were available.

As was shown in Figures 3.3, 3.4, and 3.5, there is a substantial increase in suspended particle mass between Long Beach and Riverside that occurs due to the emission of new particles into the air parcel as the air is transported across the basin and as atmospheric reaction products are added to individual particles. By the time that Trajectory 1 reaches Riverside on the afternoon of September 24, the EAA, OPC, and ATOFMS data all indicate that the aerosol population has increased in number. The character of the particles has been greatly transformed,

as can be seen by comparing the two left columns of Figure 3.8. During transport from Long Beach to Riverside, the percentage of the particles in the largest sizes that contain sodium has fallen, and the number of complex particles containing more than two marker substances has increased. In the submicron particle sizes, transport from Long Beach to Riverside is accompanied by accumulation of complex transformed particles that contain ammonium, nitrate, and either primary or secondary carbonaceous material in amounts exceeding the quantification limits used here.

The right two columns of Figure 3.8 document the transformation of the particle population along Trajectory 2 over the period from the morning of September 24 to the afternoon of September 25. As was noted earlier when discussing the filter and impactor data, the aerosol observed at Long Beach on September 24 shows a greater influence from urban emissions sources than the aerosol observed on the morning of September 23. The ATOFMS data show this as well, indicating that the aerosol as Trajectory 2 passed over Long Beach included more carbon-containing particles, more ammonium-containing particles, and greater conversion of NaCl to $NaNO_3$ than was the case as Trajectory 1 passed over Long Beach. For that reason, the relative composition of the aerosol population changes less along Trajectory 2 than along Trajectory 1 as the aerosol is advected from Long Beach to Riverside.

Chapter 4

Vehicle-Oriented Trajectory Study

4.1 Introduction

Motor vehicle exhaust emissions and their physical and chemical behavior in the atmosphere need to be clearly understood in order to judge the effectiveness of potential vehicle-related air quality control programs. Among the more complex issues that must be addressed is determination of the effect of motor vehicle exhaust on airborne fine particle concentrations. Motor vehicles contribute both primary particles that are emitted in the particle phase directly from automobile and truck tailpipes, as well as reactive gases such as NO, SO_2, ammonia and hydrocarbon vapors that can react chemically in the atmosphere to form secondary aerosols.

In late August of 1997, a field experiment was conducted in conjunction with the 1997 Southern California Ozone Study [96-98] in which a network of three airborne particle observatories was established, employing advanced instrumentation for determination of the size and chemical composition distribution of atmospheric particles. At each air monitoring site, measurements were made of the particle size distribution, bulk fine particle and PM_{10} chemical composition, chemical composition segregated into narrow particle size intervals, and single-

particle chemical composition. Two of these air monitoring station locations were chosen along a seasonally typical wind trajectory passing over downtown Los Angeles and extending downwind to Azusa, California, with the intent of first observing air parcels in an area dominated by high motor vehicle traffic density, and subsequently observing the same air parcels after they had been transported downwind. This sampling scheme was designed to provide data on the evolution over time of the size and chemical composition of ambient aerosols at the bulk, size-segregated, and single-particle levels as those particles are potentially altered by gas-to-particle conversion processes and affected by continuing emissions, dilution, and dry deposition.

Several studies of particle evolution using multiple observation points along a single air parcel trajectory have been conducted previously in the Los Angeles area. In a 1982 field study, gas- and particle-phase nitrogen species were sampled from a single air parcel which passed over or near three monitoring sites in succession: Long Beach, Anaheim, and Rubidoux, California, providing insight into the process of aerosol nitrate formation and the interrelationship between gas phase HNO_3 and NH_3 versus particulate NH_4NO_3 [13]. Measurements made at that time showed that the aerosol nitrate behaved as would be expected from analyses based on thermodynamic equilibrium between the gas and particle phases [40], and verified the presence of a large ammonia source located in the agricultural and dairy area between Anaheim and Rubidoux leading to large aerosol nitrate concentrations in the Riverside (Rubidoux) area. In 1996, a similarly designed field study was conducted using more advanced instrumentation. A battery of aerosol sampling instruments similar to those employed in the present study, including samplers for fine and total suspended particulate matter chemical composition, size-segregated particulate matter chemical composition, and single-particle size and composition measurements, were used to obtain information about the evolution of the particle population in the presence of significant aerosol nitrate formation and continuing emissions [74, 77] (see Chapters 2 and 3). Two air parcel trajectories were identified which passed

over or near three or four air monitoring stations along the Santa Catalina Island - Long Beach - Fullerton - Riverside pollutant transport corridor [74]. It was shown that the relatively fresh aerosol at Long Beach consisted largely of sea salt particles, primary carbon particles and background sulfate particles. Over a one and a half day transport period from Long Beach to Riverside, sea salt particles were transformed to sodium nitrate while the population of carbon-containing particles which consisted mostly of organic and elemental carbon at Long Beach was transformed into a population of very complex particles containing aerosol carbon as well as ammonium and nitrate ion at the single-particle level. The purpose of the present study is to apply the method of trajectory-oriented field experiments to the problem of observing air parcels that are heavily influenced by primary particle emissions from motor vehicles.

The purpose of this chapter is to document the dynamic behavior of the aerosol within the motor vehicle traffic-oriented air parcels sampled during the present experiment. These data can later be used to evaluate the accuracy of the predictions of trajectory-based and grid-based air quality models which represent the atmospheric particle population as an externally mixed collection of single particles [89]. In addition, the present data can be used to continue ongoing work in which the particle counting efficiency and chemical sensitivities of the aerosol time-of-flight mass spectrometry instruments used to measure single particle size and composition are evaluated under field sampling conditions by comparison against simultaneous measurements taken using more conventional sampling and analysis techniques [58].

4.2 Experimental Methods

4.2.1 Sample Collection and Analysis

Three urban air monitoring stations were established in the Los Angeles metropolitan area to observe ambient particulate matter concentrations in the presence of

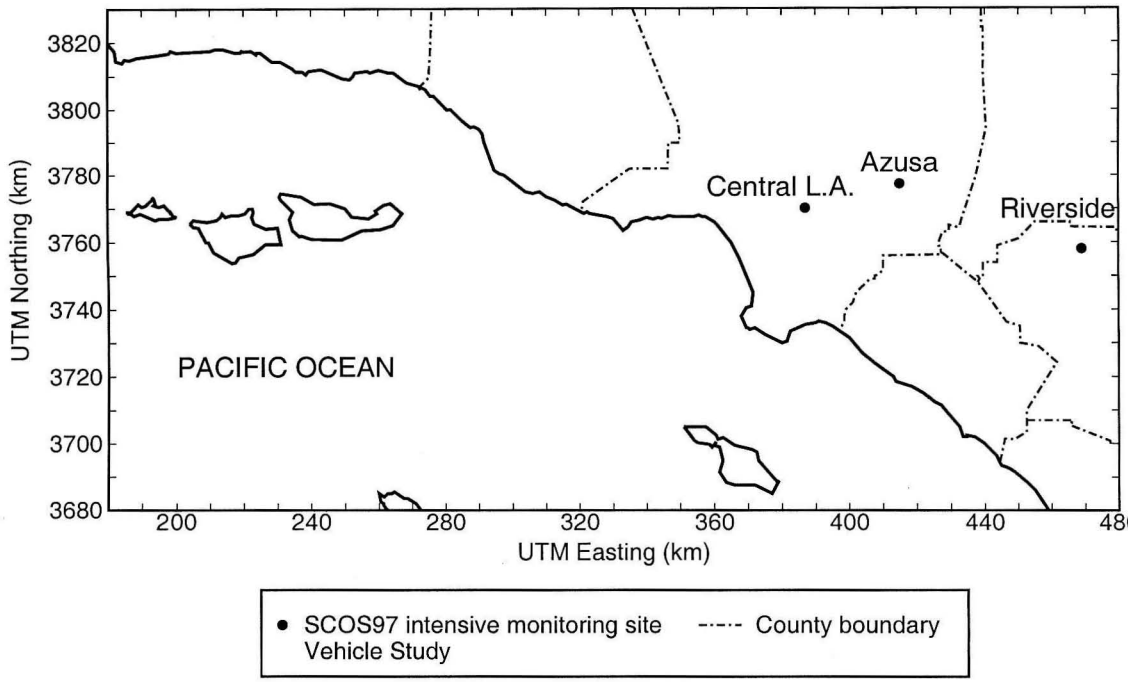

Figure 4.1: South Coast Air Basin and Vehicle Study sampling site locations.

atmospheric transport and transformation. These sites were located in Central Los Angeles, Azusa, and Riverside (see Figure 4.1). Two of the sampling sites were chosen to focus on the transport of motor vehicle-derived aerosol: Central Los Angles because of its proximity to the highest traffic densities in the South Coast Air Basin (SoCAB), and Azusa because it is often located directly downwind of Central Los Angeles. The Riverside site was chosen primarily because one of the three existing aerosol time-of-flight mass spectrometry (ATOFMS) instruments used to measure single particle size and chemical composition is permanently located there.

Sampling was conducted over two 48-h periods on August 21–23, 1997, and August 27–29, 1997. Fine particle and PM_{10} samples for mass and chemical composition determination were collected sequentially on a 5-sample per day schedule, and a pair of micro-orifice impactors (MOIs) was operated at each site for one or two of these time periods each day. Times of operation for the filter samplers and impactors are shown in Figure 4.2 for both 48-h events.

An electrical aerosol analyzer (EAA, TSI Inc., model 3030) was used at each site

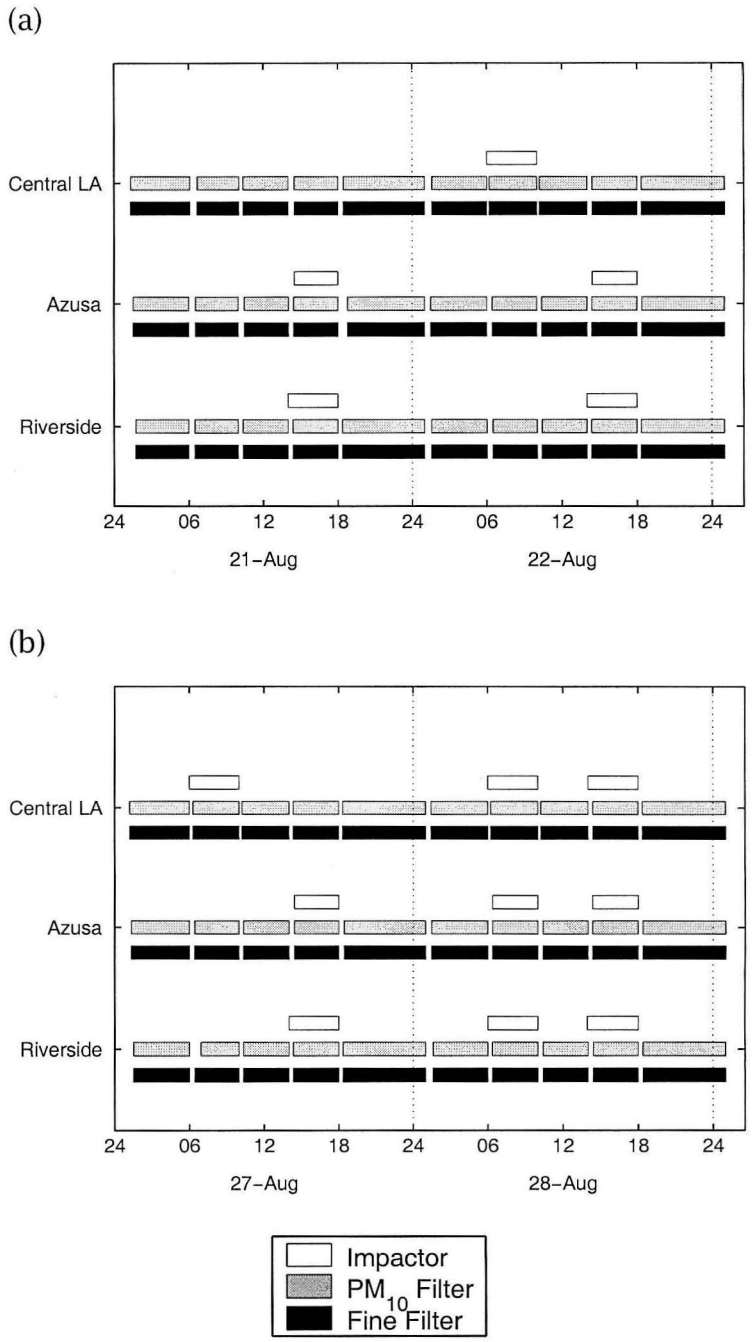

Figure 4.2: Times of operation (in PDT) of impactors and filter samplers at each site during the 48-h periods of (a) August 21-23, 1997, and (b) August 27-29, 1997.

to continuously measure particle number concentrations in the particle physical diameter, D_p, range $0.03 < D_p < 0.23$ μm. The particle number distribution over the EAA's size range was acquired once every 4–7 minutes.

Laser optical particle counters (OPC, Particle Measuring Systems, model ASASP-X at the Central Los Angeles and Azusa sites; Particle Measuring Systems, model LAS-X, at Riverside) were used to extend size distribution measurements to larger particle sizes. The OPCs at the Central Los Angeles and Azusa sites recorded particle number distributions over the size range $0.23 < D_p < 2.55$ μm in 22 channels every 5 seconds. The OPC at the Riverside site recorded particle number distributions over the size range $0.23 < D_p < 3.5$ μm in 12 channels every 21 seconds. Size distributions from the OPCs were corrected as suggested by Hering [57] to take into account the difference in the refractive index between the polystyrene latex (PSL) spheres used to calibrate the instruments and typical Los Angeles area atmospheric aerosols.

Three aerosol time-of-flight mass spectrometry (ATOFMS) instruments were used; the Central LA and Azusa sites each had a transportable ATOFMS instrument [28], and a laboratory-bound ATOFMS instrument [27] was operated in Riverside. The ATOFMS instruments operated continuously, collecting number distribution data in the particle aerodynamic diameter, D_a, range $0.2 < D_a < 5$ μm, and obtaining mass spectra for a subset of the sampled particles.

Four filter-based sampling systems were operated at each air monitoring station: one to collect PM_{10} samples ($D_a < 10$ μm) and three to collect fine particle samples ($D_a < 1.9$ μm). The PM_{10} sampler and two of the three fine particle samplers were used to collect consecutive short time average samples for bulk ionic and carbonaceous species and elemental analysis. Five complete sets of filter samples were collected each day according to the following time schedule: 0120–0600, 0620–1000, 1020–1400, 1420–1800, 1820–0100 hours PDT (see Figure 4.2). All times during this study are given in Pacific Daylight Time (PDT). This filter sampling schedule provides relatively fine temporal resolution data for comparison with the continuous ATOFMS data and future air quality model-

ing results. One fine particle sampler at each site operated over 24-h sampling intervals in order to collect enough material for later analysis for individual particulate organic compounds by GC/MS.

The PM_{10} samplers assembled for this study were similar to those deployed by Solomon et al. to collect the PM_{10} database that was used for regulatory purposes in Los Angeles from 1987 to 1995 [72]. The PM_{10} sampler drew air through an EPA-approved low volume PM_{10} inlet [72] and distributed the air between two filter holders (see Figure 4.3), one containing a polytetrafluoroethylene (PTFE) filter (Gelman Sciences, Teflo, 47mm, 1.0 μm pore size) and one containing a quartz fiber filter (Pallflex, 2500 QAO, 47mm). The air flow through each filter was controlled by a critical orifice downstream of the filter. The PTFE filter collected aerosol particles for gravimetric and inorganic species analyses, while the quartz fiber filter collected particles for aerosol carbon and organic species analyses. This sampler also housed an open face filter stack in which gas-phase ammonia was collected on two oxalic acid impregnated glass fiber filters located downstream of a PTFE pre-filter used to remove airborne particles.

In fine particle sampling systems FTQ and FTNN shown in Figure 4.3, ambient air was drawn under a stainless steel rain cap and then through an acid-washed Pyrex glass inlet line at a nominal air flow rate of 28 lpm. The air was then passed through a Teflon-coated AIHL-design cyclone separator [60] which, when operated at flow rate of 28 lpm, removed coarse particles with aerodynamic diameters larger than 1.9 μm (see Figure 4.3). Following the cyclone, the airstream containing only fine particles and gases entered a Teflon-coated sampling manifold where it was split and ducted via Teflon tubing to several low-volume filter holder assemblies arranged in parallel. Fine particles were collected in parallel on two PTFE filters, one quartz fiber filter, one nylon filter, and another nylon filter located downstream of a MgO denuder. Samplers FTQ and FTNN were operated on the 5-sampling period per day schedule described above (see Figure 4.2). Gravimetric mass, ionic species, and trace metals were determined *from the* PTFE filter samples, organic and elemental carbon from the quartz fiber filters, and aerosol

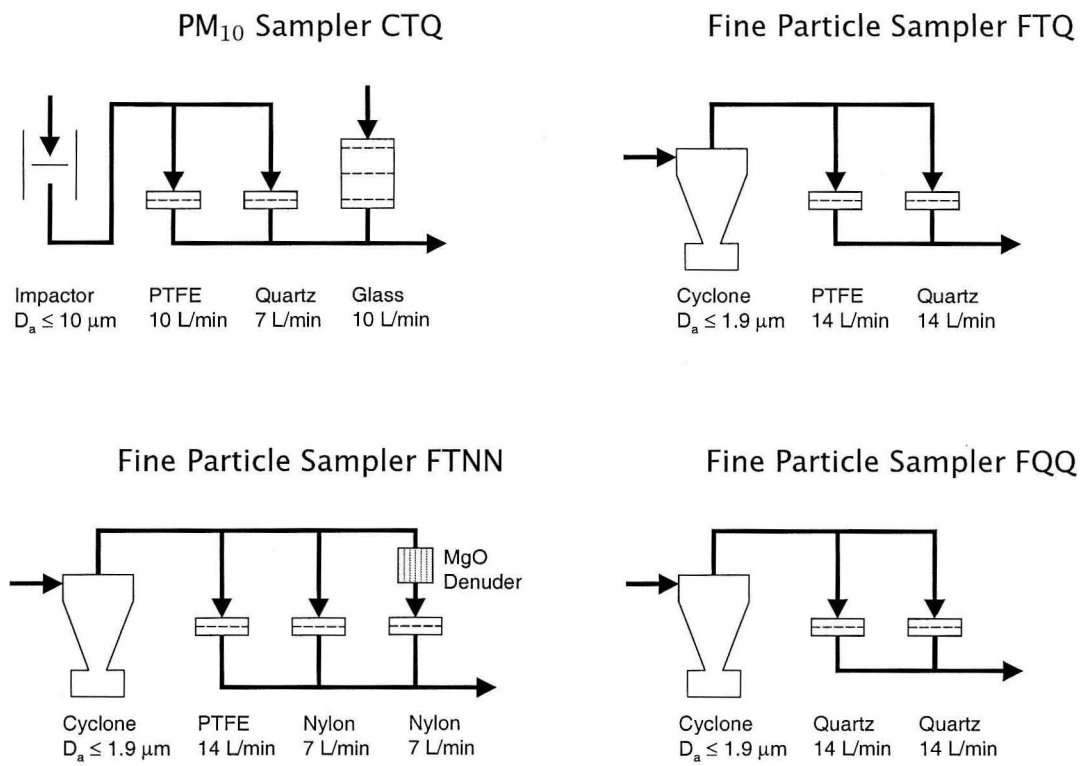

Figure 4.3: Schematic diagram of the particulate matter sampling systems used in this study.

nitrate and HNO_3 were determined by the denuder difference method from the nylon filter samples. Fine particle sampler FQQ shown in Figure 4.3 collected larger samples for organic aerosol determination over 24-hr sampling intervals.

A pair of 10-stage micro-orifice impactors (MOI, MSP Corp., model 110) [59] was operated at each air monitoring site. The impactors collocated at a site were operated simultaneously to measure fine particulate mass and chemical composition as a function of particle size. A cyclone separator [60] was placed upstream of each impactor in order to capture coarse particles ($D_a > 1.8\ \mu m$) that might otherwise enter the impactor and distort the mass distribution measurements by bouncing from their appropriate collection stages. Particles reported here were collected on stages 5–10 of the impactors over the size range $0.056 < D_a < 1.8\ \mu m$. One member of each pair of impactors was loaded with aluminum foil impaction substrates (MSP Corp.), while the other was loaded with PTFE impaction substrates (Gelman Sciences, Teflo, 47mm). No grease or oil was used on the substrates to avoid adding a source of organic contamination.

After sample collection, the PTFE, nylon, and oxalic acid-impregnated filters, and impactor substrates were stored in petri dishes which were then sealed with Teflon tape; quartz fiber filters were stored in petri dishes lined with prebaked aluminum foil and sealed with Teflon tape. All samples were refrigerated until returned from the field, a period not longer than 48 hours, and then frozen at -20°C until sample analysis.

Mass measurements were made gravimetrically before and after sampling on all PTFE filters and all PTFE and aluminum foil impaction substrates, providing the basis for atmospheric fine particle, PM_{10}, and size-distributed mass concentration determinations. Each filter or substrate was weighed at least twice before and twice after sample collection on a Mettler Model M-55-A mechanical microbalance maintained in a temperature- and humidity-controlled environment (22.9±0.3°C and 48±3% RH). Unexposed PTFE filters and substrates were equilibrated in the same controlled conditions for at least 24 hours prior to weighing. PTFE filters and substrates with collected aerosol samples were equilibrated in

the controlled environment for about 4 hours prior to weighing; a shorter equilibration time was used for collected samples to reduce the time that a sample spent at above-freezing temperatures, and so reduce the opportunity for species volatilization. A set of control filters was weighed during each daily weighing session to verify the consistency of the balance calibration between pre- and post-sample collection weighings.

Elemental carbon (EC) and organic carbon (OC) concentrations were determined by thermal-optical analysis [61, 62] of samples collected on quartz fiber filters and aluminum foil impaction substrates. Organic matter concentrations were estimated from measured organic carbon concentrations by multiplying by a factor of 1.4 to account for the additional mass of associated H, O, N, and S present in typical atmospheric organic aerosols [71]. Prior to sample collection, all quartz fiber filters were baked at 550°C in air for 8 hours to lower their carbon blank levels. Aluminum foil substrates were similarly baked at 550°C in air for 48 hours prior to initial weighing and sample collection.

Impactor and PM_{10} samples collected on PTFE substrates or filters were cut in half prior to analysis to allow the use of several chemical analysis methods. Cutting was unnecessary for the fine particle samples due to the existence of redundant samples collected on pairs of PTFE filters. Half of each set of PTFE filters and impaction substrates were extracted, and the extract analyzed using a Dionex Model 2020i ion chromatograph for determination of the atmospheric concentrations of the major ionic species: NO_3^-, $SO_4^=$, and Cl^- [63]. These extracts were analyzed for ammonium ion (NH_4^+) by an indophenol colorimetric procedure [64] using an Alpkem rapid flow analyzer (Model RFA-300). Gas phase ammonia collected on oxalic acid-impregnated glass fiber filters was measured as ammonium ion using the same procedure. Aerosol nitrate and nitric acid samples collected on nylon filters were analyzed using the ion chromatographic process prescribed by Solomon et al. [66].

The remaining half of each set of PTFE samples underwent instrumental neutron activation analysis, from which the bulk concentrations of 39 major and

minor trace elements were determined [65]. The elements measured were Al, As, Au, Ba, Br, Cd, Ce, Cl, Co, Cr, Cs, Eu, Fe, Ga, Hg, In, K, La, Lu, Mg, Mn, Mo, Na, Nd, Rb, Sb, Sc, Se, Sm, Sr, Th, Ti, U, V, Yb, and Zn. Many of these elements are rarely found in the atmospheric aerosol and thus are present at concentrations below detection limits in many samples.

4.2.2 Meteorology

Wind fields over the South Coast Air Basin for each hour of the episodes studied were reconstructed with a 5 km $\times$ 5 km grid resolution using the method of Goodin et al. [68] based on hourly averaged wind speed and direction measurements at 29 meteorological stations maintained by the South Coast Air Quality Management District (SCAQMD). From the wind fields, back trajectories from the sampling sites were calculated, establishing the time and location history of the air parcels arriving at the sampling sites.

Wind patterns were relatively consistent across the two 48-h episodes studied. Air parcels arriving at Central Los Angeles generally approached from the southwest, having crossed the coastline near Hawthorne. Air parcels reaching Azusa generally approached from the southwest as well, setting up the possibility that the same air parcel would pass over both Central Los Angeles and Azusa as planned. Air stagnation at Central Los Angeles occurred daily beginning between 1800 and 2200 PDT in the evening and ending between 1100 and 1200 PDT the following morning. Temperatures at Central Los Angeles ranged between 18.3 and 32.2°C, with relative humidities measured between 31 and 60%. By mid-day at Los Angeles, the sky was generally hazy, though most evenings were clear. On August 22 there was significant cloud cover, but all other sampling days had few clouds. Fog was seen around the Central Los Angeles site in the early morning of August 21. Air stagnation occurred at Azusa beginning between 2000 and 2100 PDT in the evening and ending between 1000 and 1200 PDT the following morning. Temperatures at Azusa were between 18.3 and 35.6°C, and relative

humidities were 24 to 86%. Mornings were generally clear, with haziness during some afternoons. Air parcels arriving at Riverside were advected from the ocean along routes passing near Long Beach and Fullerton, south of both Central Los Angeles and Azusa. This is a similar path to those taken by air parcels arriving at Riverside during September, 1996 [77] (see Chapter 3). Air stagnation occurred at Riverside beginning between 2000 and 2100 PDT and ending between 1200 and 1400 PDT the following morning. Temperatures at Riverside were between 17.8 and 35.7°C, and relative humidities were measured between 20 and 91%.

4.3 Results and Discussion

4.3.1 August 21–23, 1997, Sampling Event

Figure 4.4 shows the time series of fine particle mass and major aerosol chemical species concentrations at Central Los Angeles over the August 21–23 time period. The fine particle mass concentration shows a strong diurnal cycle, generally peaking during the morning 0600–1000 PDT peak traffic period. The fine particle mass concentration remains at a high level during the late morning and early afternoon of the second day. Elemental and organic carbon particle concentrations generally follow this strong diurnal cycle, with elemental carbon concentrations highest during the 0600–1000 PDT traffic peak and organic compounds highest during the late morning/early afternoon period from 1000–1400 PDT.

Gas phase ammonia at Central LA shows a nearly constant baseline concentration of about 8 to 9.5 μg m^{-3} (11.4–13.6 ppb) with a near doubling of ammonia concentrations during those hours when the elemental carbon concentrations are highest, possibly reflecting a traffic-derived source of NH_3 emissions as reported earlier by Fraser and Cass [88] based on experiments in the Van Nuys Tunnel. On the basis of ΔNH_3, ΔNH_4^+, and ΔEC defined as the increases in NH_3 nitrogen, fine particulate NH_4^+ nitrogen, and fine particulate EC concentrations from a previous sampling period to the time period of interest, the $(\Delta NH_3 + \Delta NH_4^+)/\Delta$EC

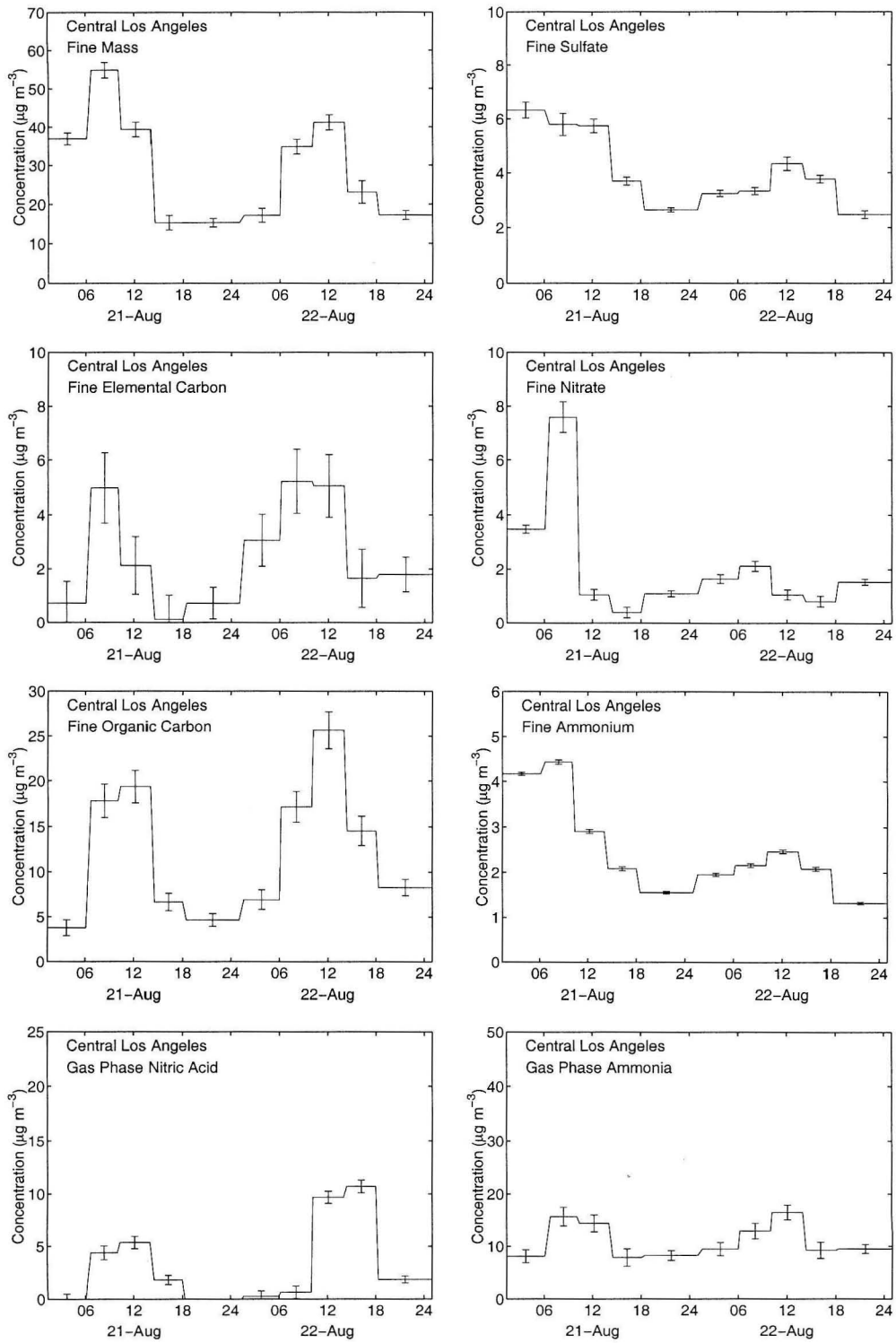

Figure 4.4: Fine particle and gas-phase concentrations for individual species measured during the August 21–23, 1997, sampling event at Central Los Angeles.

ratios for periods 0600–1000 PDT on August 21 and August 22 were 1.51±0.68 and 1.39±1.22, respectively. These ratios are approximately the same as the background-subtracted (NH_3 + NH_4^+) nitrogen to black carbon mass ratio measured in the mixed light- and heavy-duty vehicle bore of the Caldecott Tunnel on November 17, 1997, which was 1.38±0.10 [99]. For purposes of comparison, the (NH_3 + NH_4^+) nitrogen to black carbon mass ratio seen in the Van Nuys Tunnel experiments was 2.80 [88, 100], which is within ±2 standard errors of the incremental increases in the (NH_3 + NH_4^+) nitrogen to EC ratio just discussed during the time periods that contain the morning traffic peak in Figure 4.4. Nitric acid concentrations show a strong diurnal profile, with the peak concentrations during daylight hours of about 5 to 11 $\mu g\ m^{-3}$ (2.1–4.2 ppb) and nearly zero concentrations at night. Fine particle nitrate levels at Central LA are generally low throughout this experiment; the highest aerosol nitrate levels occurred overnight and during the 0600–1000 PDT period on August 21, a period with overnight fog turning to haze later in the morning. Aerosol sulfate concentrations are only marginally higher, and at times lower, than marine fine particle sulfate background levels recently reported for Santa Catalina Island (4.51 $\mu g\ m^{-3}$).

Fine aerosol behavior at Azusa over the August 21–22 episode, shown in Figure 4.5, is qualitatively similar to that at Central Los Angeles, except that the organic aerosol diurnal peak is broader and extends later into the day than at Central LA, possibly reflecting both early morning local traffic plus transport of organic aerosol to Azusa from upwind later in the same day. Fine particle sulfate concentrations are generally lower than at Central LA, indicating that the effects of dilution and surface removal are exceeding new sulfate formation between Central LA and Azusa. Nitric acid vapor concentrations at Azusa still show the strong diurnal cycle expected for a photochemically generated pollutant. Gaseous ammonia concentrations at Azusa do not show a diurnal variation that peaks during the early morning traffic peak, suggesting less influence from NH_3 emissions from autos with three-way catalytic converters. *Elemental carbon* shows strong early morning concentration peaks, suggesting that considerable

diesel truck traffic occurs near the Azusa monitoring site.

Figure 4.6 shows the time series of fine particle mass and major aerosol chemical species concentrations at Riverside over the August 21-23 time period. Fine aerosol mass concentrations at Riverside show a diurnal variation that differs from that seen at Central LA and Azusa, which is not surprising since Riverside does not lie on the same air parcel trajectory pathway as Central LA and Azusa. Relative peaks that correspond in time to peaks in individual aerosol chemical species can be seen clearly in the overall Riverside fine particle mass concentration time series. The fine elemental carbon particle concentrations increase sharply during the morning traffic peak. The organic aerosol concentration peaks are detached from the timing of the EC peak, with OC concentrations increasing later in the day as aerosol is transported to this inland location from the city upwind. Ammonia concentrations at Riverside are quite high, as expected given Riverside's location downwind of the agricultural ammonia sources in the Chino dairy area [21, 38, 39]. Nitric acid concentrations, however, are generally lower than at Central LA and Azusa, and on these days there is little aerosol nitrate, suggesting that HNO_3 formation from NO_2 was not running much faster than dry deposition of HNO_3 during the August 21-23 period.

4.3.2 August 27-29, 1997, Sampling Event

During the August 27-29 experiments, fine aerosol mass concentrations at Central Los Angeles and Azusa ranged between 12.8 and 30.1 $\mu g\ m^{-3}$ with a diurnal variation having comparable minimum values but smaller peak values than were seen during the August 21-23 episode. Elemental and organic carbon concentrations at Central LA were similar between the two experiments, while sulfate aerosol levels at that site were generally lower than in the earlier episode. Nitric acid showed peak concentrations of about 10 $\mu g\ m^{-3}$ (3.9 ppb) during the middle of the day at Central LA and 20.5-22.5 $\mu g\ m^{-3}$ (8.2-8.9 ppb) at Azusa with the usual daytime concentration peak and near-zero values at night. Aerosol nitrate

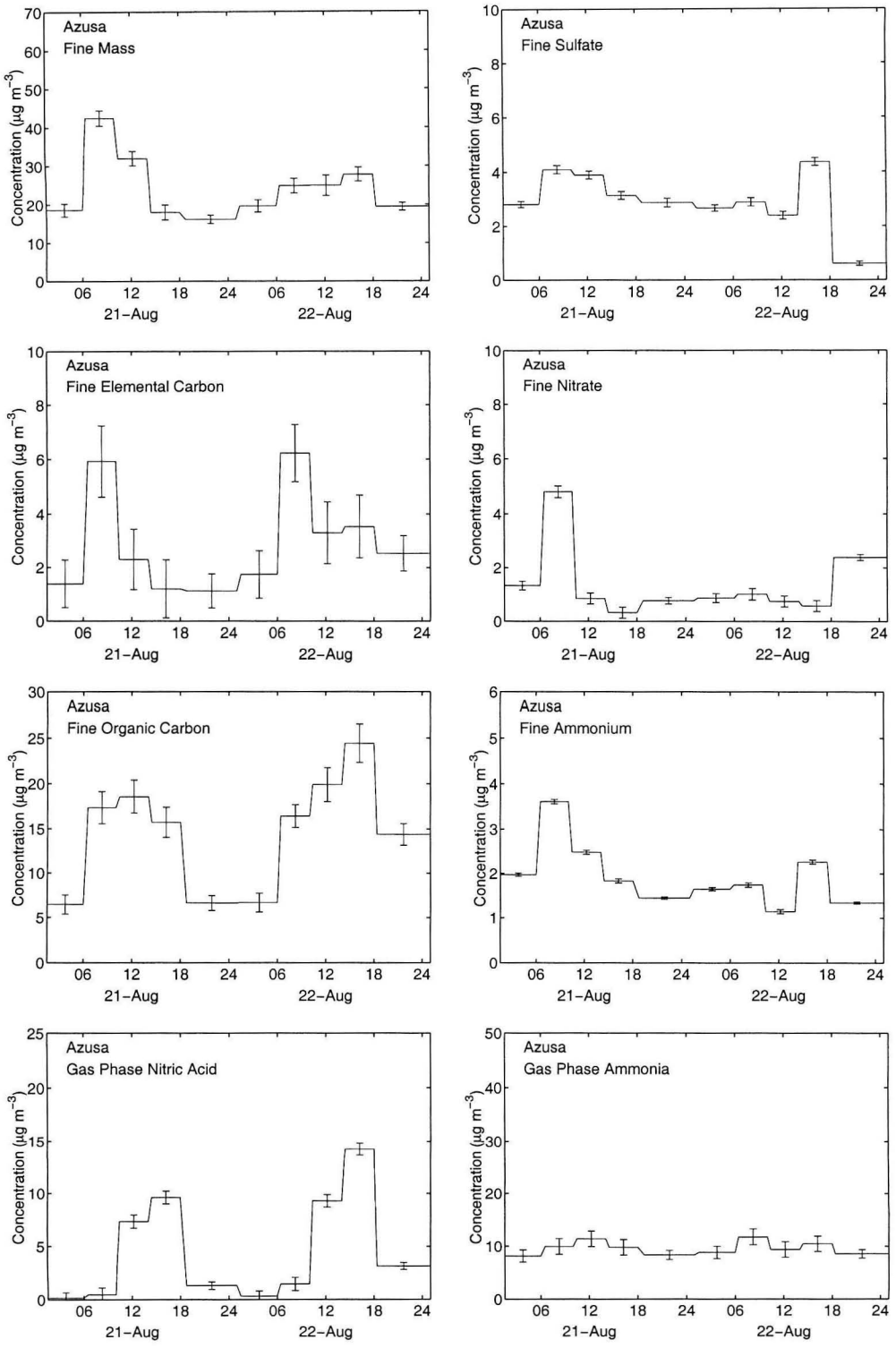

Figure 4.5: Fine particle and gas-phase concentrations for individual species measured during the August 21-23, 1997, sampling event at Azusa.

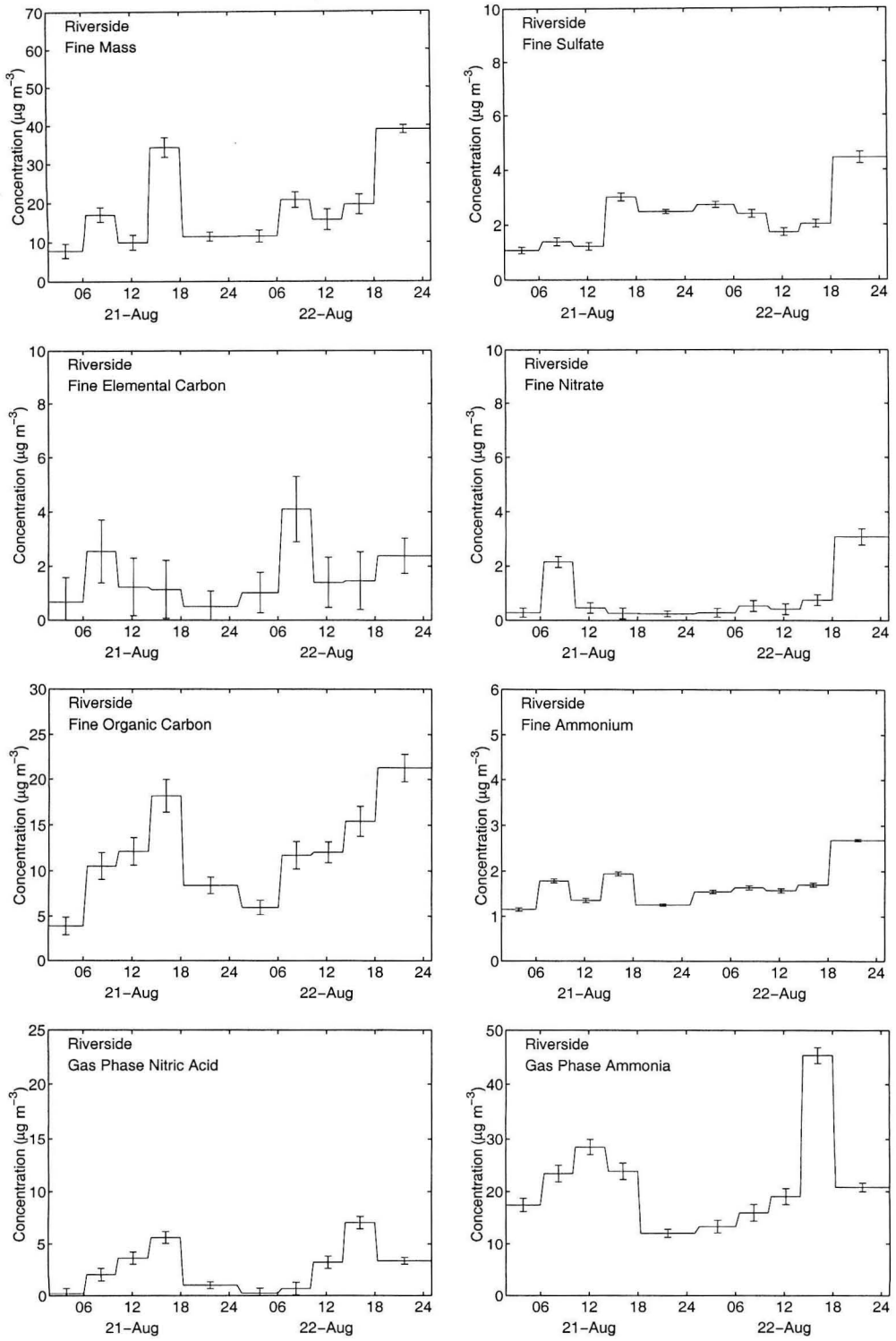

Figure 4.6: Fine particle and gas-phase concentrations for individual species measured during the August 21-23, 1997, sampling event at Riverside.

concentrations were low, generally between 1-2.5 $\mu g\ m^{-3}$ at both Central LA and Azusa.

Fine particle concentration and composition trends at Riverside likewise were fairly similar between the August 21-23 and August 27-29 episodes, and thus will not be described further.

Figure 4.7 shows a material balance on fine particle chemical composition at Central Los Angeles during the August 27-29 episode from the filter-based data during all sampling periods, as well as the size-segregated mass distribution and chemical composition of the fine particulate matter ($D_a < 1.8\ \mu m$) collected by the micro-orifice impactors during two sampling time periods: 0600-1000 PDT and 1400-1800 PDT on August 28, 1997. In these plots, as well as in mass balance presentations in Figures 4.8, 4.9, and 4.10, the designation "Unidentified" applies to the difference between mass concentration determined gravimetrically and the sum of species concentrations identified by chemical analysis methods. Silicon- and calcium-containing mineral matter are among the materials not detected by the methods used in the present study, and these make up some portion of the unidentified matter. In addition, because samples were equilibrated and weighed in an environment with controlled low relative humidity, water may have been retained by some ionic species. "Metals and Metal Oxides" refers to the sum of trace elements measured by neutron activation analysis, with elemental concentrations converted to equivalent concentrations of their most common oxides, where appropriate. See Table 4.1 for a list of these oxides and the conversion factors used.

The decreases in fine EC, OC, and aerosol nitrate apparent between the 0600-1000 PDT versus 1400-1800 PDT in Figure 4.7a also can be seen by a comparison of the two sets of impactor data. The EC concentration reduction between the morning traffic rush hour period versus the later period is accompanied by a size shift from an EC concentration peak in the 0.1-0.18 μm particle size range during the morning traffic peak to a relatively even distribution of EC between 0.1 and 0.56 μm diameter particles later in the day. The OC concentration re-

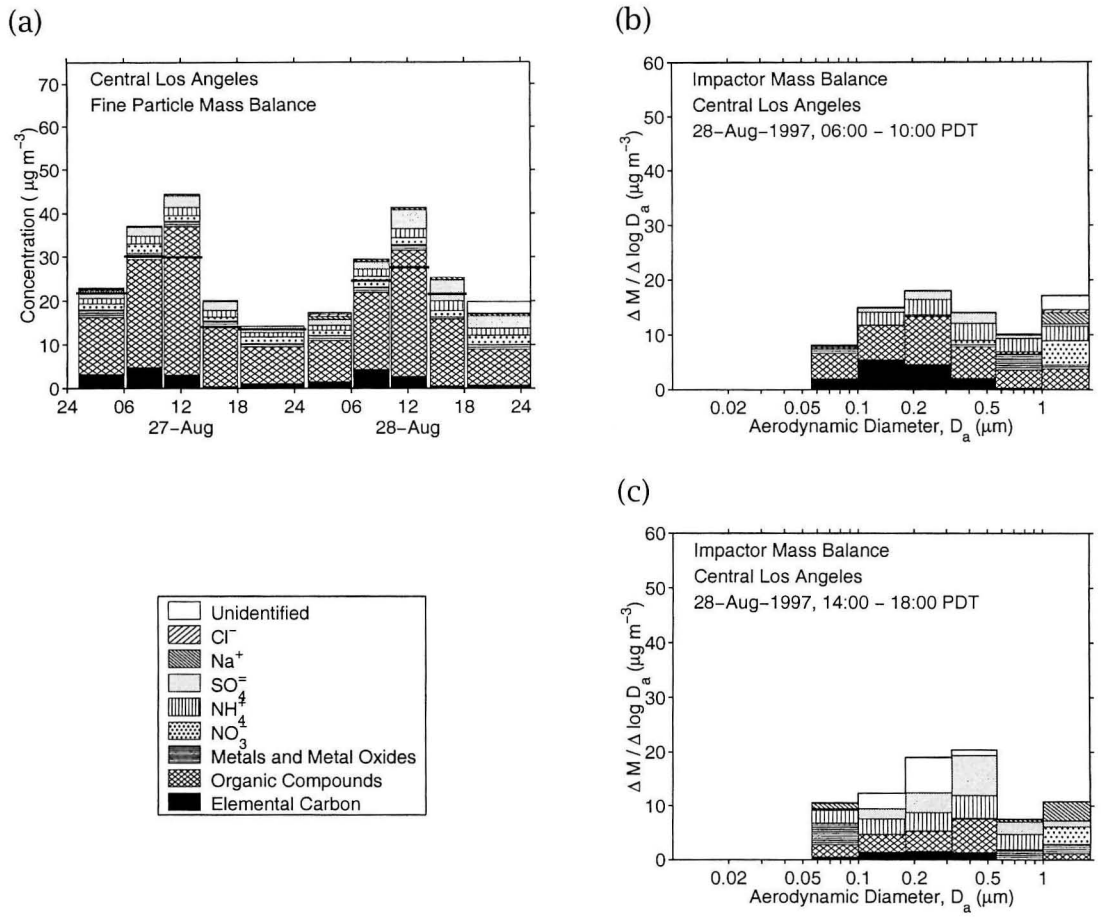

Figure 4.7: Fine particle results for a typical sampling event at Central Los Angeles. (a) Bulk fine particle concentrations and chemical compositions measured during the August 27–29, 1997, sampling event. (b) Size-resolved fine particle mass distribution and chemical composition measured on August 28, 1997, during the 0600–1000 PDT sampling period. (c) Size-resolved fine particle mass distribution and chemical composition measured on August 28, 1997, during the 1400–1800 PDT sampling period.

Table 4.1: Common oxide forms of measured elements and mass conversion factors.

Element	Oxide	Conversion Factor
Al	Al_2O_3	1.9
Fe	Fe_2O_3	1.43
Ba	BaO	1.12
Cd	CdO	1.14
Cr	CrO_3	1.92
In	In_2O_3	1.2
K	K_2O	1.2
Mn	Mn_2O_7	2.02
Sb	Sb_2O_5	1.33
Ti	TiO_2	1.67
V	V_2O_5	1.78
Ga	Ga_2O_3	1.69
As	As_2O_5	1.53
Se	SeO_3	1.61
Hg	HgO	1.08
Mo	MoO_3	1.5
Zn	ZnO	1.24

duction over this same pair of time periods is likewise accompanied by a shift of the peak in the OC size distribution to a larger size, moving from the 0.18-0.32 μm size range in the 0600-1000 PDT time period to the 0.32-0.56 μm size range in the 1400-1800 time period. The EC and OC concentration peaks during the morning in the 0.18-0.32 μm particle size range occur in the same size range as the predominant fine particle emissions from gasoline- and diesel-powered engines [101]. The appearance of EC and OC in larger particle sizes late in the day could result from advection into Central Los Angeles of aged aerosol having accumulated coatings of gas-to-particle conversion products over time. Alternatively, additional sources may contribute to the afternoon aerosol. NO_3^-, Cl^-, and Na are found in significant quantities only in the largest size range measured by the impactor ($1.0 < D_a < 1.8$ μm); these substances are associated with sea salt or transformed sea salt, which is generally found in particle sizes larger than 1 μm in diameter. If all of the Na and Cl^- began as NaCl in sea salt particles, then the Cl^- measured between 0600 and 1000 PDT suggests that about 82% of the sea salt has undergone a chloride substitution reaction during atmospheric transport prior to that time. The lack of Cl^- seen between 1400 and 1800 PDT implies that all of the Cl^- has been driven from the aerosol by late in the afternoon on the day studied. The reaction of nitric acid vapor with NaCl to produce $NaNO_3$ aerosol and hydrochloric acid vapor is well-documented [28, 94, 102-106]. The nitric acid concentration peaks in the daylight hours between 1000 and 1800 PDT. The air parcels which were sampled on the morning of August 28, 1997, at Central Los Angeles were over the ocean during the previous day's nitric acid peak, and crossed the coast at about 1800 PDT on August 27, 1997, arriving at Central LA before the time of the HNO_3 peak on August 28. In contrast, air parcels sampled at Central Los Angeles on the afternoon of August 28, 1997, stagnated over or near the ocean the night before, but were exposed to peak nitric acid concentrations during transport over land at mid-day on August 28, driving the chloride substitution reaction to completion.

Figure 4.8a shows the time series of fine particle ($D_a < 1.9$ μm) concentrations

and chemical compositions measured on August 27-29, 1997, during a typical sampling event at Azusa. As in Los Angeles, the highest concentrations of EC occurred during the 0600-1000 PDT time period when vehicle traffic was heavy, and OC concentrations were much larger during daylight hours than at night.

Figures 4.8b and c show the size-segregated mass distribution and chemical composition of the fine particulate matter (D_a < 1.8 μm) at Azusa during the two sampling time periods: 0600-1000 PDT and 1400-1800 PDT on August 28, 1997. The air parcels sampled in the morning of August 28 at Azusa stagnated over the ocean on the evening of August 26-27, crossed the coastline at approximately 1400 PDT August 27, and proceeded to Azusa, where stagnation occurred overnight between August 27-28. The air parcels sampled in the afternoon at Azusa on August 28 stagnated overnight over land, having come inland across the coast the afternoon before. Elemental and organic carbon particle concentrations and size distributions measured in the morning of August 28 at Azusa are similar to those measured at Azusa that afternoon. As in the Los Angeles morning and afternoon impactor samples (Figure 4.7), sulfate is present in greater quantities in the afternoon, particularly in the 0.32-0.56 μm size range. On this day, NO_3^- and Na are found only in particles larger than 1 μm, and the sea salt had been exposed to enough nitric acid vapor for complete Cl^- substitution to have occurred. The afternoon impactor samples show a larger NH_4^+ concentration in the 0.1-0.56 μm particle diameter size range than was the case in the morning, corresponding to the increased $SO_4^=$ concentration.

4.3.3 Evolution Along Air Parcel Trajectories

Several air parcel trajectories during the study were determined to have passed over or near the Central Los Angeles and Azusa air monitoring sites in succession, thereby permitting a comparison of aerosol evolution over time; two such air parcel trajectories are examined closely here. These two air parcel trajectories are of similar character; in each case the air mass which stagnated overnight

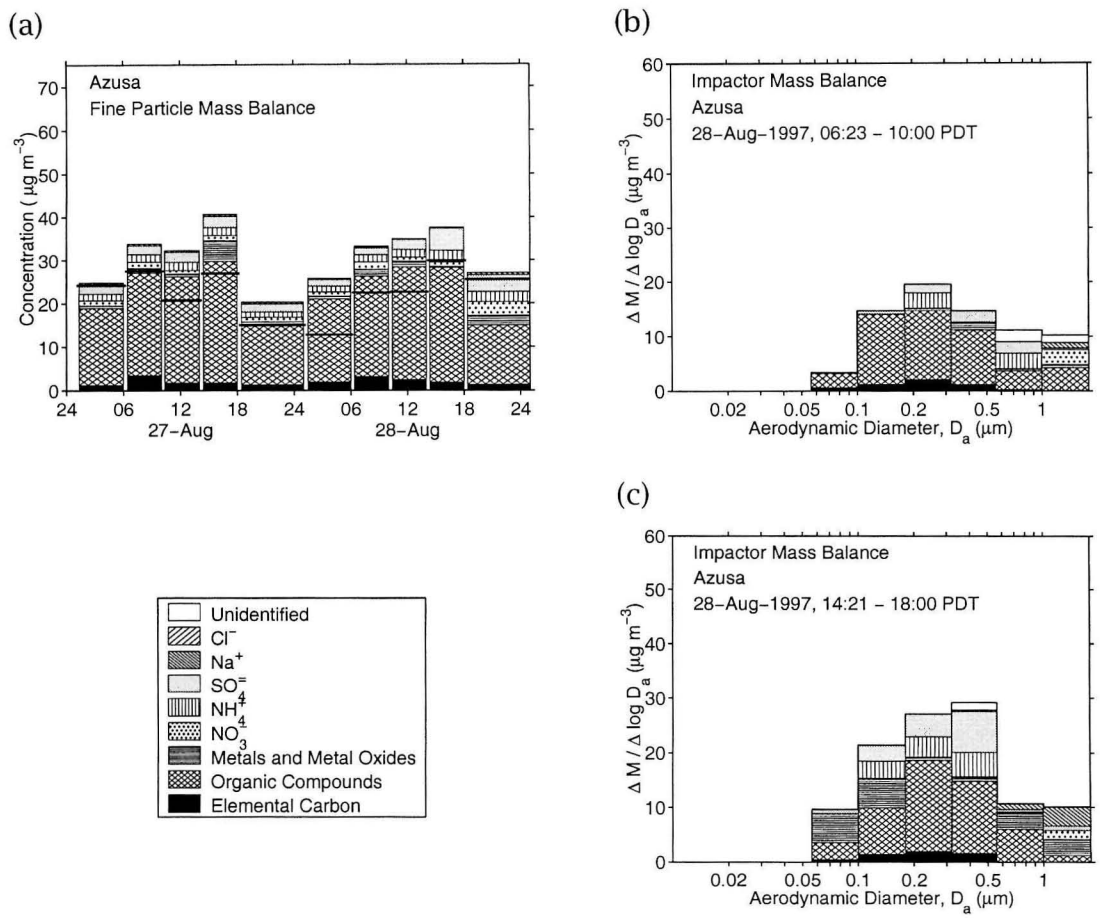

Figure 4.8: Fine particle results for a typical sampling event at Azusa. (a) Bulk fine particle concentrations and chemical compositions measured during the August 27–29, 1997, sampling event. (b) Size-resolved fine particle mass distribution and chemical composition measured on August 28, 1997, during the 0600–1000 PDT sampling period. (c) Size-resolved fine particle mass distribution and chemical composition measured on August 28, 1997, during the 1400–1800 PDT sampling period.

within 5 km of Azusa passed within 5 km of the Central Los Angeles monitoring site during the afternoon of the previous day. Trajectory analysis indicates that the air mass stagnating overnight within 5 km of Azusa on the night of August 21–22, 1997, passed within 5 km of Central LA at around 1400–1600 PDT on the afternoon of August 21. Figure 4.9a shows that air parcel path; each open circle indicates the air parcel location at successive hours during transport. Similarly, during the second 48-h experiment, the air mass stagnating overnight within 5 km of Azusa on the night of August 27–28 passed within 5 km of Central LA at around 1500–1630 PDT on the afternoon of August 27. This air parcel path is shown in Figure 4.10a. Examination of data obtained from these sites and time periods permits study of particle evolution within the same air mass.

Figures 4.9b and 4.10b show the composition of the nitrogen-containing air pollutant concentrations present within the August 21–22 and the August 27–28 air parcels studied, respectively. Most notable in both cases are the sharp increases in NO, by factors of 2.3–3.6, and NO_2, by factors of 1.4–1.8, that occur between the 0100–0600 PDT and 0600–1000 PDT time periods. These increases are presumably due to the increase in motor vehicle exhaust emissions during the morning traffic peak. While ammonia is present at noticeable concentrations in the range 4.0–13.6 μg N m^{-3} (equivalent to 7.0–24.5 ppb NH_3), there is little HNO_3 and little aerosol nitrate. This indicates that there is little NH_4NO_3 formation from HNO_3, and that HNO_3 formation from NO_2 is not faster than HNO_3 dry deposition along these trajectories. This is consistent with the comparatively low level of photochemical oxidant formation during the episodes studied here when compared to historical conditions in Southern California. Daily peak concentrations of hourly-averaged ozone ranged between 50 and 70 ppb at Central Los Angeles and 70 and 100 ppb at Azusa over the August 21–23 and August 27–29 sampling events. California air quality standards specify that the hourly average ozone concentration should not exceed 90 ppb. This standard was exceeded during two hours of the sampling events in this study at Azusa; the standard was not exceeded at the other two sites. In general, the smog season of 1997 was mild

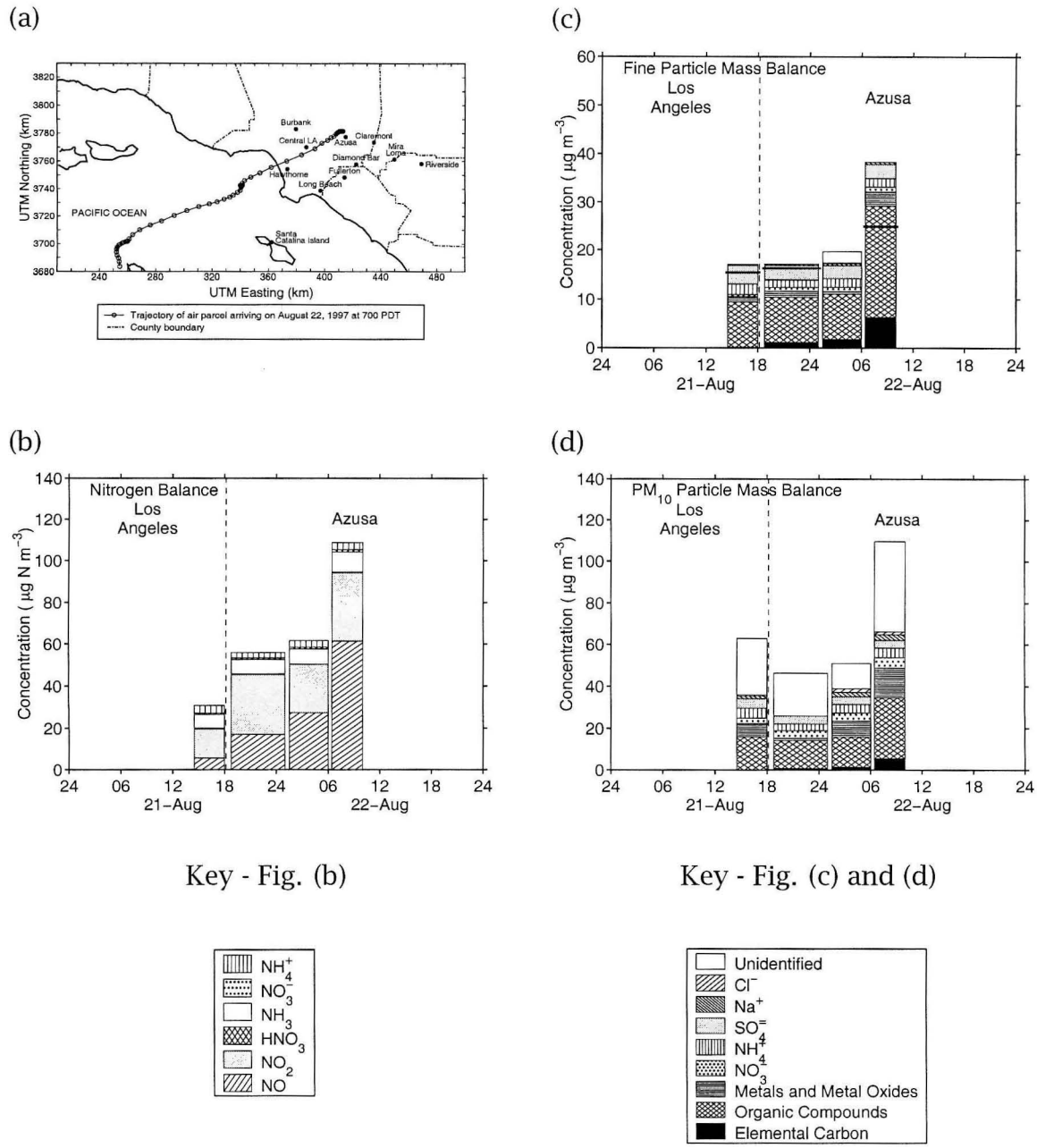

Figure 4.9: Aerosol evolution along the trajectory between Central Los Angeles and Azusa, August 21-22, 1997. (a) Representative air parcel trajectory which reached Azusa at 0700 PDT August 22, 1997. The air parcel passed within 5 km of the Central Los Angeles sampling site between 1400 and 1800 PDT on August 21 before stagnating at Azusa over the night and morning of August 21-22. Circles represent air parcel location at consecutive hours. (b) Nitrogen balance, (c) Fine particle mass balance, and (d) PM_{10} mass balance.

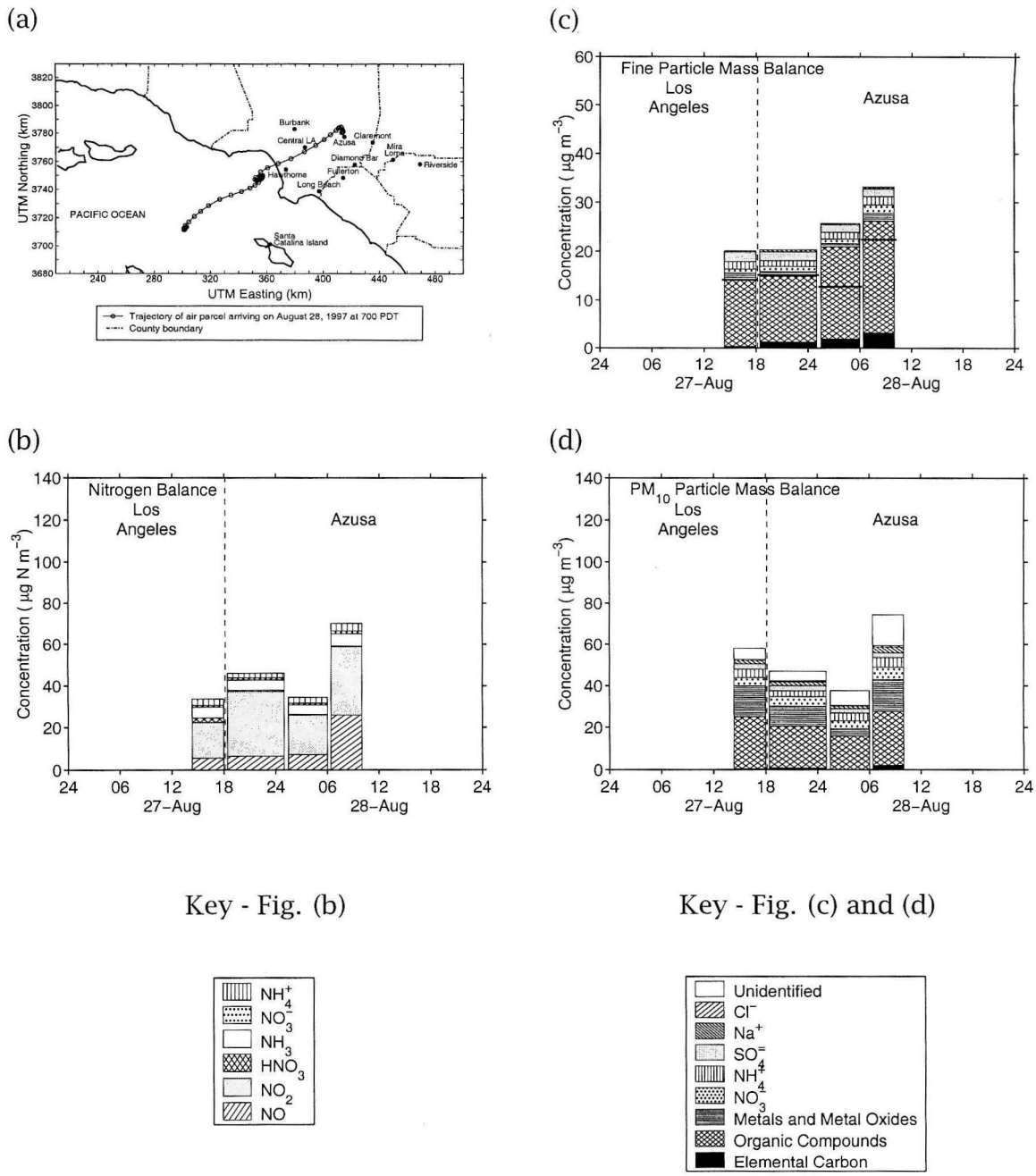

Figure 4.10: Aerosol evolution along the trajectory between Central Los Angeles and Azusa, August 27-28, 1997. (a) Representative air parcel trajectory which reached Azusa at 0700 PDT August 28, 1997. The air parcel passed within 5 km of the Central Los Angeles sampling site between 1400 and 1800 PDT on August 27 before stagnating at Azusa over the night and morning of August 27-28. Circles represent air parcel location at consecutive hours. (b) Nitrogen balance, (c) Fine particle mass balance, and (d) PM_{10} mass balance.

in comparison with previous years; there was only one Stage One ozone episode during the entire year (hourly average O_3 concentration > 200 ppb), in contrast to 41, 24, 23, 14, and 7 such episodes over the 5 consecutive years 1992–1996, respectively [98].

Figures 4.9c and 4.10c show material balances on fine particle ($D_a < 1.9\ \mu m$) chemical composition along the August 21–22 trajectory and the August 27–28 trajectory, respectively. "Unidentified" material indicates the difference between gravimetrically determined mass concentrations and the sum of the identified analyte concentrations. A thick horizontal line indicates the gravimetrically determined mass concentration on the one occasion when this is less than the sum of the identified analyte concentrations. During transport along both trajectories, the relative composition of the aerosol did not change appreciably between 1400 PDT at Central Los Angeles and 0600 PDT the next morning at Azusa. The exception to this observation is that elemental carbon concentrations increased steadily over time in both air parcels, as did organic aerosol during the early morning hours on August 28 at Azusa. There was not significant NO_3^- or $SO_4^=$ formation during the overnight stagnation periods up until 0600 PDT. In both cases, on the second morning of each experiment the particle population changed noticeably during the morning traffic peak period through increases in aerosol elemental carbon (65–258% increase), organic matter (21–146% increase), metals and metal oxides (138–538% increase), nitrate (17–84% increase), ammonium (6–25% increase), and fine aerosol mass (27–75% increase) during periods when the air mass motion was relatively stagnant.

Figures 4.9d and 4.10d show PM_{10} material balances on aerosol chemical composition along the August 21–22 and the August 27–28 air parcel trajectories studied, respectively. At least a portion of the large unidentified mass concentrations includes silicate minerals and calcium-containing mineral matter which were not measured by neutron activation analysis in this experiment. These minerals are found primarily in dust and crustal material, which are largely present in the coarse particle size range; therefore, unidentified matter is generally greater

for PM_{10} particulate matter than for fine particle matter. As with fine aerosol, on the second morning of each experiment the PM_{10} particle population changed significantly during the morning peak traffic period through increases in aerosol organic matter (60–100% increase), metals and metal oxides (88–353% increase), nitrate (27–58% increase), ammonium (13–24% increase), and fine aerosol mass (97–115% increase).

4.3.4 Evolution Along an Air Parcel Trajectory at the Single Particle Level

Aerosol time-of-flight mass spectrometry instruments operated continuously in dual-ion mode at the Central Los Angeles and Azusa air monitoring sites during this study. Through these ATOFMS data, changes in an aerosol population within an air mass as it is transported from Los Angeles to Azusa can be examined at the single particle level by analyzing and categorizing the thousands of particles collected at those two sites during the air parcel trajectory events identified in the previous section. Statistically large numbers of particles were sampled over the size range 0.56–3.50 μm aerodynamic diameter. The ATOFMS instruments undercount ambient particles by a factor which is a function of particle size; detection efficiency decreases with decreasing size. This detection efficiency as a function of size can be determined through field calibration against collocated impactor measurements [58]. Once this field calibration procedure has been completed, each particle detected by the ATOFMS is taken to represent a number of similar but uncounted particles present in the atmosphere, with that number determined by the ATOFMS counting efficiency function and the particle's size.

A particle "hit" by the ATOFMS instrument ablation laser has a positive and a negative mass spectrum associated with it. Each particle is categorized according to whether it contains one of a number of major chemical species, as determined by the presence of key indicator ions. These species and the rules by which they are defined are described here generally; precise definitions are given in Table 4.2.

Sodium is indicated by a peak at mass-to-charge ratio (m/z) 23 (Na^+); ammonium by m/z 18 (NH_4^+); nitrate by m/z 30 (NO^+), 108 ($Na_2NO_3^+$), -46 (NO_2^-), or -62 (NO_3^-); carbon by m/z 12 (C^+), 36 (C_3^+), 37 (C_3H^+), 60 (C_5^+), 72 (C_6^+), -12 (C^-), -24 (C_2^-), -36 (C_3^-), -48 (C_4^-), or -72 (C_6^-); sulfate by m/z 165 ($Na_3SO_4^+$), or -96 (SO_4^-); and soil or dust by large peaks at m/z 7 (Li^+), 27 (Al^+), 40 (CaO^+), 56 (Fe^+/CaO^+), or 96 (Ca_2O^+). Source studies on local soil samples have also shown that a very large peak at low mass-to-charge ratios ($m/z < 2.5$) is an unique indicator of a soil dust particle. The more detailed criteria used for considering a given peak present in a mass spectrum are listed in Table 4.2.

Figure 4.11 provides a color-coded display that illustrates the character of the counting efficiency-corrected particle populations, separated by size, during the sampling periods at Central Los Angeles and Azusa which encompass the air parcel trajectory that passed through Central Los Angeles on the afternoon of August 21, 1997, before stagnating overnight on August 21–22 within 5 km of Azusa. As with Figure 3.8, each of the 100 dots within a square plot represents one percent of the particle population at the time and location indicated, within the specified range of particle aerodynamic diameters. Each dot is striped with the colors that correspond to the indicator ion peaks found within a particular one percent of particles. The exception to this rule is the dust category; all mineral dust-containing particles are represented as solid gray dots because the peaks associated with dust often have areas so large that they blow scale and produce noise in the rest of the mass spectrum, making detection of any other peaks unreliable. Therefore, any or all of the other classified species may be present within the particles represented by a "dust" dot. A color stripe only qualitatively indicates the presence of the corresponding chemical species; no conclusions can be drawn about the relative amounts of each substance. Only the presence or absence of these six defined classes was considered in producing the figure; the presence of one or few colors in a dot does not necessarily imply that those particles are of "simple" composition, as any number of species that were not included in the analysis may also be present, for example potassium

Table 4.2: Criteria used for classifying particle mass spectra.

Class	Ion	m/z[a]	Peak Search Rules
Sodium	Na^+	23	Peak Area > 100
Ammonium	NH_4^+	18	Peak Area > 30
Nitrate	NO^+	30	Peak Area > 30 OR
	$Na_2NO_3^+$	108	Peak Area > 50 OR
	NO_2^-	-46	Peak Area > 1000 OR
	NO_3^-	-62	Peak Area > 1000
Sulfate	$Na_3SO_4^+$	125	Peak Area > 125 OR
	SO_4^-	-96	Peak Area > 100 AND no peak at m/z=-72 (C_6^-)[b]
			(Restriction limits C_8^- interference at m/z=-96)
Carbon	C^+	12	Peak Area > 50 OR Relative Peak Area > 0.5% OR
	C_3^+	36	Peak Area > 50 OR Relative Peak Area > 0.5% OR
	C_3H^+	37	Peak Area > 50 OR Relative Peak Area > 0.5% OR
	C_5^+	60	Peak Area > 50 OR Relative Peak Area > 0.5% OR
	C_6^+	72	Peak Area > 50 OR Relative Peak Area > 0.5% OR
	C^-	-12	Peak Area > 50 OR Relative Peak Area > 0.5% OR
	C_2^-	-24	Peak Area > 50 OR Relative Peak Area > 0.5% OR
	C_3^-	-36	Peak Area > 50 OR Relative Peak Area > 0.5% OR
	C_4^-	-48	Peak Area > 50 OR Relative Peak Area > 0.5% OR
	C_6^-	-72	Peak Area > 50 OR Relative Peak Area > 0.5%
Dust	Fe^+/CaO^+	54–57	Peak Area > 1500 OR
	Al^+	25.5–28	Peak Area > 1500 OR
	H^+	0.5–2.5	Peak Area > 1500 OR
	Li^+	5–9	Peak Area > 200 OR
	CaO^+	40	Peak Area > 2500 OR
	Ca_2O^+	96	Peak Area > 100 AND no peak at m/z=72 (C_6^+)[c]

[a] Unless otherwise specified, m/z range is ±0.5

[b] Restriction on C_6^- limits C_8^- interference at m/z=-96

[c] Restriction on C_6^+ limits C_8^+ interference at m/z=96

(K^+, m/z 39), vanadium (V^+, m/z 51), or chloride (Cl^-, m/z -35). The "many types" category, shown in purple, is the sum of those particle types which each encompass less than approximately 0.5% of the particle population and which would therefore not warrant representation by an entire dot. Note the color differences between this figure and the similarly constructed figure in Chapter 3; in the previous figure, ammonium was represented by yellow and "many types" by green, while in Figure 4.11, ammonium is represented by green and "many types" by purple. With the recently added ability to simultaneously detect positive and negative ions from each particle with the transportable ATOFMS instruments stationed at Los Angeles and Azusa, sulfate indicator ions became available, and sulfate-containing particles are represented here by a yellow stripe or dot.

Figure 4.11 qualitatively shows the changes in the particle population during transport along the trajectory between Los Angeles and Azusa on August 21-22, 1997. The corresponding $PM_{1.9}$ and PM_{10} mass balances and nitrogen species balances along this trajectory are shown in Figure 4.9. The first column of the single particle data plots shows particles sampled in Central Los Angeles, August 21, 1400-1800 PDT, and the second and third columns show the particle populations at Azusa on August 22 at 0100-0600 PDT and 0600-1000 PDT, respectively. A prominent component of the largest size range, $1.80 < D_a < 3.50$ μm, is sodium-containing particles. Although there are combustion sources of sodium, at these large sizes the likely original source of sodium-containing particles is sea salt. At all three times along the trajectory shown, most of the non-dust particles with diameters > 1.0 μm contain sodium. The fraction of sodium-containing particles in this size range that also contain sulfate is about the same during all three time periods; this implies that the sulfate is present in the primary sea salt particles, and agrees with fine and PM_{10} measurements that show very little change in sulfate concentrations during transport through the Los Angeles area. Sodium-containing particles often also contain some combination of nitrate, carbon, and/or ammonium, probably as a result of alteration of the sea salt particles by gas-to-particle conversion processes.

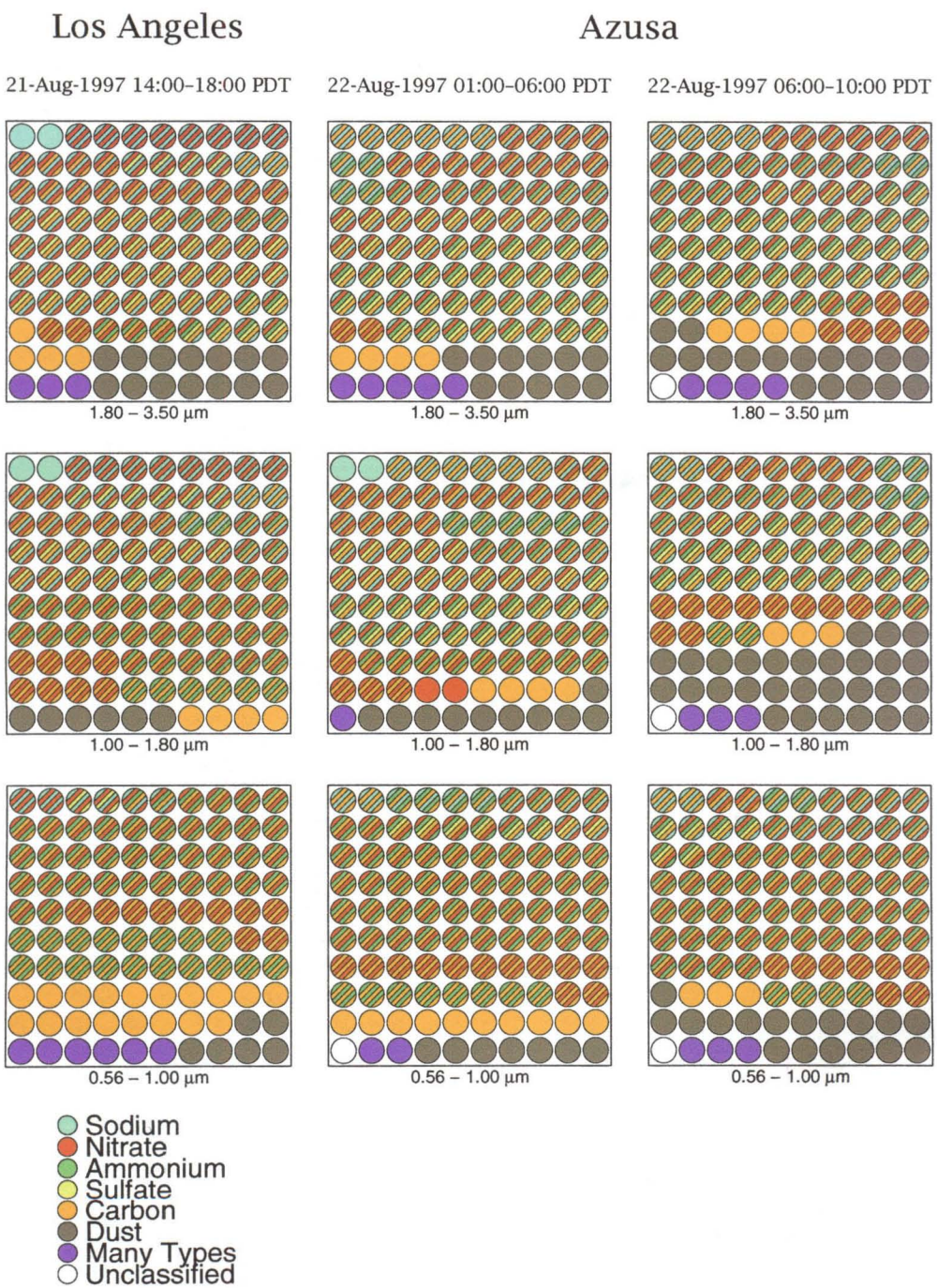

Figure 4.11: The chemical compositions of size-segregated particle populations during the August 21–22, 1997, trajectory between Los Angeles and Azusa as measured by the ATOFMS instruments. Each dot represents one percent of the particle population within the indicated aerodynamic particle diameter range.

In the smaller particle size range $0.56 > D_a > 1.00$ μm, carbon-containing particles dominate the aerosol populations during all three time periods. A large fraction of these particles are classified as containing carbon, ammonium, and nitrate (orange, green, and red stripes). There is a larger fraction of "carbon only" particles present in Los Angeles in the afternoon. This may be the result of fresh motor vehicle emissions during the afternoon traffic peak in Los Angeles, though diesel and gasoline engines primarily emit particles with diameters less than about 0.3 μm.

Another prominent feature of Figure 4.11 is the increase in dust-containing particles at Azusa during the 0600–1000 PDT sampling period; counting efficiency-corrected particle counts show that the number of dust-containing particles increased by factor of greater than 4 in size ranges larger than 1.0 μm diameter. The Azusa sampling site is located near a quarry, and the increase in dust-containing particles occurs with the onset of business hours. This increased presence of dust is also seen in PM_{10} and $PM_{1.9}$ time series data at Azusa.

Chapter 5

Nitrate-Oriented Trajectory Study

5.1 Introduction

In autumn of 1997 a field experiment was conducted in conjunction with the 1997 Southern California Ozone Study [96–98] in which a network of three air monitoring stations was established, with the purpose of determining the size and chemical composition of the airborne particle population in an area having high secondary ammonium nitrate aerosol formation. Measurements were made of the particle size distribution, bulk fine particle and PM_{10} chemical composition, chemical composition segregated into narrow particle size intervals, and single particle chemical composition. Air monitoring locations were chosen along a seasonally typical wind trajectory that crosses an agricultural area located to the east of Los Angeles, California, that has significant ammonia emissions due to livestock husbandry operations and fertilizer use. The intent was to first observe air parcels at the leading edge of the ammonia source area, and to subsequently observe the same air parcels after they have been carried downwind through the source area. This sampling scheme was designed to provide data on the evolution over time of the size and chemical composition of ambient aerosols at the bulk, size-segregated, and single-particle levels as those particles are poten-

tially altered by gas-to-particle conversion processes and affected by continuing emissions, dilution, and dry deposition.

Several studies of nitrate-containing particle evolution using multiple observation points along a single air parcel trajectory have been conducted previously in the Los Angeles area. In a 1982 field study, gas- and particle-phase nitrogen species were sampled from a single air parcel which passed over or near three monitoring sites in succession: Long Beach, Anaheim, and Rubidoux, California, providing insight into the process of aerosol nitrate formation and the interrelationship between gas-phase HNO_3 and NH_3 versus particulate NH_4NO_3 [13, 21, 40]. Measurements made at that time showed that the aerosol nitrate behaved as would be expected from analyses based on thermodynamic equilibrium between the gas and particle phases and verified the presence of a large ammonia source located in the agricultural and dairy area between Anaheim and Rubidoux leading to large aerosol nitrate concentrations in the Riverside (Rubidoux) area.

In 1996, a similarly designed field study was conducted using more advanced instrumentation (see Chapters 2 and 3). A battery of aerosol sampling instruments similar to those employed in the present study, including samplers for fine and total suspended particulate matter chemical composition, size-segregated particulate matter chemical composition, and single particle size and composition measurements, were used to obtain information about the evolution of the aerosol as particles aged in the presence of significant aerosol nitrate formation as well as continuing emissions [74, 77]. Two air parcel trajectories were identified which passed over or near three or four air monitoring stations along the Santa Catalina Island - Long Beach - Fullerton - Riverside pollutant transport corridor [74]. Notable in the results of this study was the observation of large increases in particulate ammonium and nitrate concentrations between Fullerton and Riverside in air parcels which stagnated overnight in the area of large livestock and agricultural ammonia sources just west of Riverside. The present study differs from previous work in that for the first time, air monitoring stations are placed just upwind of and directly within the Chino dairy area in order

to observe the effect of a major source of ammonia emissions at close range.

The purpose of this chapter is to document the dynamic behavior of the aerosol within the air parcels sampled during the present experiment. These data can later be used to evaluate the accuracy of the predictions of trajectory-based and grid-based air quality models which represent the particle population as externally mixed single particles. In addition, these data can be used in ongoing work which determines the particle counting efficiency and chemical sensitivities of the ATOFMS instruments to atmospheric particles as measured under field sampling conditions by comparison to simultaneous measurements using conventional sampling and analysis techniques.

5.2 Experimental Methods

5.2.1 Sample Collection and Analysis

Three urban air monitoring stations were established in the Los Angeles metropolitan area to measure the effect of nitrogen species emissions on ambient particulate matter concentrations. These sites were located in Diamond Bar, Mira Loma, and Riverside, as labeled on the map in Figure 5.1. The three sites were chosen because they are located along a seasonally typical wind path inland across the South Coast Air Basin. This allows the possibility of successive sampling of the same air parcels at multiple locations as they are transported downwind. In addition, the area traversed by an air parcel advected between two or more of these sites is exposed to substantial agricultural and livestock ammonia sources (see Figure 2 of [38]).

Sampling was conducted at all three sites during one 48-h period on October 31–November 2, 1997. In addition, continuous sampling at the Mira Loma monitoring station alone was conducted during one 59-h period, September 27–29, 1997. Fine particle and PM_{10} samples for mass and chemical composition determination were collected sequentially on a five-sample per day schedule, and

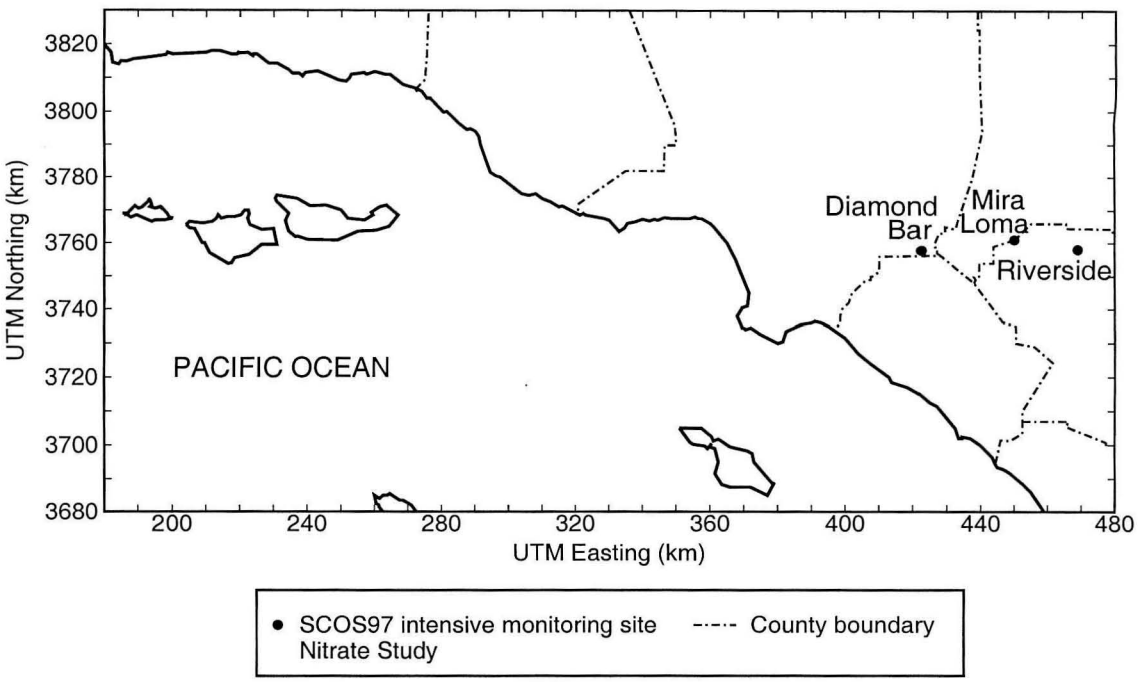

Figure 5.1: South Coast Air Basin and Nitrate Study sampling site locations.

a pair of micro-orifice impactors (MOIs) were operated at each site for one or two of these time periods each day. Times of operation for the filter samplers and impactors are shown in Figure 5.2 for both sampling events.

During the September 27–29, 1997, sampling at Mira Loma, a transportable aerosol time-of-flight mass spectrometry (ATOFMS) instrument [28] was in operation at that site. During the October 31–November 2, 1997, sampling period, a laboratory-bound ATOFMS instrument [27] was operated in Riverside. Where used, the ATOFMS instruments operated continuously, collecting number distribution data in the particle aerodynamic diameter, D_a, range $0.2 < D_a < 5$ μm, and obtaining mass spectra for a subset of the input particle population.

Four filter sampling systems were used to collect particles at each air monitoring station: one to collect PM_{10} samples ($D_a < 10$ μm) and three to collect fine particle samples ($D_a < 1.9$ μm). The PM_{10} sampler and two of the three fine particle samplers were used to collect consecutive short time average samples for bulk and elemental analysis. Five complete sets of filter samples were collected each day according to the following time schedule: 0120–0600 hours,

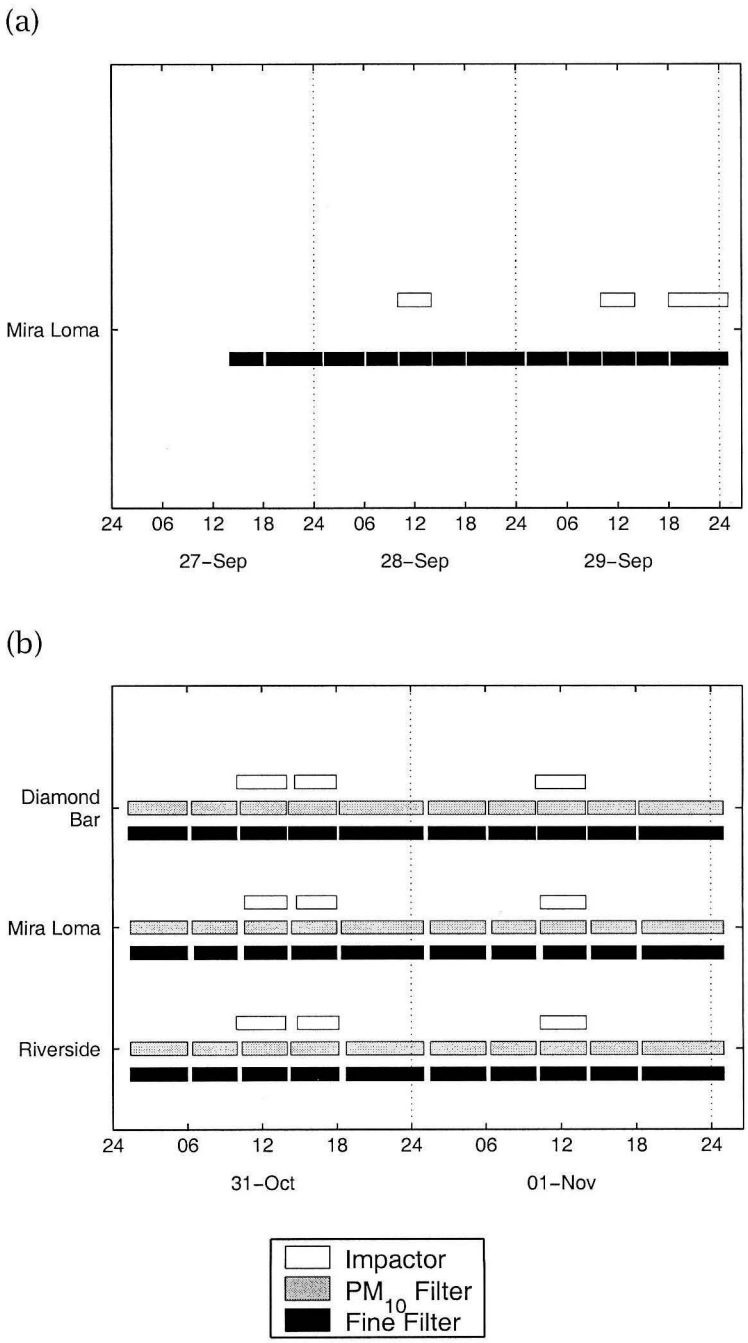

Figure 5.2: Times of operation of impactors and filter samplers at each site during the two sampling events, stated in terms of local time during the experiments. (a) Extended sampling at Mira Loma, September 27–20, 1997 (local time was PDT). (b) Three-site experiment, October 31–November 2, 1997 (local time was PST).

0620-1000 hours, 1020-1400 hours, 1420-1800 hours, 1820-0100 hours (the following day). All times in this study were recorded in the local time system; therefore, times before October 26, 1997, are in Pacific Daylight Time (PDT), and times after October 26, 1997, are in Pacific Standard Time (PST). The sampling schedule provides relatively fine temporal resolution data for comparison with the continuous ATOFMS data and future air quality modeling results. One fine particle sampler at each site collected 24-h average samples to facilitate collection of enough material for later analysis of individual particulate organic compounds by GC/MS. In addition, a pair of MOIs (MSP Corp., Model 110) was used at each site to collect particles in the aerodynamic diameter range $0.056 < D_a < 1.8$ μm, in six size intervals during one or two 4-h sampling periods each day.

The impactors, filter samplers, and sample analysis methods are identical to samplers used in the Vehicle-Oriented Trajectory Study, and are described in detail in Chapter 4. Impactor substrates and filter samples were analyzed for mass gravimetrically, for Cl^-, NO_3^-, and $SO_4^=$ by ion chromatography, for NH_4^+ by indophenol colorimetry, for elemental black carbon and organic carbon by thermal evolution and combustion analysis, and neutron activation analysis for 39 trace elements. HNO_3 was measured using the denuder difference method. Gas-phase NH_3 was detected as NH_4^+ collected on oxalic acid-impregnated glass fiber filters used downstream of a PTFE pre-filter. Measurement methods are discussed in more detail in Chapter 4. A factor of 1.4 was applied to measured organic carbon concentrations to convert these measurements to an estimate of organic compound concentrations. This scale factor accounts for the additional mass of associated H, O, N, and S present in the organic matter of typical atmospheric organic aerosols [71].

5.2.2 Meteorology

Wind fields over the South Coast Air Basin were reconstructed over a 5 km $\times$ 5 km grid system superimposed over the airshed for each hour during the study

using the method of Goodin et al. [68], based on hourly averaged wind speed and direction measurements at 27–28 meteorological stations maintained by the South Coast Air Quality Management District (SCAQMD). From the wind fields, back trajectories from the sampling sites were calculated, establishing the time and location history of the air parcels arriving at the sampling sites.

At Mira Loma during the September 27–30 sampling event, temperatures were between 17.2 and 39.2°C, relative humidity was 15 to 94%, and optical conditions were hazy. Air stagnation occurred beginning between 2000 and 2300 PDT in the evening until between 0900 and 1100 PDT the following morning.

Temperatures at Diamond Bar during the October 31–November 2 sampling episode ranged between 11.5 and 34.8°C, with relative humidities measured between 12 and 78%. Air stagnation occurred at Diamond Bar beginning at about 1700 PST in the evening each day until about 1300 PST the afternoon of the following day. Mornings were hazy, and the haze cleared in the afternoon of November 1. During the same sampling event at Mira Loma, the temperature range was 8.5 to 34.8°C and the relative humidity range was 10 to 85%. Air stagnation occurred at Mira Loma on the evening of October 31 at about 1700 PST, lasting until about 0600 PST the following morning; no air stagnation occurred the evening of November 1. Mornings were hazy and misty; the afternoon of October 31 was hazy, but conditions cleared beginning early in the morning of November 1. Temperatures at Riverside during this sampling event ranged between 12.4 and 33.3°C, and the relative humidity range was 26 to 62%. Air stagnation occurred at Riverside on the evening of October 31 at about 1700 PST, and lasting until about 0700 PST the following morning; no air stagnation occurred at Riverside the evening of November 1. October 31 was hazy, but November 1 was clear from the early morning on. None of the three sites had significant cloud cover at any time during sampling, and air quality cleared significantly at all three sites beginning on the morning or early afternoon of November 1 and lasting through the rest of that day. Wind pattern shifts likely explain this phenomenon; air parcels reaching Mira Loma and Riverside for the latter half of November 1 were trans-

ported from the north, rather than across the heavily populated area to the west of those locations.

5.3 Results and Discussion

5.3.1 September 27–30, 1997, Sampling Event

Figure 5.3 shows the time series of fine particle mass and major aerosol chemical species concentrations at Mira Loma over the September 27–30 sampling period. Fine particle mass concentrations were high, averaging 81.9 $\mu g\ m^{-3}$, 63.9 $\mu g\ m^{-3}$ and 58.2 $\mu g\ m^{-3}$ on September 27 (after 1400 PDT), September 28, and September 29, respectively. By comparison, the recently proposed Federal $PM_{2.5}$ air quality standard limits 24-h average fine particle concentrations to not more than 65 $\mu g\ m^{-3}$ and annual average $PM_{2.5}$ concentrations to not more than 15 $\mu g\ m^{-3}$. The fine particle mass concentration at Mira Loma on these days was dominated by ammonium nitrate aerosol, with significant quantities of organic aerosol also present.

September 27, 28, and 29 fell on Saturday, Sunday, and Monday, respectively, and it is interesting to note the differences between species concentration patterns on a weekend and a weekday. For example, Monday, September 29 exhibits a strong peak in the elemental carbon concentration during the 0600–1000 PDT time period. This pattern was also noted on weekdays in Central LA and Azusa, areas in which vehicle traffic emissions are a major source (see Figures 4.4 and 4.5). However, this pattern does not appear on Sunday, September 28.

In addition to the weekend/weekday distinctions, some of the concentration time series behaviors can be explained by the source of the air mass sampled. Concentrations of fine particulate nitrate, ammonium, and mass are all relatively high and constant from the evening of September 27 through the morning of September 28. Fine particulate sulfate concentrations were relatively high, but steadily decreased with time. Average concentrations during this time period

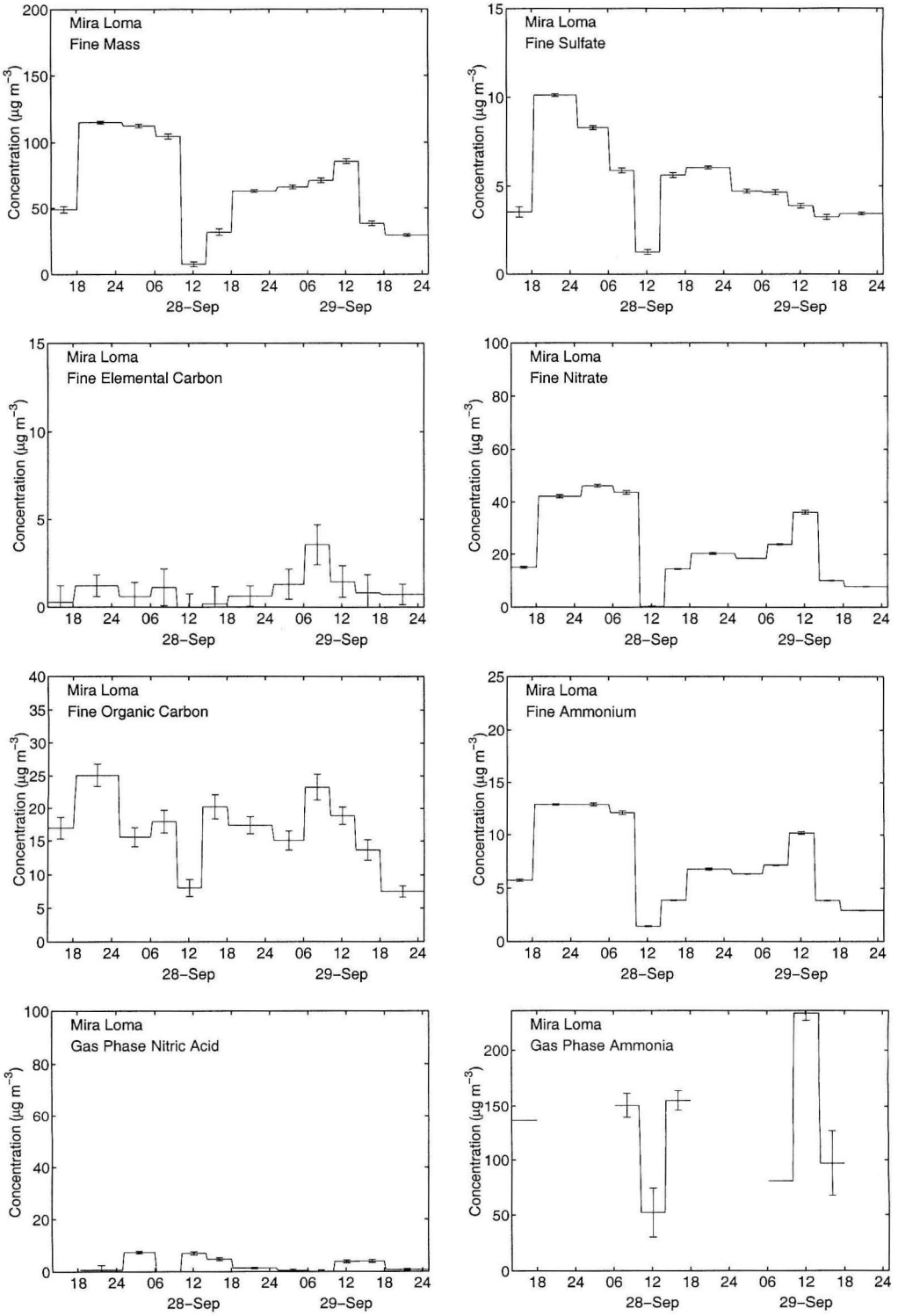

Figure 5.3: Fine particle and gas-phase results for individual species measured during the September 27–30, 1997, sampling event at Mira Loma.

were 8.5 μg m^{-3} fine $SO_4^=$, 43.9 μg m^{-3} fine NO_3^-, 12.7 μg m^{-3} fine NH_4^+, and 111 μg m^{-3} fine particulate mass. The consistency of these concentrations over time was due to the fact that this air mass was stagnant at Mira Loma overnight. After 1000 PDT, air mass stagnation ended, and the air parcels transported into the Mira Loma area came from north of Mira Loma, an area absent the ammonia source-driven ammonium nitrate production associated with the dairy area near Mira Loma. This difference in air mass origin is reflected in the precipitous drop in measured concentrations of gas-phase ammonia and fine particle mass, EC, organic compounds, sulfate, nitrate, and ammonium. (Two independent gravimetric measurements of this minimum in the fine particle mass concentration agreed to within 6%.) The fine mass concentration minimum during this time period was 7.5 $\pm$ 1.9 μg m^{-3}, compared to maximum and average fine particle mass concentrations of 114.9 $\pm$ 1.1 μg m^{-3} and 64.5 $\pm$ 0.50 μg m^{-3}, respectively, over the entire sampling event. Later in the afternoon of September 28, particulate species concentrations increased again; the air arriving at Mira Loma in these time periods had stagnated the night before in the corridor between Claremont, Diamond Bar, and Fullerton, and most calculated trajectories indicate several hours of travel across the ammonia sources between Diamond Bar and Mira Loma before these air parcels reached Mira Loma.

Figure 5.4a shows a material balance on the fine particle chemical composition at Mira Loma during the September 27–30 episode. Ammonium nitrate is the most abundant species present, followed by organic compounds. In this plot, as well as in mass balance presentations in Figures 5.6, 5.8, 5.10, 5.11 and 5.12, the designation "Unidentified" applies to the difference between mass concentration determined gravimetrically and the sum of species concentrations identified by chemical analysis methods. Silicates and calcium-containing mineral matter are among the materials not detected by the methods used in the present study, and these may be included in the unidentified matter. While samples were equilibrated and weighed in an environment with low relative humidity, some water may have been retained in the samples despite desiccation. "Metals and Metal

Oxides" refers to the sum of trace elements measured by neutron activation analysis, with elemental concentrations converted to the equivalent concentrations of their most common oxides, where appropriate. See Table 4.1 for a list of these oxides and the conversion factors used.

Figure 5.4b shows a material balance on nitrogen-containing air pollutant concentrations present at Mira Loma during the September 27–30 episode. Data are presented in terms of μg of nitrogen m^{-3}. Gas-phase NH_3 data for this sampling period were taken by Dr. Dennis Fitz' group at CE-CERT, UC-Riverside. Ammonia was measured only during daylight hours, 0600–1800. Dashed lines connect the intervals where ammonia data are missing to indicate the extrapolated ammonia concentrations. The most important point demonstrated in Figure 5.4 is that ammonia concentrations are extraordinarily high at the Mira Loma site; so high that virtually all of the HNO_3 produced in the plume downwind of the Los Angeles/Long Beach/Orange County urban complex will be converted to ammonium nitrate aerosol to the extent that that plume passes over the dairy area. The nitrogen species concentrations echo the mid-day minimum concentrations seen on September 28 and mid-day maximum concentrations seen on September 29 in the fine particle species data of Figures 5.3 and 5.4a. NO and NO_2 concentration patterns are similar between the two days. During both days, there is a general increase in NO + NO_2 nitrogen concentrations after 1800, peaking in the 0600–1000 PDT time period, after which NO + NO_2 concentrations decrease, followed by HNO_3 concentration peaks between the hours of 1000 and 1800 PDT.

5.3.2 October 31–November 2, 1997, Sampling Event

During the October 31–November 2, 1997, sampling period, all three of the air monitoring stations were in operation. All three sites had periods of relatively high pollutant concentrations on Friday, October 31, and all three sites experienced drastic reductions in particle concentrations beginning in the morning of November 1 and lasting for the rest of that day. Changing wind patterns account

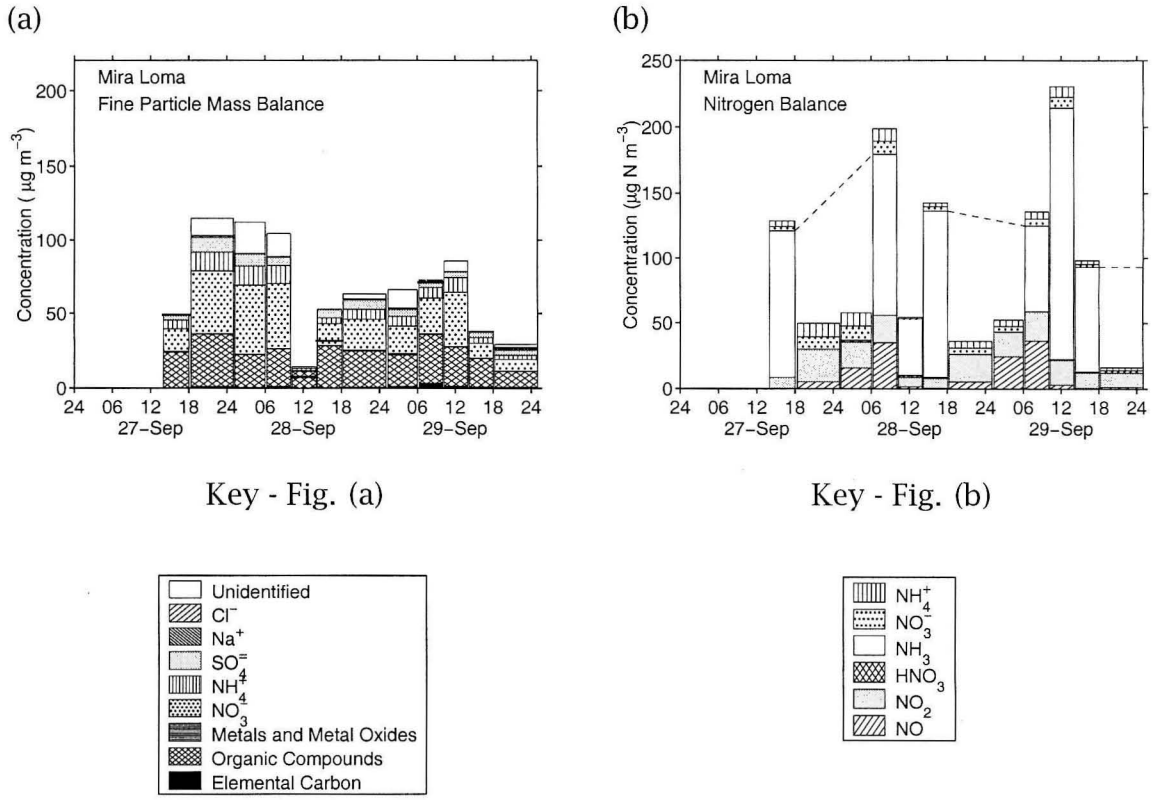

Figure 5.4: (a) Fine particle mass balance and (b) nitrogen species mass balance during sampling at Mira Loma, September 27-30, 1997. NH_3(g) measurements were not taken by CE-CERT at UC-Riverside between the hours of 1800 and 0600 each day; dashed lines indicate the extrapolated overnight ammonia concentrations.

for the sudden change in conditions. During the period of clean air at the end of the day on November 1, incoming air parcels at Mira Loma and Riverside approached from the mountains to the north and northeast instead of from urban and agricultural areas to the west.

Figure 5.5 shows the time series of fine particle mass and major fine aerosol chemical species concentrations at Diamond Bar over the October 31–November 2, 1997, sampling period. Fine particulate mass, NO_3^-, and NH_4^+ concentrations were essentially constant for the first half of the day on October 31. These concentrations are relatively high; fine particle mass averaged 98.6 ± 1.7 $\mu g\ m^{-3}$ of which 40.8 ± 0.7 $\mu g\ m^{-3}$ was particulate NO_3^- and 10.5 ± 0.2 $\mu g\ m^{-3}$ was particulate NH_4^+. The air parcels reaching Diamond Bar during this night and morning period of low-to-stagnant wind speeds approached Diamond Bar from the northeast during a condition of mild off-shore wind flow after having crossed the Pacific Coast along the Santa Monica Bay two to three days earlier. The air mass stagnating overnight at Diamond Bar in this case already contained high particulate ammonium nitrate concentrations. In contrast, air parcels arriving during the 1400–1800 time period were transported by on-shore winds after stagnating only once overnight near Fullerton; these air parcels were over the urban area for a much shorter time, and there are minimums in the particulate NO_3^-, NH_4^+, and fine mass concentrations accordingly. The fine particulate elemental carbon concentration increased by more than a factor of 2.5 during the 0600–1000 PST morning traffic peak period on October 31 when compared to the previous time period. This 0600–1000 PST peak in EC concentrations did not occur on Saturday, November 1, reflecting the differences between weekday and weekend traffic patterns.

Figure 5.6a shows the time series of fine particle concentrations and chemical compositions measured at Diamond Bar during the October 31–November 2, 1997, sampling event. Figures 5.6b and 5.6c show the size-segregated mass distribution and chemical composition of the fine particulate matter ($D_a < 1.8\ \mu m$) at Diamond Bar during the two sampling time periods 1000–1400 PST and 1400–

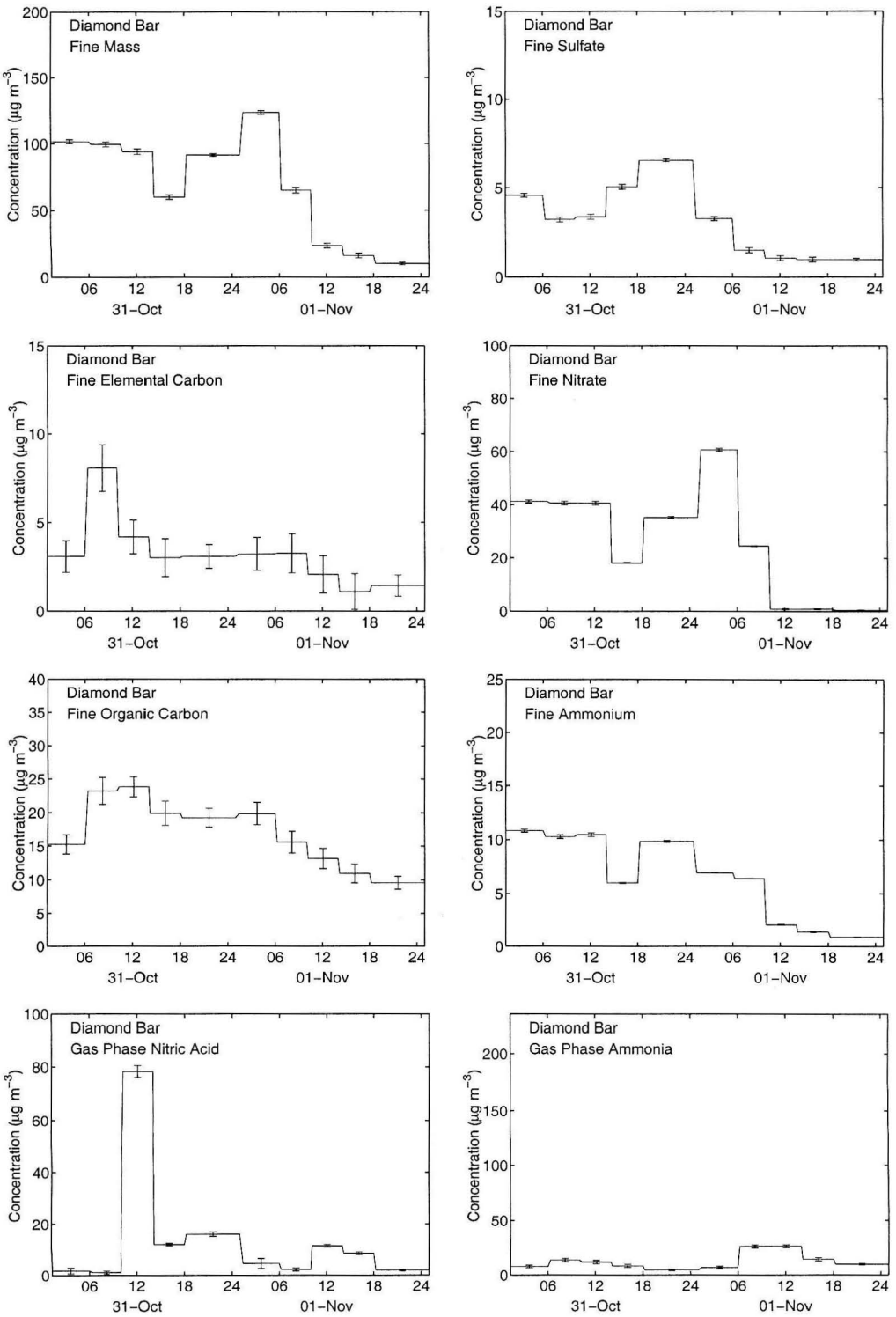

Figure 5.5: Fine particle and gas-phase results for individual species measured during the October 31–November 2, 1997, sampling event at Diamond Bar.

1800 PST on October 31, 1997. The particle size distribution data show that aerosol nitrate accumulation is occurred largely on particles larger than 0.3 μm aerodynamic diameter. The air sampled during the 1000–1400 PST time period stagnated overnight in and to the northeast of the Diamond Bar area; the air sampled in the subsequent time period had been transported from west of Diamond Bar. The decreases in fine particulate NO_3^-, NH_4^+, and mass, the slight decrease in fine aerosol carbon, and the slight increase in fine particle $SO_4^=$ between the two time periods apparent in Figure 5.6a can also be seen in the size-segregated chemical composition data.

Figure 5.7 shows the time series of fine particle mass and major aerosol chemical species concentrations at Mira Loma over the October 31–November 2, 1997, sampling period. Gas phase NH_3 concentrations between 1000 PST and 0100 PST October 31–November 1 were among the highest concentrations measured during the study, peaking at 123.9 $\pm$ 2.3 $\mu g\ m^{-3}$ (equivalent to 180 $\pm$ 3.4 ppb). Fine elemental carbon and organic compound concentrations peaked during the 0600–1000 PST peak traffic period on Friday, October 31. Other fine particulate species remained relatively constant from 0100 through 1000 hours PST on October 31. Air parcel trajectories arriving at Mira Loma changed around 1100 hours PST from a pattern which approached Mira Loma from the north to one which approached Mira Loma from the west. Air parcels arriving after 1100 hours PST contained higher concentrations of fine particulate NO_3^- and NH_4^-, and gas-phase NH_3, and lower concentrations of EC. The center of the Chino dairy area is located to the west of Mira Loma, and thus it is not surprising that the highest ammonia concentrations recorded occur during periods of easterly flow. Overnight between October 31 and November 1 as air parcels stagnated at Mira Loma, the concentrations of all species remained relatively high. As mentioned previously, the wind direction shifted to produce flow from the north after 0700 PST on November 1, resulting in very low fine particle concentrations for the rest of that day.

Figure 5.8a shows a chemical material balance on the time series of fine parti-

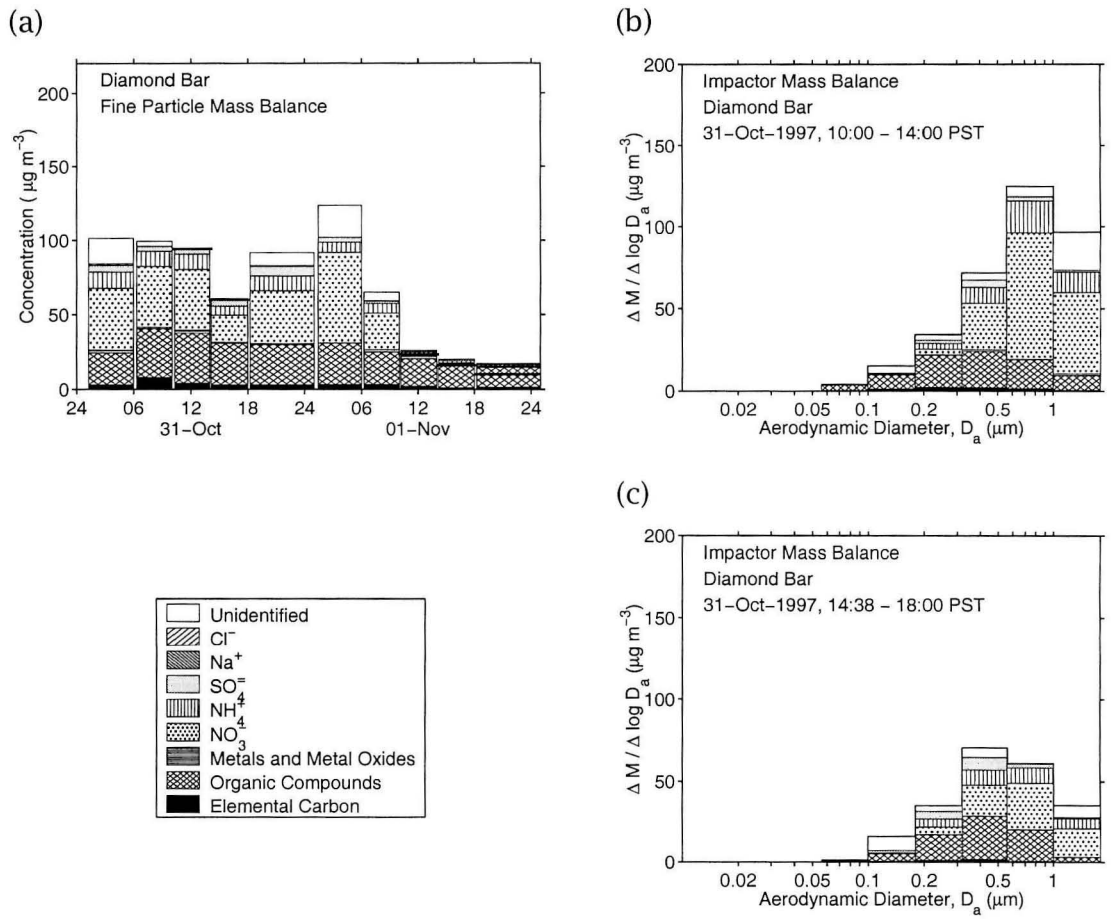

Figure 5.6: Fine particle concentration and chemical composition at Diamond Bar. (a) Bulk fine particle concentrations and chemical compositions measured during the October 31–November 2, 1997, sampling event. (b) Size-resolved fine particle mass distribution and chemical composition measured on October 31, 1997, during the 1000–1400 PST sampling period. (c) Size-resolved fine particle mass distribution and chemical composition measured on October 31, 1997, during the 1400–1800 PST sampling period.

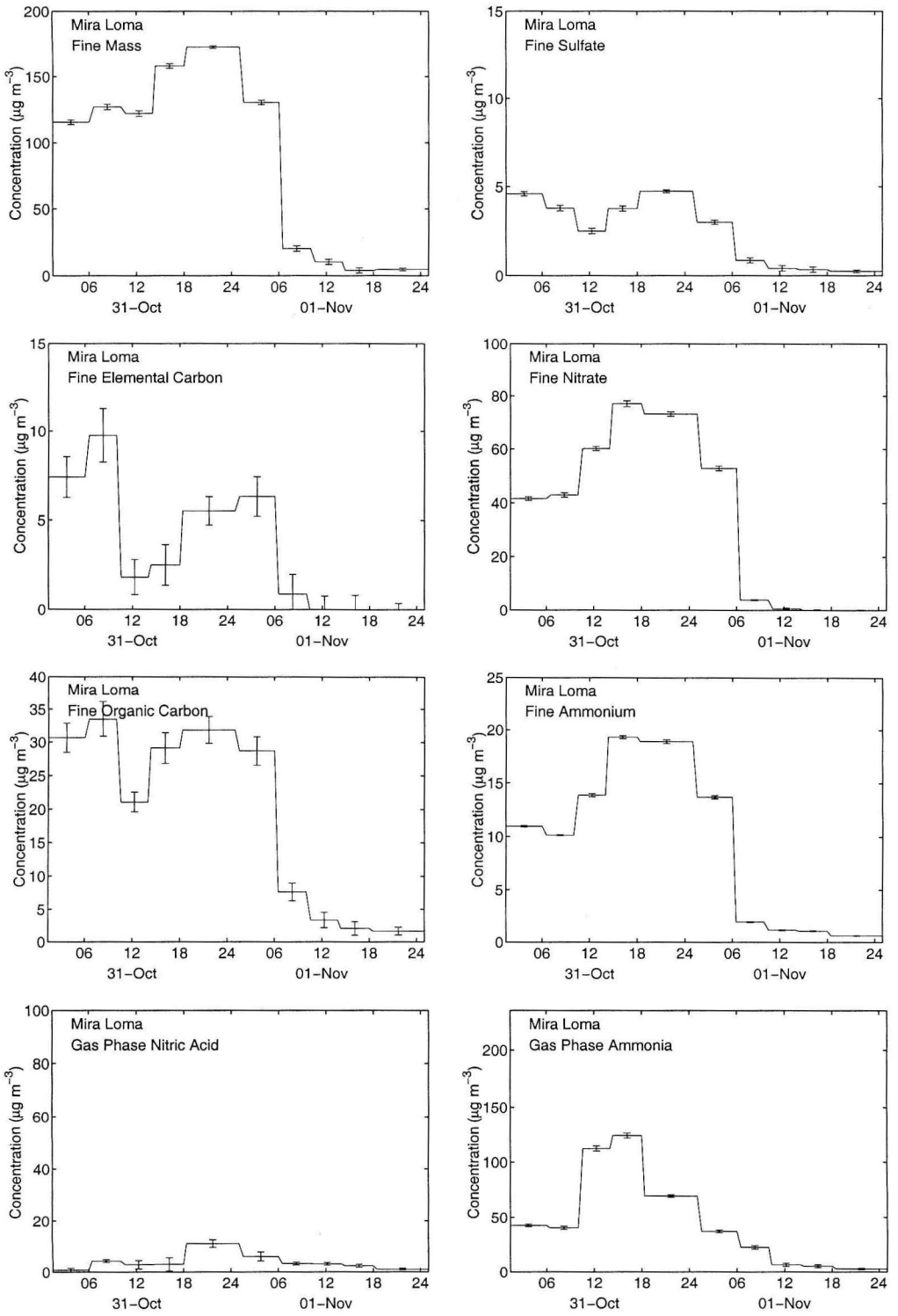

Figure 5.7: Fine particle and gas-phase results for individual species measured during the October 31–November 2, 1997, sampling event at Mira Loma.

cle concentrations and chemical compositions measured at Mira Loma during the October 31–November 2, 1997, sampling event. Figures 5.8b and 5.8c show the size-segregated mass distribution and chemical composition of the fine particulate matter ($D_a < 1.8$ μm) at Mira Loma as measured by the cascade impactors during the two sampling time periods 1000–1400 PST and 1400–1800 PST on October 31, 1997. Increases in fine particle mass, EC, organic compounds, NO_3^-, $SO_4^=$, and NH_4^+ between the mid-day and afternoon time periods seen in Figure 5.8a also can be seen in the size-segregated fine particle composition data as well. Again, the greatest accumulation of nitrate occurred on particles larger than 0.3 μm aerodynamic particle diameter.

Figure 5.9 shows the time series of fine particle mass and major aerosol chemical species concentrations at Riverside over the October 31–November 2, 1997, sampling event. Elemental carbon concentrations were relatively constant through October 31 and the following morning. Fine particulate mass, organic compounds, NH_4^+, and NO_3^- peaked during the 1400–1800 PST time period on October 31; wind speeds increased at this time after the overnight stagnation period ended, thereby transporting more polluted air parcels into Riverside from the west. $SO_4^=$ concentrations peaked at 3.0 ± 0.1 $\mu g\ m^{-3}$ in the 1800–0100 PST period.

Figure 5.10a shows a material balance on the time series of fine particle concentrations and chemical compositions measured at Riverside during the October 31–November 2, 1997, sampling event. Figures 5.10b and c show the size-segregated mass distribution and chemical composition of the fine particulate matter ($D_a < 1.8$ μm) at Riverside as measured from the cascade impactor samples during the two sampling time periods 1000–1400 PST and 1400–1800 PST on October 31, 1997. Again, the ammonium nitrate concentration increase between these two time periods occurs in the form of additional ammonium nitrate accumulation in particles larger than 0.3 μm aerodynamic diameter.

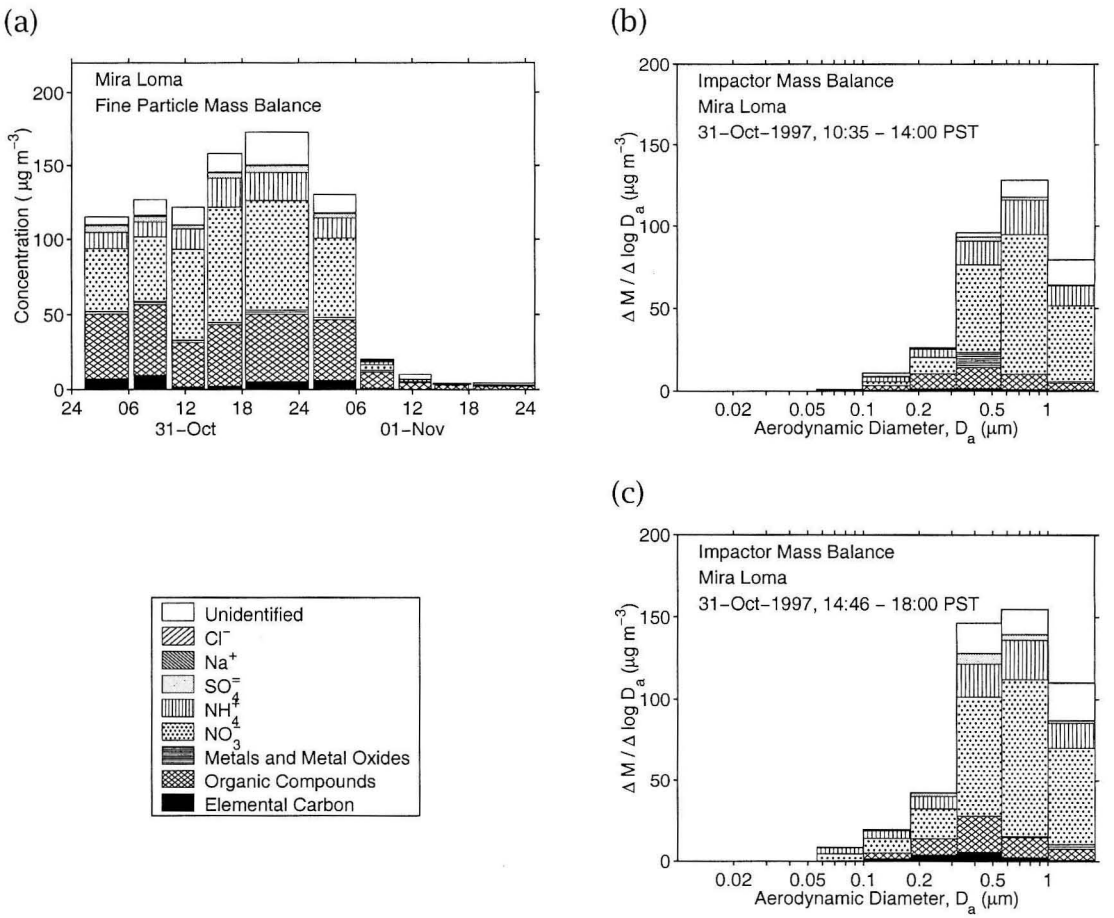

Figure 5.8: Fine particle concentration and chemical composition at Mira Loma. (a) Bulk fine particle concentrations and chemical compositions measured during the October 31-November 2, 1997, sampling event. (b) Size-resolved fine particle mass distribution and chemical composition measured on October 31, 1997, during the 1000-1400 PST sampling period. (c) Size-resolved fine particle mass distribution and chemical composition measured on October 31, 1997, during the 1400-1800 PST sampling period.

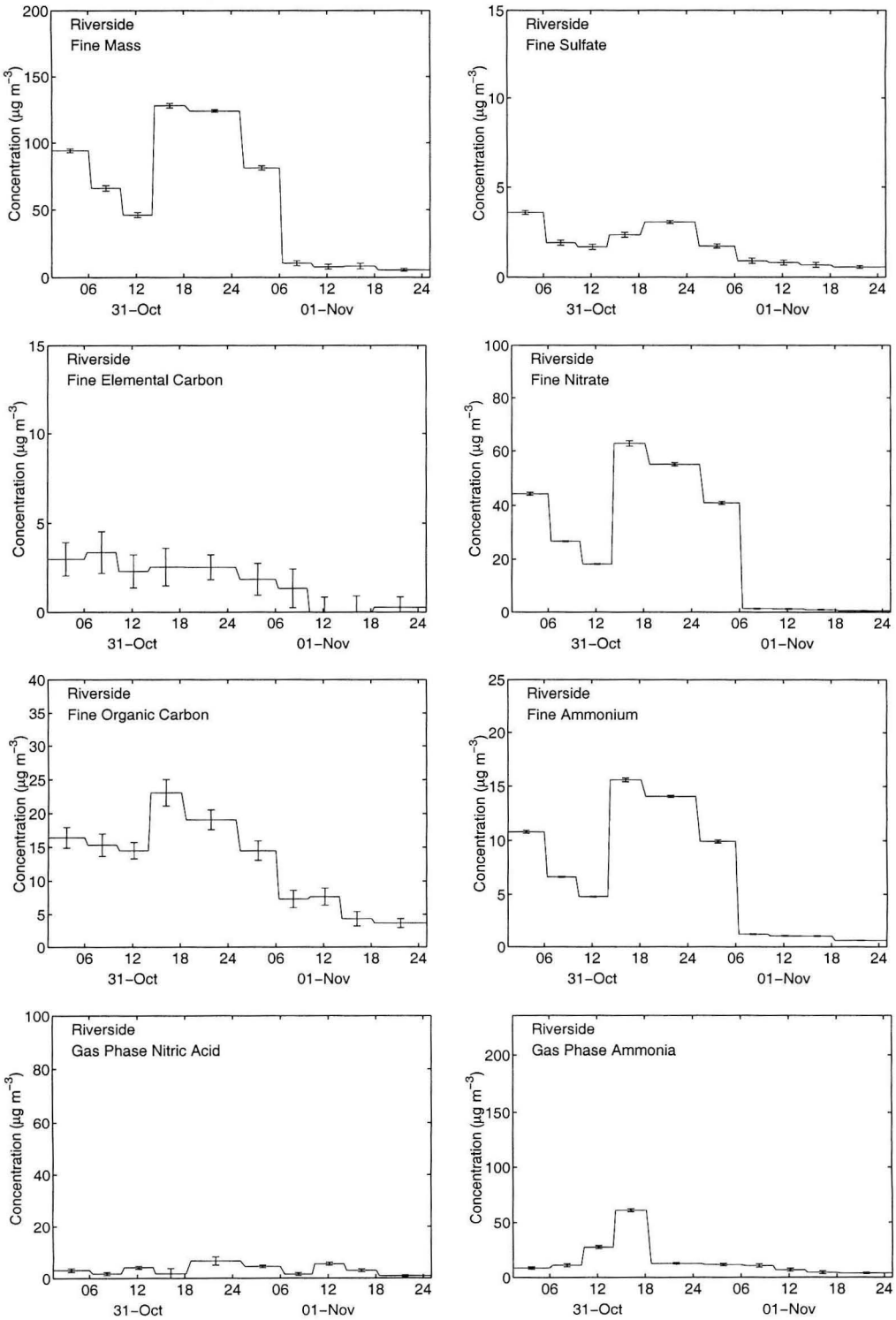

Figure 5.9: Fine particle and gas-phase results for individual species measured during the October 31–November 2, 1997, sampling event at Riverside.

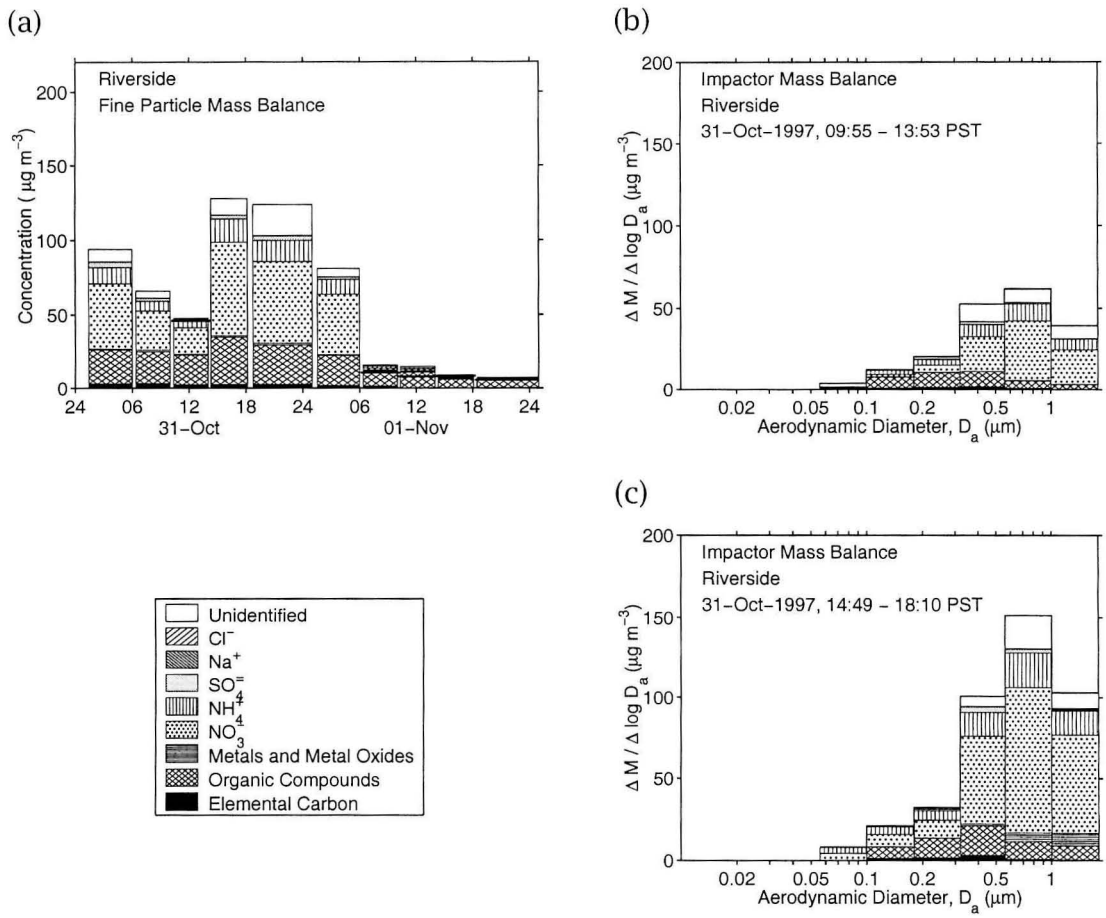

Figure 5.10: Fine particle concentration and chemical composition at Riverside. (a) Bulk fine particle concentrations and chemical compositions measured during the October 31–November 2, 1997, sampling event. (b) Size-resolved fine mass distribution and chemical composition measured on October 31, 1997, during the 1000–1400 PST sampling period. (c) Size-resolved fine mass distribution and chemical composition measured on October 31, 1997, during the 1400–1800 PST sampling period.

5.3.3 Evolution Along Air Parcel Trajectories

Several air parcel trajectories during the October 31–November 2 sampling event passed over or near two of the three air monitoring stations in succession, allowing a comparison of the pollutant concentrations and aerosol populations within single air parcels as pollutants age in the presence of continuing emissions and dry deposition.

The first of these air parcel trajectories to be discussed is shown in Figure 5.11a; each open circle indicates the air parcel location at successive hours during transport across the air basin. Trajectory analysis shows that an air parcel passing within 5 km of Diamond Bar between 0830–0930 hours PST on October 31 later was advected across the ammonia sources in the Chino dairy area and arrived within 5 km of the Mira Loma site between 1800–2200 PST later that day. Study of particle evolution within this air parcel provides direct insight into the effect of transport across the largest ammonia source area in Southern California. A material balance on the nitrogen-containing pollutants within this air parcel is shown in Figure 5.11b. The air parcel begins its travels that morning at Diamond Bar with more than 100 μg N m^{-3} present as NO and lesser quantities of NO_2; nitric acid concentrations initially are close to zero while excess NH_3 is still present in the gas phase, indicating that NH_4NO_3 present at Diamond Bar is limited by the amount of inorganic nitrate (e.g., HNO_3) available to form aerosol. Figure 5.11b shows that NO is converted to NO_2 during transport from Diamond Bar to Mira Loma; that same reaction system will lead eventually to NO_2 oxidation to form additional nitric acid. Ammonia concentrations increase by more than a factor of 5 between Diamond Bar and Mira Loma as the air parcel passes over the local ammonia sources. The additional ammonia drives the additional HNO_3 formed into the particle phase and aerosol nitrate concentrations increase, as shown in Figure 5.11c.

Trajectory analysis also shows that the air parcels stagnating near the Riverside air monitoring station in the early morning hours (0100–0800 PST) of Novem-

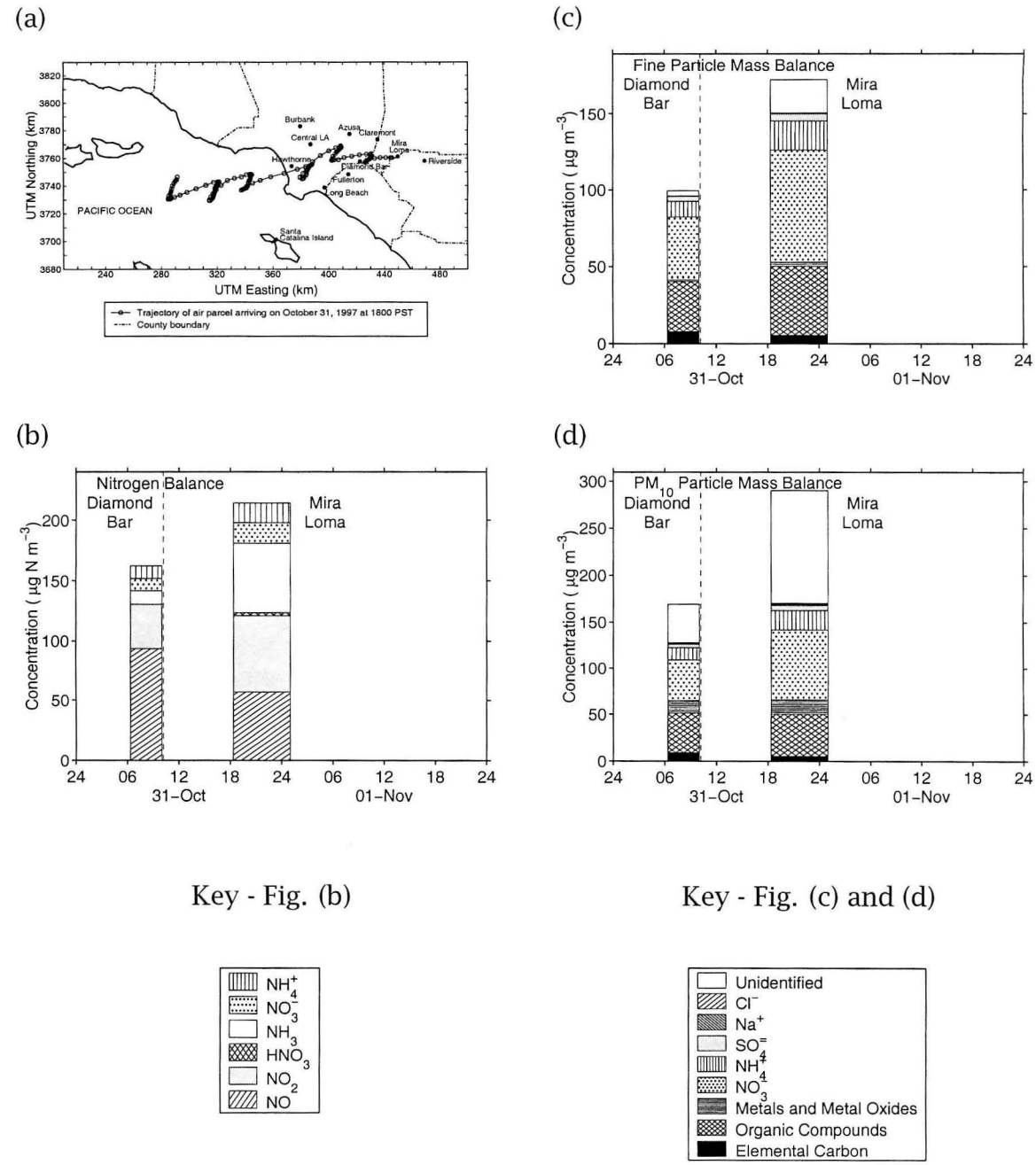

Figure 5.11: Aerosol evolution along the trajectory between Diamond Bar and Mira Loma, October 31–November 1, 1997. a) Representative air parcel trajectory which reached Mira Loma at 1800 PST November 1, 1997. The air parcel passed within 5 km of Diamond Bar at 0830–0930 PST on October 31 before being transported to near Mira Loma during 1800–2200 PST later that day. Each circle represents an elapsed hour. b) Nitrogen balance, c) Fine particle mass balance, and d) PM_{10} mass balance.

ber 1 passed slowly near the monitoring station at Mira Loma approximately 24 hours earlier, on October 31 from about 0100–0700 hours PST. This air parcel path is shown in Figure 5.12a; again, each open circle indicates the air parcel location at successive hours. This air parcel was over land for approximately 3 days before arriving at Mira Loma, and was over land for 4 days before arriving at Riverside.

Figures 5.12b, c, and d show a material balance on the nitrogen-containing pollutant, fine particulate matter, and PM_{10} concentrations present over time within that air parcel. NH_3 concentrations at Riverside decreased to about 25% of the concentration present at Mira Loma, within the NH_3 source area. This NH_3 concentration decrease is consistent with the dilution expected as one moves away from the virtual point source of ammonia in the Chino dairy area (see Russell et al., [38]). NO_3^- and NH_4^+ concentrations are approximately the same at both Mira Loma and Riverside, reflecting a balance between NH_4NO_3 aerosol formation versus pollutant dispersion and dry deposition. PM_{10} mass decreased proportionally more than fine particle mass; the 24-h transit time facilitated deposition of PM_{10}.

A final perspective on the aerosol nitrate formation problem in the South Coast Air Basin can be gained from Figure 5.13. That figure shows a nitrogen balance on the air masses over consecutive time periods at all three air monitoring sites over the October 31–November 2 sampling period. Generally, NO and NO_2 concentrations are much higher than either HNO_3 concentrations or aerosol nitrate concentrations. Thus the precursor gases needed for more HNO_3 production are available in abundance. Excess ammonia is present at most times, thus any HNO_3 formed usually will be driven quickly into the aerosol phase. Although the aerosol nitrate concentrations are small relative to the total nitrogen burden in the atmosphere, the resulting NH_4NO_3 aerosol is large in comparison to both other aerosol species as well as the fine particle air quality standards recently proposed by the US EPA.

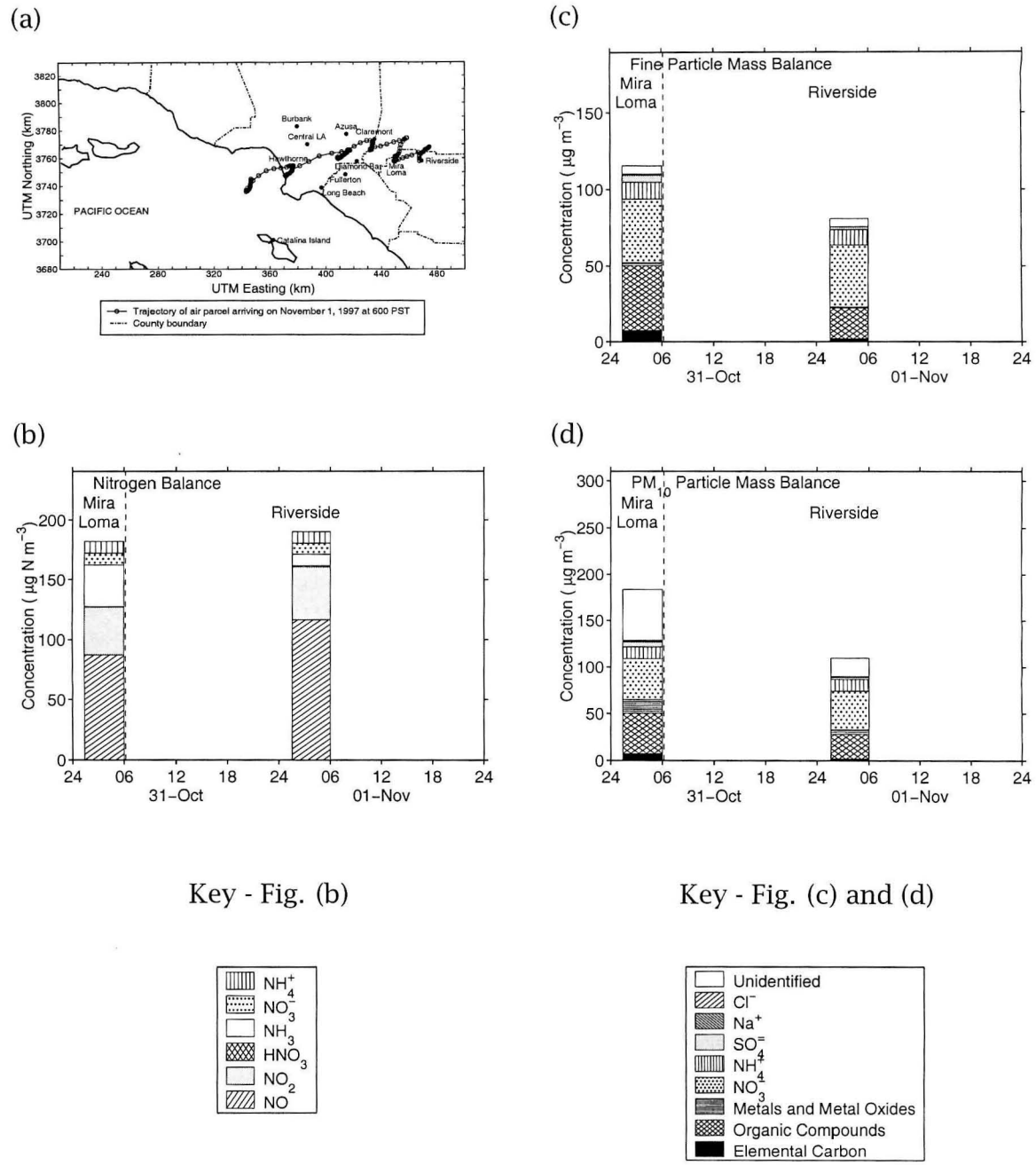

Figure 5.12: Aerosol evolution along the trajectory between Mira Loma and Riverside, October 31–November 1, 1997. a) Representative air parcel trajectory which reached Riverside at 0600 PST November 1, 1997. The air parcel passed within 5 km of Mira Loma during 0100–0700 PST on October 31 before passing within 5 km of Riverside during 0100–0800 PST on November 1. Each circle represents an elapsed hour. b) Nitrogen balance, c) Fine particle mass balance, and d) PM_{10} mass balance.

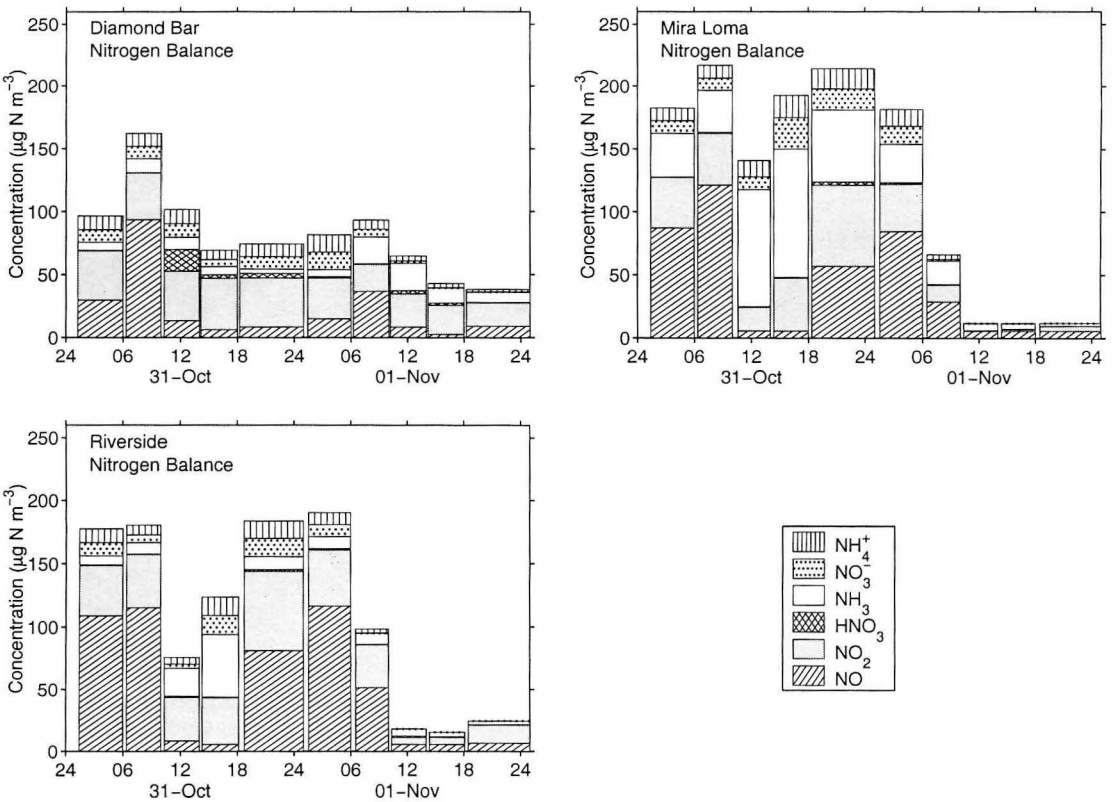

Figure 5.13: Nitrogen balances at the three sites monitored during the October 31–November 2, 1997, sampling event.

5.3.4 Changes in the Riverside Aerosol at the Single Particle Level

In addition to the bulk and size-segregated samples taken during this study, an ATOFMS instrument gathered continuous data on single particle size and chemical composition at the Riverside monitoring site during the October 31–November 2 sampling period. While single particle data are not available for multiple points along an air parcel trajectory, interesting observations can be made at the single particle level at the Riverside location. Each particle is categorized according to whether it contains one or more of a number of major chemical species, as determined by the presence of key indicator ions. Particle counts are corrected according to the counting efficiency as a function of particle size of the Riverside ATOFMS instrument, determined through comparison of ATOFMS data to impactor data at that site throughout the study [58]. The particle categorizations and the rules by which they are defined are described here generally; precise definitions are given in Table 5.1. Relative peak area is defined as the ratio of the area of a given mass spectrum peak to the total peak area of the mass spectrum. Sodium is indicated by a peak at mass-to-charge ratio (m/z) 23 (Na^+); ammonium by m/z 18 (NH_4^+); nitrate by m/z 30 (NO^+) or 108 ($Na_2NO_3^+$); carbon by m/z 12 (C^+), 36 (C_3^+), 37 (C_3H^+), 60 (C_5^+), or 72 (C_6^+); and soil or dust by large peaks at m/z 7 (Li^+), 27 (Al^+), 40 (CaO^+), 56 (Fe^+/CaO^+), or 96 (Ca_2O^+). Studies of local soil samples have also shown that a very large peak at low mass-to-charge ratios (m/z < 2.5) is a unique indicator of a soil particle. The ATOFMS instrument at Riverside is able to detect either positive or negative ion spectra for a particle, and during this study it was operated mainly in positive ion mode. Sulfate particles are not categorized here, because the SO_4^- ion was not measured. Details on the criteria used for considering that a given peak is present in a mass spectrum are given in Table 5.1. These criteria differ from those presented in Table 4.2 because the laboratory-bound instrument in Riverside is of a different design than the transportable ATOFMS instruments.

Figures 5.14 and 5.15 each show the character of the size-segregated particle

Table 5.1: Criteria used for classifying particle mass spectra.

Class	Ion	m/z[a]	Peak Search Rules
Sodium	Na^+	23	Peak Area > 100
Ammonium	NH_4^+	18	Peak Area > 30
Nitrate	NO^+	30	Peak Area > 30 OR
	$Na_2NO_3^+$	108	Peak Area > 50
Carbon	C^+	12	Peak Area > 50 OR Relative Peak Area > 0.5% OR
	C_3^+	36	Peak Area > 50 OR Relative Peak Area > 0.5% OR
	C_3H^+	37	Peak Area > 50 OR Relative Peak Area > 0.5% OR
	C_5^+	60	Peak Area > 50 OR Relative Peak Area > 0.5% OR
	C_6^+	72	Peak Area > 50 OR Relative Peak Area > 0.5%
Dust	Fe^+/CaO^+	54-57	Peak Area > 1500 OR
	Al^+	25.5-28	Peak Area > 1500 OR
	H^+	0.5-2.5	Peak Area > 1500 OR
	Li^+	5-9	Peak Area > 200 OR
	CaO^+	40	Peak Area > 2500
	Ca_2O^+	96	Peak Area > 100 AND no peak at m/z=72 (C_6^+)[b]
All			Total Positive Spectrum Area > 100

[a] Unless otherwise specified, m/z range is ±0.5

[b] Restriction on C_6^+ limits C_8^+ interference at m/z=96

populations as determined by classification of particle mass spectra during sampling periods of October 31–November 1, 1997, at Riverside. Each of the 100 dots within a square plot represents one percent of the particle population at the time and location indicated within the specified aerodynamic diameter range. Each dot is striped with the colors that correspond to the indicator ion peaks found within a particular one percent of the particles. The exception to this rule is the dust category; all dust-containing particles are represented as solid gray dots because the peaks associated with dust often have areas so large that they blow scale and produce noise in the rest of the mass spectrum, making detection of any other peaks unreliable. Therefore, any or all of the other classified species may be present in the particles represented by a "dust" dot. A color stripe only qualitatively indicates the presence of the corresponding chemical species; no conclusions can be drawn about the relative amounts of each substance. The ATOFMS detection sensitivity varies widely by ion; the instruments are approximately 71 times more sensitive to Na^+ than to NH_4^+, for example. This explains the prominent appearance of sodium in Figures 5.14 and 5.15 while sodium was found in impactor samples at concentrations so small that it cannot be seen separately in the plots of Figure 5.10. Only the presence or absence of these six major substances was considered in producing Figures 5.14 and 5.15. The presence of one or a few colors in a dot does not necessarily imply that those particles are of "simple" composition, as any number of species that were not included in the analysis may also be present. This is especially true for the laboratory-based ATOFMS instrument at Riverside, as many particles are hit "lightly," yielding mass spectra with few peaks and small peaks. In these cases, the ions to which the instrument is less sensitive may be present in the particles, but may remain undetected. This situation was partially mitigated by considering only those mass spectra which had a total peak area of at least 100 arbitrary units. The "many types" category, shown in purple, is the sum of those particle types which each encompass less than approximately 0.5% of the particle population and which would therefore not warrant representation by an entire dot.

From the early morning of October 31 and through the early morning of November 1, air parcels approached Riverside from the east after crossing over urban pollution sources and the Chino dairy area. Figure 5.14 shows that the qualitative character of the particle population changed very little throughout October 31. This agrees with the size-segregated impactor data presented in Figures 5.10b and c, in which relative aerosol chemical compositions are proportionally very similar, though concentrations were higher in the 1400–1800 PST time period than in the 1000–1400 PST time period. Particles larger than 1.8 μm are largely dust-containing, and carbon-containing particles dominate the smaller sizes, often also containing ammonium and nitrate. There are peaks in the percentage of particles classified as "carbon only" in the smallest size range ($0.32 < D_a < 0.56$ μm) in the 0600–1000 PST and 1800–0100 PST time periods, perhaps due to fresh motor vehicle emissions from nearby traffic.

During the morning of November 1, 1997, the wind at all three air monitoring sites changed direction. The new wind direction approached Riverside from the northeast, from over the mountains. This air was much cleaner than the air from the west, as evidenced by the 87% drop in fine particle mass concentration and 75% drop in PM_{10} mass concentration between the 0100–0600 PST and 0600–1000 PST sampling periods on November 1 at Riverside (see Figure 5.9). Counting efficiency-corrected particle counts recorded by the ATOFMS instrument within the size range $0.32 < D_a < 3.50$ μm dropped from 1.2×10^8 particles during the 0100-0600 PST period to 1.7×10^7 particles during the 0600-1000 PST time period, a decrease of 86%. Figure 5.15 shows the results of the categorization of the counting efficiency corrected particles during a time period before (0100–0600 PST) and a time period after (1000–1400 PST) this wind direction change on November 1. The character of the particle population before the shift in wind direction is similar to what was seen on October 31 (see Figure 5.14): dust-containing particles at sizes larger than 1.8 μm and smaller particles contining mainly carbon, usually also containing ammonium and nitrate. However, after the wind shift, there is a much larger proportion of dust-containing parti-

Figure 5.14: The chemical compositions of size-segregated particle populations at Riverside on October 31, 1997, as measured by the ATOFMS instruments. Each dot represents one percent of the particle population within the indicated aerodynamic particle diameter range.

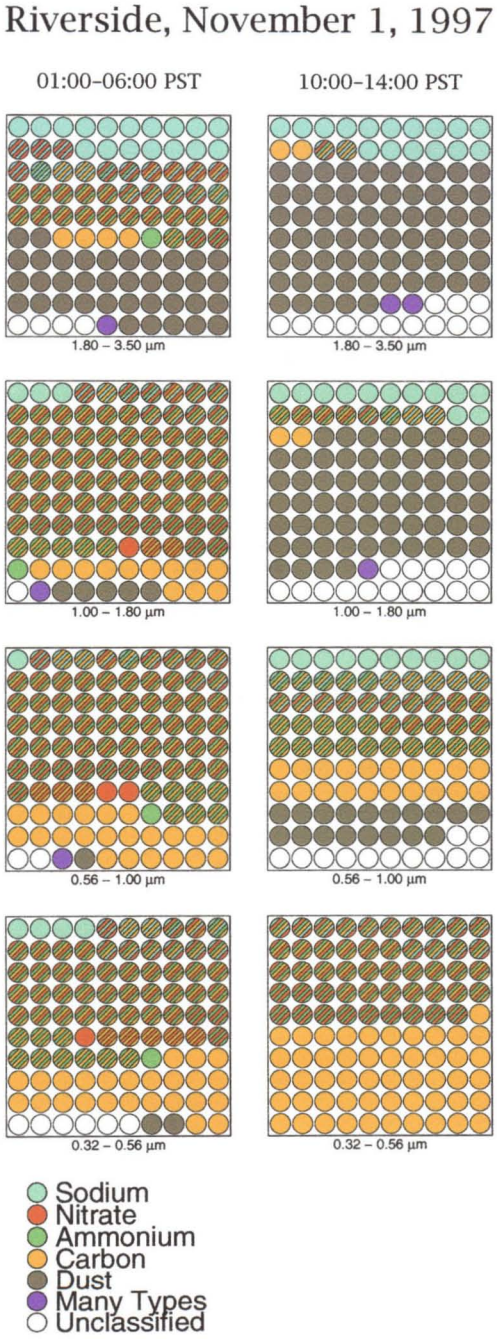

Figure 5.15: The chemical compositions of size-segregated particle populations as measured by the ATOFMS instruments at Riverside on November 1, 1997, before (0100-0600 PST) and after (1000-1400 PST) the shift in wind direction. Each dot represents one percent of the particle population within the indicated aerodynamic particle diameter range.

cles at larger sizes and a larger proportion of “carbon only” particles at smaller sizes.

Chapter 6

Physical and Chemical Characterization of Atmospheric Ultrafine Particles in the Los Angeles Area

6.1 Introduction

Recent epidemiological studies that have examined air pollutant concentrations in relation to health statistics conclude that elevated fine particulate matter concentrations ($D_p \leq 2.5\ \mu m$) are associated with increased mortality and morbidity [1, 2]. Effects are reported at total particulate matter concentrations below 100 $\mu g\ m^{-3}$; in some cases there is no easily discerned threshold concentration below which the adverse effects of particulate matter exposure are seen to vanish. The particulate concentrations reported to be associated with adverse effects in epidemiological studies are much lower than those observed to cause health effects in laboratory toxicology studies, and toxicologists historically have not been able to demonstrate the mechanisms by which such low fine particulate matter concentrations might cause serious health damage [107]. Motivated by

Reproduced with permission from "Physical and Chemical Characterization of Atmospheric Ultrafine Particles in the Los Angeles Area," by L. S. Hughes, G. R. Cass, J. Gone, M. Ames, and I. Olmez; *Environmental Science and Technology*, 32:1153-1161, 1998.

this paradox, there is particular interest in examining those aspects of airborne particulate matter that might be capable of producing injury while at the same time not contributing greatly to measured airborne particle mass concentrations.

Certain toxicological investigations suggest that atmospheric ultrafine particles may be responsible for some of the adverse effects observed due to exposure to atmospheric particulate matter concentrations. For the purposes of the present discussion, ultrafine particles will be defined in accordance with current practice in the community of toxicologists as those particles which are smaller than about 0.1 μm in diameter. Many thousand particles of that size may be present within each cm^3 of outdoor air while at the same time accounting for a negligibly small fraction of the airborne particle mass concentration. Several current hypotheses about the possible mechanisms for damage to the respiratory system due to ultrafine particles give clues as to the particle chemical properties that might be important. Oberdorster et al. [3–6] have proposed that ultrafine particles even at small mass concentrations may have serious negative health effects because of their high number concentration and ability to penetrate into the interstitial space of the lungs; it is possible that the sheer number of such particles can overwhelm the alveolar macrophages, whose job it is to clear the lungs of inhaled substances. In this case the distinction between solid particles such as black carbon versus nearly neutralized soluble particulate components such as ammonium sulfate aerosol might be expected to be important, because if the ultrafine particles were soluble they could be cleared without requiring the intervention of particle-scavenging macrophages. Ironically, it is also conceivable that when subjected to a high ultrafine particle number concentration, "overload" may occur, in which the alveolar macrophages themselves cause injury to the lungs by releasing excessive quantities of oxygen radicals, proteases, and certain proteins [3]. Alternatively, others have suggested that ultrafine particles coated with unneutralized strong acids may, upon deposition, cause tissue damage due to their acidity [108–110]. In that case a finding that ultrafine particles were largely made of sulfuric acid would be an interesting result. In addition, acids or

catalytic metals on the surfaces of irritant particles can be more efficiently transferred to the lungs by ultrafines than by an equal mass of larger particles. This is both because of the larger surface area to mass ratio inherent in the smaller particles and because the ultrafines have a higher deposition efficiency in the alveolar region. Finally, investigators have suggested that trace metals distributed widely throughout the lung on ultrafine particles could catalyze the formation of oxidants within the lung which in turn produce tissue damage [111, 112]. In this case a finding that ultrafine particles contained catalytically active species such as Fe, Mn, V, or Ni from metallurgical fumes or fuel combustion, or Pt, Pd and Rh from motor vehicle catalytic converters, or Lanthanide series catalysts (e.g., Ce) could be significant.

If these distinctions attributed to ultrafine particles turn out to be physiologically important, they may help to explain the difference between epidemiological findings inferred from exposure to real ambient particles versus those laboratory toxicology studies that in the past have been based largely on synthetic, pure-substance, lab-generated aerosols consisting of smaller number concentrations of circa 0.5 μm diameter (fine, but not ultrafine) particles. The few inhalation experiments that have been conducted to date using ultrafine particles have been conducted with model Teflon and TiO_2 aerosols [3, 5-7]. In order to construct future experiments that represent ambient atmospheric ultrafine particles as accurately as possible, it is first necessary to know the chemical composition of actual atmospheric ultrafine particles.

Though ultrafine number concentrations may be large, ultrafine mass concentrations are so small that they are in no way constrained by current air quality standards. Over the past decade, national ambient air quality standards in the United States for particles smaller than 10 μm in diameter (PM10) required that ambient particle mass in that size range not exceed 150 $\mu g\ m^{-3}$ over 24-h periods, nor average more than 50 $\mu g\ m^{-3}$ on an annual basis. Recently adopted new national ambient air quality standards for fine particles smaller than 2.5 μm in diameter limit fine particle concentrations such that they should not exceed

65 $\mu g\ m^{-3}$ over 24-h periods or 15 $\mu g\ m^{-3}$ as an annual average. The ultrafine particles studied here constitute only a small fraction of the new fine particle mass concentration limit. For that reason emission control strategies designed to attain the new fine particle standards will not necessarily have to reduce ultrafine particle concentrations in order to meet the required mass concentration limits. Ultrafine particles are emitted from certain sources, particularly combustion sources [53, 113]. Controls applied to combustion sources for the purposes of meeting fine particle standards directed mainly at control of somewhat larger accumulation mode particles may or may not have the indirect effect of lowering ultrafine particle concentrations as well. While control equipment applied to stationary combustion sources (e.g., electrostatic precipitators, bag houses) may more effectively reduce ultrafine particle emissions than is the case for accumulation mode fine particles [114], design changes applied to other combustors to reduce particle mass emissions may not have a similar effect. That a reduction in ultrafine particles is by no means assured is indicated by recent examination of particles emitted from a newer (1991) diesel engine in which ultrafine particle emissions increased relative to 1988 engines even as particle mass emission rates were decreased [115, 116]. This could occur if the newer engine causes incomplete burnout of soot particles, causing particle agglomerates to disintegrate into many smaller particles in a manner somewhat analogous to the production of many small particles from the combustion of a single coal particle (see Figure 6.13 of [114]). Ultrafine particle emissions measurements must be made on a larger number of engines before the observations to date can be generalized.

Little work has been done to simultaneously measure both the number distribution and chemical composition of atmospheric ultrafine particles in an urban environment. Number counts for particles in this size range were obtained as early as the 1930's using Aitken's condensation nucleus counter. Detailed size distribution measurements for ultrafine particles were later acquired using electrical mobility analyzers. For example, the 1969 Pasadena Smog Aerosol Project [117, 118] made use of such an instrument, an automated Whitby Aerosol

Analyzer (WAA) [119] to measure the particle number distribution over the particle diameter range 0.0075–0.6 μm; two Lundgren impactors [120] were also used in that project to measure particle mass concentration and chemical composition, but the size range over which those impactors operate did not extend to the very small sizes needed to specifically examine the chemical composition of the ultrafines.

More recently, cascade impactors have been developed which can collect particles within the ultrafine size range, allowing chemical analysis as well as mass distribution measurement to take place more readily. The low pressure impactor (LPI) designed by Hering (size range 0.05–4.0 μm) [121] was used to collect fine and ultrafine particles in the desert at Zilnez Mesa, AZ, followed by analysis for sulfur compounds by flash volatilization/flame photometric detection and elemental analysis by PIXE [122]. The aim of those measurements was to determine the light scattering coefficient of various-sized particles. During the 1987 Southern California Air Quality Study (SCAQS), a variety of impactors were deployed simultaneously to measure a broader range of aerosol chemical components. Berner impactors (size range 0.075–16 μm) [123] were used for inorganic ions analysis [41]; Micro-Orifice Uniform Deposit Impactors (MOUDIs), size range 0.056–18 μm, were used for organic carbon and elemental carbon particle size distributions [42, 43]; and a Davis Rotating drum Unit Monitoring (DRUM) sampler (size range 0.069–8.54 μm) [44] was deployed to obtain elemental composition data by PIXE analysis [44]. The impactor data from the SCAQS study are presented separately for the various chemical components measured, and for that reason an overall picture of ultrafine aerosol composition is difficult to glean.

Other chemical analyses of size-segregated atmospheric aerosol samples include the work of Dodd et al. [124], who measured the concentrations of 44 elements in rural air using a prototype horizontally configured micro-orifice impactor [125] with a particle diameter size range of 0.083–1.03 μm and an 8-stage MOUDI (size range 0.092–4.9 μm). Measurements made at the Grand Canyon as part of the 1990 Navajo Generating Station Visibility Study [24, 126] included

size-segregated samples collected with three simultaneously operated MOUDIs, for the ultimate purpose of studying the hygroscopicity of ambient particles in the desert southwestern U.S. These samples were analyzed for elemental and organic carbon concentrations, for trace elements by PIXE, and for $SO_4^=$ and NO_3^- by ion chromatography.

The aim of the present paper is to describe a measurement program designed to systematically measure both the number distribution and chemical composition of the ultrafine particles present in polluted urban air. In order to collect comprehensive data on number counts, size, and composition, particle counters and several impactors running at the same time are needed, in effect the simultaneous application of all of the individual techniques noted above. Accordingly, these experiments were conducted using a high resolution scanning differential mobility analyzer and condensation nucleus counter (DMA/CNC), a laser optical counter (OPC) and a pair of identical impactors (Micro-Orifice Uniform Deposit Impactors, abbreviated MOUDI when rotated and MOI when not rotated). Samples were analyzed to create a material balance on the chemical composition of the ultrafine particles. Comparisons will be made to the composition and mass concentration of the entire fine particle complex ($D_p < 2\ \mu m$) in order to explore the extent to which the properties of ultrafine particles can or cannot be judged from more widely available fine particle filter data.

6.2 Experimental Methods

Size distribution measurements and sampling of fine and ultrafine ambient particles were carried out over the course of one winter month in January and February, 1996. Measurements were made at six-day intervals from a rooftop in Pasadena, California, and all instruments were operated continuously for a 24-h period during each sampling event. Two cascade impactors, a differential mobility analyzer/CNC combination, a laser optical particle counter, and a filter-based fine particle sampler were all operated simultaneously and used to obtain

several different measurements of particle number distribution, mass concentration, and chemical composition. A schematic diagram of the equipment used is presented in Figure 6.1.

A differential mobility analyzer (DMA, TSI Inc., Model 3071) was used in conjunction with a condensation nucleus counter (CNC, TSI Inc., Model 3760) to measure particle number concentrations in 175 size intervals over the particle size range $0.017 < D_p < 0.250$ μm. The ultrafine particle size range, $D_p < 0.1$ μm, was examined in 120 measured size intervals. Both instruments were interfaced with a personal computer which operated the DMA as a scanning electrical mobility spectrometer [127] and enabled the acquisition of particle number distributions over the complete range of sizes every 90 seconds during each 24-h period studied.

A laser optical particle counter (OPC, Particle Measuring Systems, Model ASASP-X) was used to corroborate the size distribution data from the DMA/CNC combination over the size range where the two instruments overlap and to extend size distribution measurements to larger particle sizes. This instrument recorded particle number distributions in 31 channels over the size range $0.090 < D_p < 3.0$ μm every 4–10 seconds.

Two 10-stage Micro-Orifice Uniform Deposit Impactors (MOUDI, MSP Corp., Model 100) [59] were simultaneously operated to measure 24-h average fine particulate mass and chemical composition as a function of particle size. A Teflon-coated cyclone separator was placed ahead of the inlet of each impactor in order to capture coarse particles ($D_a > 1.8$ μm) that might otherwise enter the impactor and distort the mass distribution measurements by bouncing from their appropriate collection stages. The fine and ultrafine particles reported here were collected on stages 5–10 of the impactors over the size range from 0.056–1.8 μm particle diameter; the upper stages of the impactor also were loaded with impaction substrates, but were not analyzed chemically. An afterfilter downstream of the impaction stages collected particles smaller than 0.056 μm diameter. One impactor was equipped with aluminum foil substrates (MSP Corp.) and a quartz

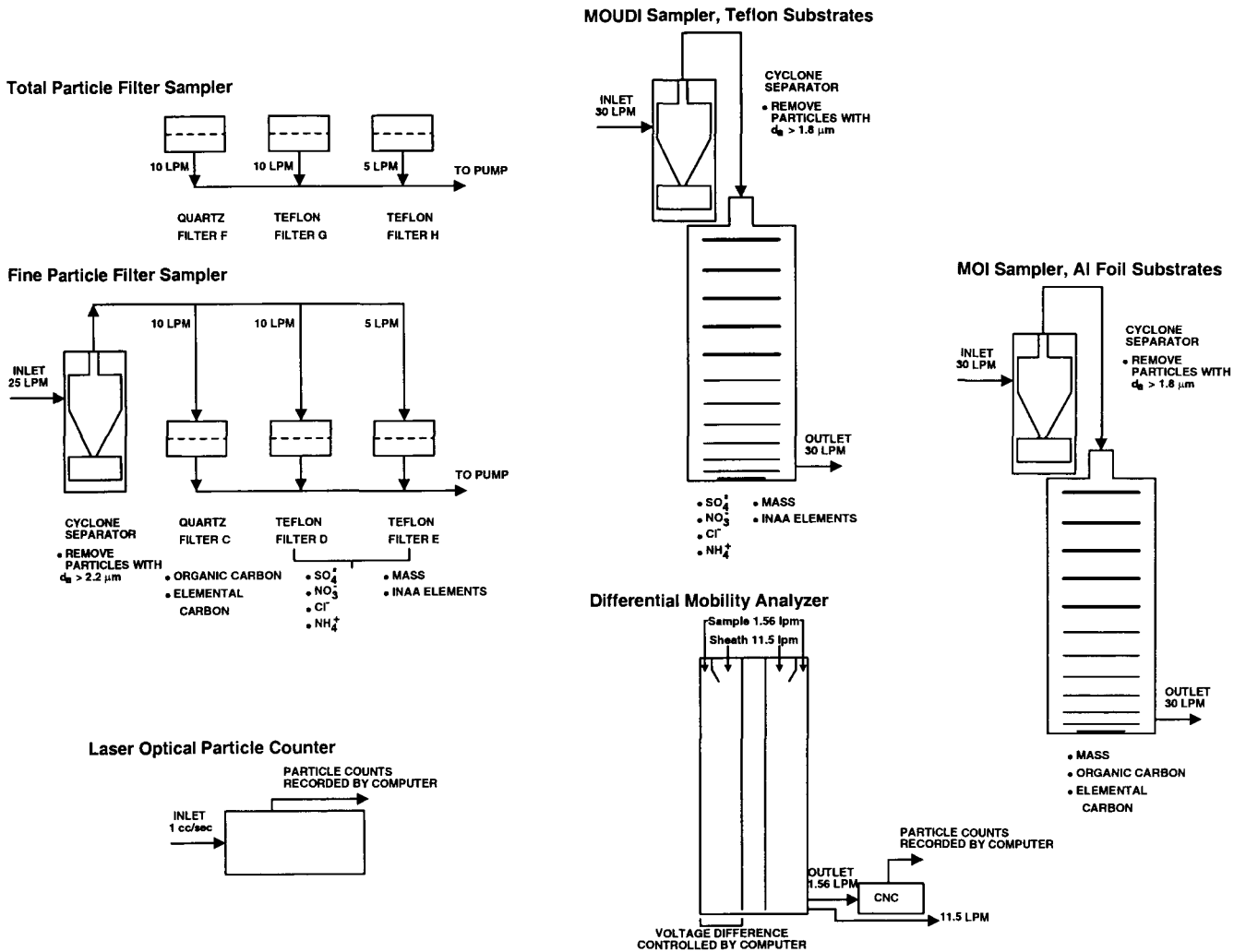

Figure 6.1: Schematic diagram of equipment used to measure fine and ultrafine particle size distribution and chemical composition.

fiber afterfilter (Pallflex, 2500 QAO), while the other impactor was operated with Teflon filter substrates (Teflo, Gelman Science, 1.0 μm pore size) and a Teflon afterfilter (Zefluor, Gelman Science, 1.0 μm pore size). Since one key objective of this experiment was to measure the size distribution of fine organic aerosols, and since the fine aerosol in Los Angeles generally has a sticky liquid film, no grease or oil was used on the substrates in order to avoid organic contamination. The impactor containing the foil substrates was operated as a micro-orifice impactor (MOI) and was not rotated during operation so that lubricant was not necessary to that system; a uniformly deposited sample was not needed for elemental and organic carbon analysis.

In addition to the above instruments, 24-h samples of total (no size separation) and fine ($D_a < 2.2$ μm) airborne particulate matter were collected using a filter-based system. Total particulate matter was collected on one open-faced quartz fiber filter (Pallflex, 2500 QAO) and on two parallel Teflon filters (Gelman Sciences, Teflo, 2.0 μm pore size) at the flow rates shown in Figure 6.1. For fine particle samples, ambient air was passed through a glass inlet line to a Teflon-coated cyclone separator [60] at a nominal flow rate of 25 lpm before particle collection on another set of one quartz (Pallflex, 2500 QAO) and two Teflon (Gelman Sciences, Teflo, 2.0 μm pore size) filters, also as shown in Figure 6.1. The air flow rate through each filter was measured with a rotameter before and after each 24-h sampling period. While these filter samples did not offer the size-specific information available from the impaction substrate samples, they served as an important check on the entire quantity of fine particle material in the atmosphere. These samples have the advantage of a greater available mass, thereby facilitating chemical analysis procedures.

Mass concentration determinations were made on all foil and Teflon substrates and Teflon afterfilters, by repeated weighing before and after use on a Mettler Model M-55-A mechanical microbalance maintained in a temperature- and humidity-controlled environment (21.8 ± 0.2°C, 38 ± 3% RH). Foil substrates were precleaned by baking for 40–50 h at 550°C, and all quartz fiber filters were pre-

cleaned by baking for at least 10 h at 550°C. All impactor substrates and filters were cut in half before chemical analysis to allow the use of several different chemical analysis methods. The samples collected on aluminum foil and quartz fiber filter material were analyzed for elemental and organic carbon using the thermal-optical carbon analysis method of Huntzicker et al. [61] as modified by Cary [62]. Samples collected on Teflon substrates underwent analysis by ion chromatography (Dionex Corp, Model 2020i) for the anions NO_3^-, $SO_4^=$, and Cl^- [63], analysis by an indophenol colorimetric procedure for NH_4^+ [64] using an Alpkem rapid flow analyzer (Model RFA-300), as well as neutron activation analysis for trace elements detection [65]. Only the bottom 6 stages ($0.056 \leq D_a \leq 1.8\mu m$) and afterfilter of the micro-orifice impactors were analyzed chemically; the ultrafine particles of special interest here were collected on the substrate of the last impaction stage ($0.056 \leq D_a \leq 0.097\ \mu m$) and on the afterfilter ($D_a \leq 0.056\ \mu m$).

6.3 Results

An example of the number distribution of airborne fine and ultrafine particles as measured by each of the instruments used in this study is illustrated in Figure 6.2. Impactor mass concentrations measured gravimetrically are converted to equivalent number concentrations using an assumed particle density of 1.7 g cm^{-3}. The data from the four instruments used generally coincide over the size range from 0.09 μm to just above 1 μm diameter where the DMA, the OPC and both impactors overlap in whole or in part. The OPC signal terminates below 0.09 μm diameter, the quartz fiber afterfilter that is loaded into the impactor used for carbon analysis is not suited to gravimetric determination of mass concentration, and in the case of the Teflon MOUDI afterfilter, there is no well-defined size at which to plot a point on the number distribution curve. Therefore, the particle number distribution shown in the ultrafine particle size range below 0.056 μm particle diameter depends largely on the data from the differential mobility analyzer/CNC combination. Table 6.1 shows the number concentration of atmospheric ultra-

Table 6.1: Airborne ultrafine particle number concentration over the size range $0.017 < D_p < 0.1$ μm averaged over 24-h periods at Pasadena January–February, 1996.

Date	Number Concentration cm^{-3} air
1/23/96	1.4×10^4
1/29/96	7.1×10^3
2/4/96	9.0×10^3
2/10/96	2.9×10^4
2/17/96	8.7×10^3

fine particles in winter months in Pasadena obtained by integrating the aerosol size distributions like the one shown in Figure 6.2 over the size range from 0.017 to 0.1 μm particle diameter. 24-hour average ultrafine particle number concentrations fall in the range $1.3 \times 10^4 \pm 8.9 \times 10^3$ particles per cm^3 air. To put this in perspective, at a tidal volume of 1.2 liters per breath and a respiration rate of about 10 breaths per minute, a person breathing such urban air would take on the order of 2×10^{11} ultrafine particles per day into their respiratory tract. Taking into account the deposition efficiency as a function of the size distribution of the particles [26, 128], approximately 10^{11} ultrafine particles in the size range 0.017–0.1 μm diameter will deposit daily in the respiratory tract of such a person.

Ultrafine particle number concentration exposure can vary as a function of time of day. Figure 6.3 illustrates two examples of the daily time series of hourly average ultrafine particle number concentrations for particles in the size range 0.017 to 0.1 μm particle diameter. Figure 6.3a shows the time series data at Pasadena for Tuesday, January 23, 1996. There is a pronounced peak in ultrafine particle number concentration that day that occurs during the time of the

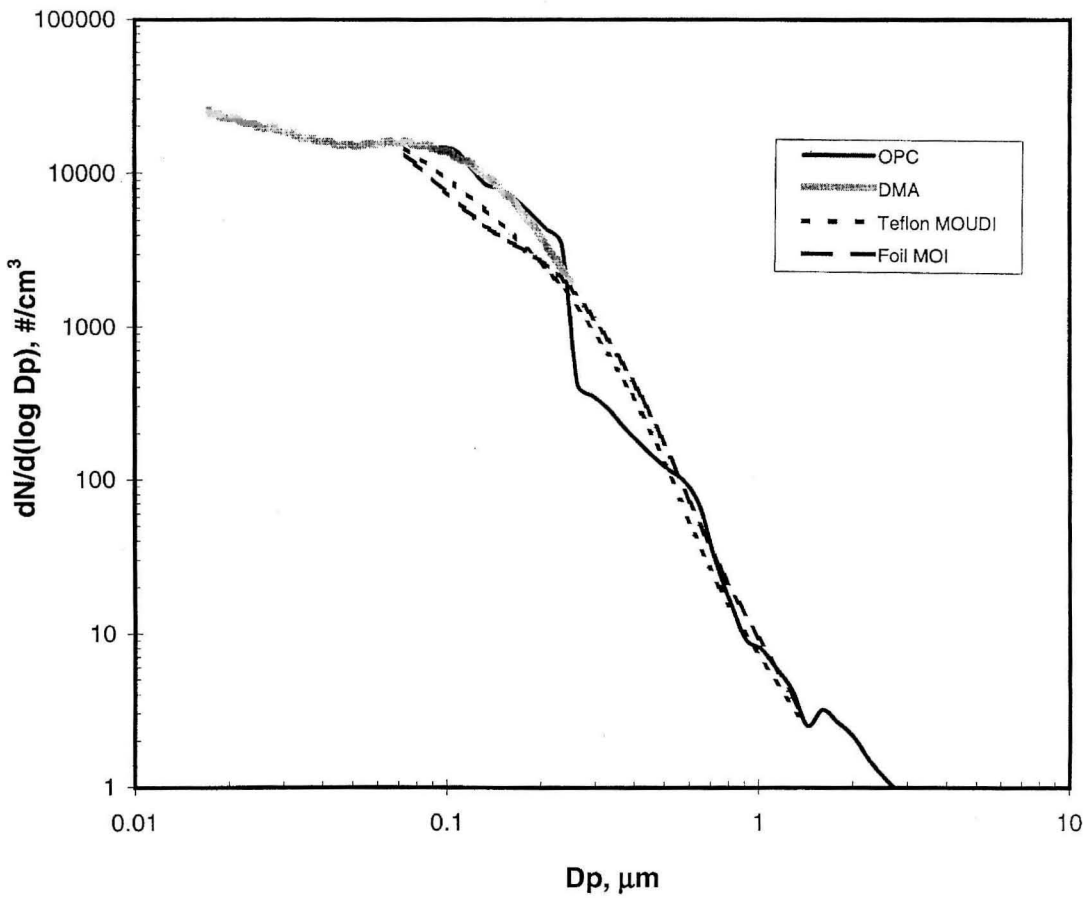

Figure 6.2: Atmospheric particle number distribution as a function of particle size averaged over the 24-h period of January 23, 1996, at Pasadena. Results from all four instruments used in these experiments show degree of agreement between measurement methods.

morning rush hour traffic peak, and higher than average values during the period around midnight, which is often a time with low mixing depths and low wind speeds in the Los Angeles area. In contrast, Figure 6.3b presents the time series data for Saturday, February 10, 1996, showing concentrations close to the long-term average value over the whole study during the early hours of that day, followed by a peak in ultrafine particle concentrations late in the day. The early morning hours of February 10 were accompanied by fog with droplets large enough to create a persistent downward flux of fog drops settling under the influence of gravity. The fog drops may have scavenged some of the ultrafine particles that otherwise would have been present during the early morning hours. Data presented later in this paper (Figure 4) that describe the size distribution of the chemical composition of the fine and ultrafine particles on February 10 show an enrichment in sulfates in particles having diameters from 0.5 to 1.0 μm, which is symptomatic of sulfate production in fog drops in the Los Angeles area [15, 53, 129]. Whether or not the afternoon peak in ultrafine particles on February 10 is in any way related to fog processing is unknown. The remaining days studied show diurnal patterns more like Figure 6.3a than Figure 6.3b, but with generally lower ultrafine particle counts during the morning traffic peak.

While ultrafine particle number concentrations are very large, the particle mass concentration contributed by ultrafines is small by comparison to those air quality standards that have been established to protect public health from damage due to airborne particles. Table 6.2 shows that the mass concentration of ultrafine particles in the aerodynamic diameter range 0.056–0.097 μm ranges from 0.60–1.17 μg m^{-3}. The value for the mass concentration of extremely small particles measured on the Teflon impactor afterfilters is an uncertain estimate of the true mass concentration because the impactor afterfilter used to collect those samples could be subject to positive or negative artifacts due to gaseous pollutant adsorption or semi-volatile particle evaporation [130]. An alternate estimate of the mass concentration of particles smaller than 0.056 μm diameter can be obtained by integrating the size distribution measured by the differen-

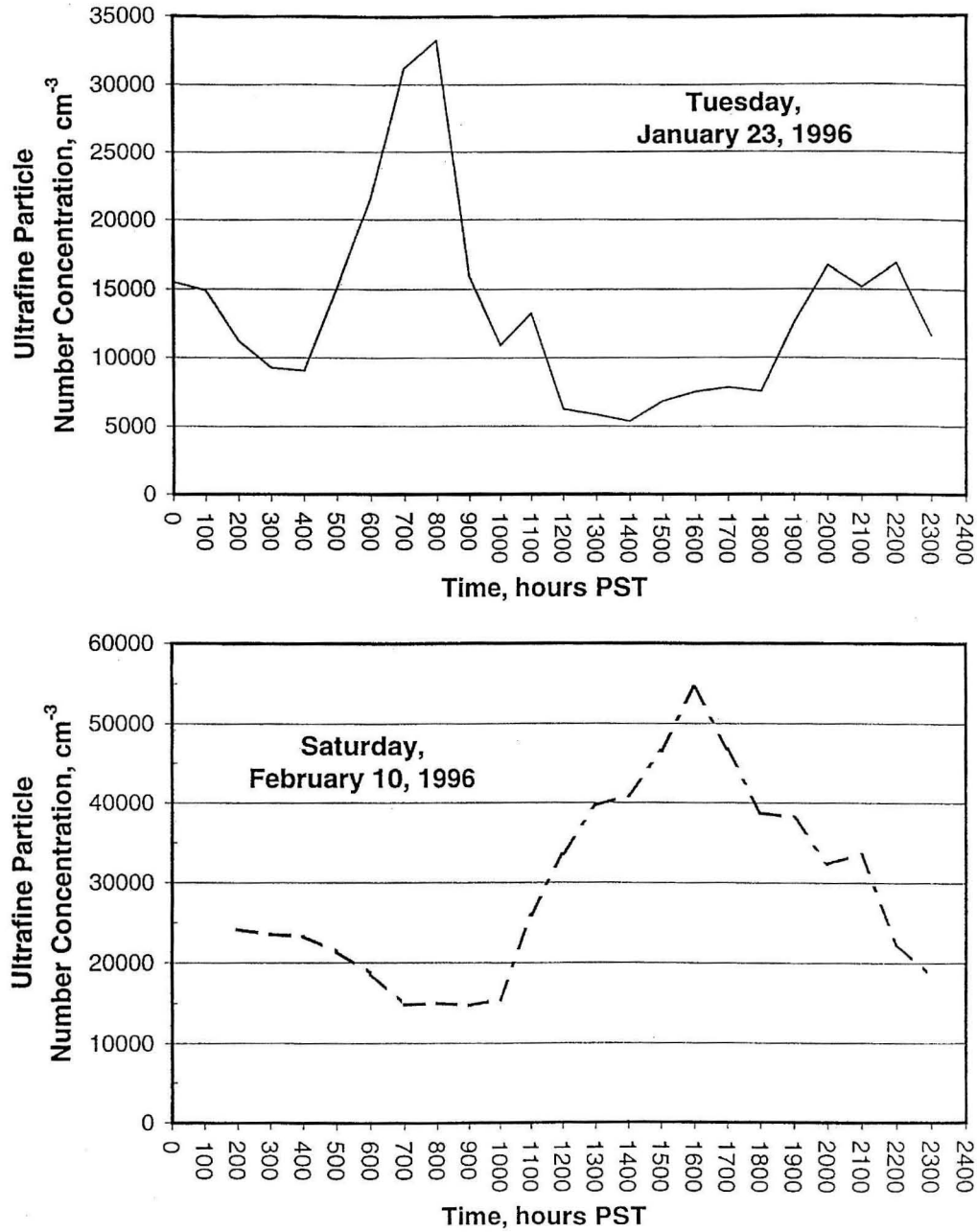

Figure 6.3: Time series of 24-h average ultrafine particle ($0.017 < D_p < 0.1$ μm) number concentrations, as measured by the DMA/CNC combination showing (a) Tuesday, January 23, 1996, with high concentrations near midnight and at the time of the morning traffic peak, and (b) Saturday, February 10, 1996, a day with early morning fog.

Table 6.2: Airborne ultrafine and fine particle mass concentrations averaged over 24-h periods at Pasadena, January–February, 1996.

Date	Fine Particle Mass Conc.[a], μg m^{-3} $D_a < 1.8$ μm	Ultrafine Particle Mass Conc.[a], μg m^{-3} $0.056 < D_a < 0.097$ μm	Ultrafine Particle Mass Conc.[b], μg m^{-3} $0.017 < D_a < 0.056$
1/23/96	21.49	1.17	0.36
1/29/96	25.52	0.60	0.20
2/4/96	14.86	0.88	0.24
2/10/96	24.89	0.67	0.91
2/17/96	14.02	0.76	0.20

[a] Obtained gravimetrically from impactor substrates.
[b] Obtained by integration of differential mobility analyzer/CNC data and using an assumed particle density of 1.7 g cm^{-3}.

tial mobility analyzer/CNC combination (DMA in Figure 6.1) over the size range 0.017–0.056 μm. At an assumed particle density of 1.7 g cm^{-3}, the mass concentration of these very small particles would total 0.20–0.91 μg m^{-3} over the days studied, as shown in Table 6.2. Combining the data in the two columns farthest to the right in Table 6.2 on a daily basis, the mass concentration of ultrafine particles of size 0.017–0.097 μm was in the range 0.80–1.58 μg m^{-3} over 24-h averaging times.

In order to provide data that are relevant to the hypotheses outlined in the Introduction about the possible relationship between ultrafine particle chemical composition and health, the impactor samples taken here were subjected to extensive chemical analysis as described earlier. Size distributions of the chemical composition of the entire fine particle portion of the atmospheric aerosol during these experiments are shown in Figure 6.4. In constructing that figure, as well as Figure 6.5, organic compound mass concentrations are estimated as 1.4 times the organic carbon measured, in order to account for H, O, S and N present in organic compounds [131], and the most abundant trace elements other than Na and Mg are shown at the equivalent mass concentration of their common oxides. The

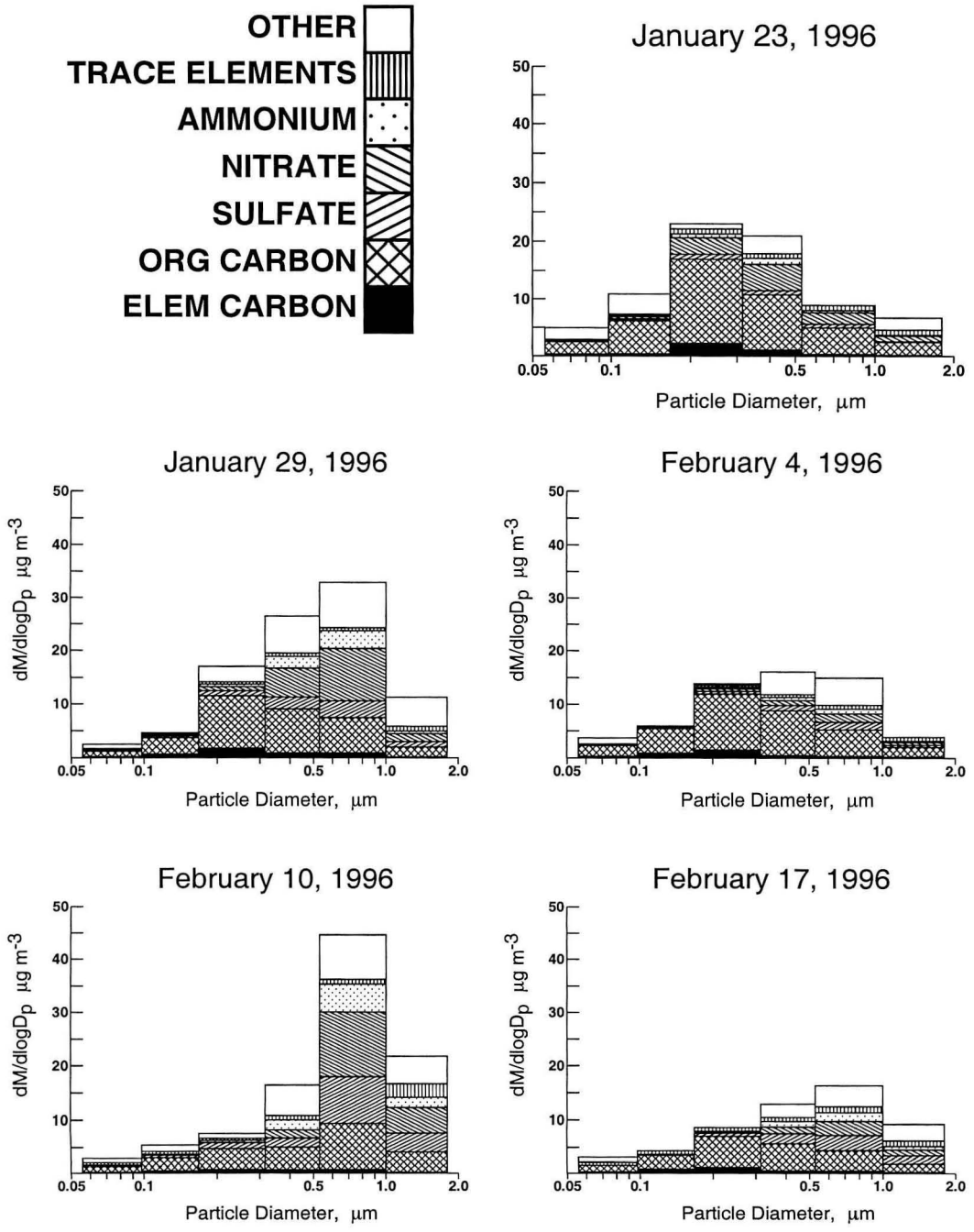

Figure 6.4: The mass distribution of the chemical composition of wintertime fine and ultrafine particles measured at Pasadena. Distributions are 24-h averages for the dates shown. The most abundant trace elements other than Na and Mg are shown at the molecular weight of their common oxides.

"other" category refers to the apparent particle mass concentration determined gravimetrically that cannot be assigned to identified chemical components. It is possible that this unidentified mass includes additional organic compound mass, which would be the case if the ultrafine organics consist largely of oxygenated organics with a mass to organic carbon ratio of greater than 1.4 (the actual compounds present are not known). As expected, the fine particle mass concentration is dominated by particles larger than 0.1 μm diameter. Nitrates and sulfates are commonly found in particles larger than 0.2 to 0.3 μm diameter, with the highest concentrations of these water soluble inorganic ionic species present in particles larger than 0.5 μm diameter. In contrast, particles $0.1 < D_a < 0.3$ μm are largely carbonaceous, and particles in the ultrafine range $D_a < 0.1$ μm are found to consist of 46–62% elemental carbon plus organic compounds.

Figure 6.5 shows pie charts which display the chemical composition of the ultrafine particles collected on impactor stage 10 (diameter range 0.056–0.097 μm). As in Figure 6.4, the apparent particle mass concentration that cannot be assigned to identified chemical components is labeled as "other" material. Typically when constructing material balances on aerosol chemical composition, unidentified components constitute zero to 35% of the fine particle mass [73, 122, 132–135]. Here, the unidentified material in the ultrafine particle size range amounted to 23–40%; the slightly larger discrepancy is expected due to the very small amounts of material available for analysis. Organic compounds are the largest contributors to these wintertime ultrafine particles followed by black elemental carbon particles. The organic carbon (OC) and elemental carbon (EC) in ultrafine particles collected on the last stage of the impactors at Pasadena during the January–February 1996 experiments can be compared to the OC and EC collected on the lowest stages of the impactor samples reported by McMurry [42] during the 1987 Southern California Air Quality Study. The data described in this paper show an average concentration of 0.26 $\mu g\ m^{-3}$ OC and 0.06 $\mu g\ m^{-3}$ EC between 0.056 and 0.097 μm particle diameter at Pasadena in the winter of 1996. The SCAQS data show an average concentration of 0.35 $\mu g\ m^{-3}$ OC and 0.10 $\mu g\ m^{-3}$ EC between

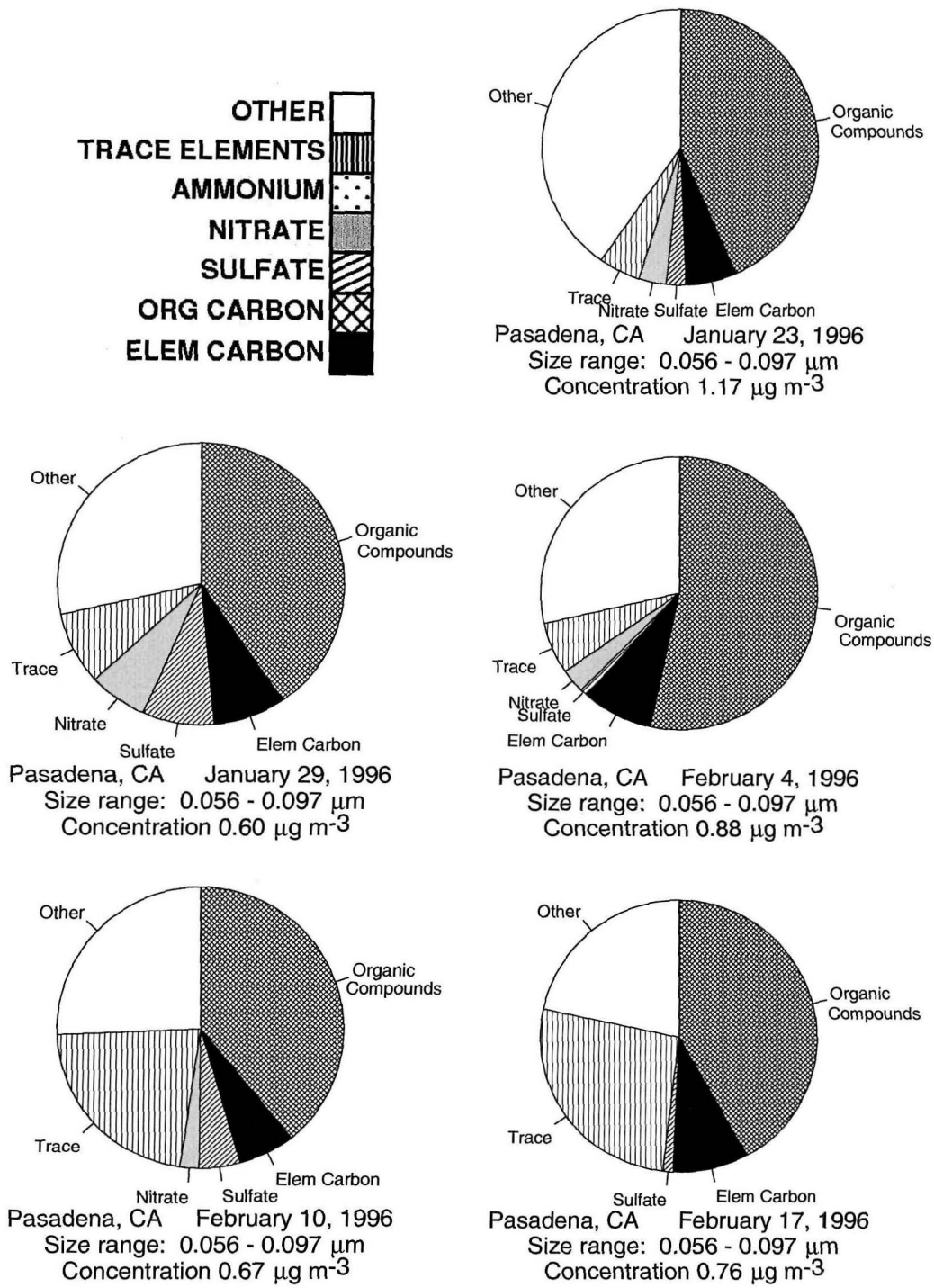

Figure 6.5: The chemical composition of wintertime ultrafine particles of size $0.056 < D_a < 0.097$ μm measured at Pasadena. The most abundant trace elements other than Na and Mg are shown at the molecular weight of their common oxides.

0.046 and 0.086 μm particle diameter at Claremont, California, in the summer of 1987; an average of 0.11 $\mu g\ m^{-3}$ OC and 0.00 $\mu g\ m^{-3}$ EC between 0.036 and 0.072 μm particle diameter at Rubidoux, California, in the summer of 1987; an average of 0.48 $\mu g\ m^{-3}$ OC and 0.18 $\mu g\ m^{-3}$ EC between 0.034 and 0.062 μm particle diameter at Long Beach, California, in the fall of 1987; and an average of 0.51 $\mu g\ m^{-3}$ OC and 0.25 $\mu g\ m^{-3}$ EC between 0.036 and 0.072 μm particle diameter at Los Angeles, California, in the fall of 1987.

The sulfate content of the ultrafine particles measured during these wintertime Los Angeles area experiments is very low, averaging 3.4 $\pm$ 3.0% of the ultrafine particulate matter collected on impactor stage 10 (i.e., typically less than 10 ng m^{-3} as sulfur). This eliminates the possibility that the ultrafine particles are mostly sulfuric acid at the place and time studied. An ion balance on these ultrafine particles shows that $SO_4^=$ exceeds NH_4^+, leaving open the possibility that some unneutralized sulfuric acid is present; the measurements are inconclusive, however, since the mass in the ultrafine sizes is small enough that even if NH_4^+ were present in quantities necessary to balance $SO_4^=$, it would still be below the detection limits of the NH_4^+ analysis procedure. By comparison, ultrafine sulfur concentrations reported for the 1987 SCAQS experiments by [44] using DRUM impactors show higher concentrations, generally above 100 ng m^{-3} as sulfur (exact comparison is not possible due to differences in the size cuts used by the micro-orifice versus DRUM impactors).

The potentially catalytic transition element content of the ultrafine particles (both impactor stage 10 samples and afterfilter samples) is described in Table 6.3. The most abundant catalytic trace metal present is iron, which is one of the metals shown by Dreher et al. [112] to be capable of catalyzing the production of oxidative damage in pulmonary systems. Pt, Pd, and Rh are not detected by the neutron activation analysis performed here; therefore, the contribution of noble metal emissions from motor vehicle catalytic converters cannot be estimated. Lanthanide series elements that also are used as catalysts are present in the ultrafine particle data set shown in Table 6.3. Cerium concentrations in ultrafine

Table 6.3: Elemental content of ultrafine particles compared to content of fine particles measured over 24-h periods at Pasadena, January-February, 1996.

Element	Fine particle mass from filter sampler mean conc. (range) ng m^{-3} D_a < 2.2 μm	Fine particle mass from sum of impactor stages and afterfilter mean conc. (range) ng m^{-3} D_a < 1.8 μm	Ultrafine particle mass from final impactor stage plus afterfilter mean conc. (range) ng m^{-3} D_a < 0.097 μm
Groups I and II			
Na	226.7 (84.3-420.0)	190.2 (64.9-416.1)	27.0 (0.75-34.8)
K	243.4 (40.5-441.5)	240.6 (166.9-278.0)	*
Cs	0.083 (0.041-0.13)	0.18 (0.15-0.24)	0.016 (0.0081-0.028)
Ba	22.4 (6.5-45.7)	12.0 (8.4-15.6)	1.04 (*-2.8)
Transition Metals			
Sc	0.022 (0.0016 - 0.068)	0.015 (0.010 - 0.022)	0.0046 (* - 0.0081)
Ti	46.7 (13.4 - 110.0)	46.7 (34.2 - 64.1)	7.65 (4.07 - 10.2)
V	5.46 (1.72 - 11.8)	5.27 (1.37 - 12.3)	0.059 (* - 0.14)
Cr	25.0 (0.18 - 78.7)	19.9 (2.46 - 61.2)	7.32 (* - 26.2)
Mn	7.89 (2.10 - 17.4)	4.79 (2.42 - 6.94)	0.74 (* - 2.43)
Fe	382.4 (115.8 - 790.0)	285.8 (132.6 - 470.2)	67.5 (* - 148.3)
Zn	44.2 (7.01 - 120.0)	24.9 (7.70 - 57.7)	3.68 (* - 6.56)
Mo	1.33 (* - 3.15)	0.40 (0.068 - 0.59)	0.072 (* - 0.19)
Cd	0.72 (0.061 - 1.44)	0.26 (0.093 - 0.44)	0.061 (* - 0.12)
Au	0.0031 (0.0016 - 0.0067)	0.00050 (* - 0.0014)	*
Hg	0.036 (0.016 - 0.068)	0.049 (0.026 - 0.071)	0.0052 (0.00014 - 0.012)
Lanthanides			
La	0.36 (0.20 - 0.43)	0.36 (0.17 - 0.68)	0.11 (0.00082 - 0.51)
Ce	0.37 (0.12 - 0.70)	0.43 (0.081 - 0.99)	0.19 (* - 0.82)
Sm	0.013 (0.0050 - 0.031)	0.023 (0.0047 - 0.080)	0.015 (0.00030 - 0.073)
Eu	0.077 (0.039 - 0.19)	0.076 (0.058 - 0.12)	0.013 (* - 0.023)
Yb	0.015 (* - 0.028)	0.014 (0.0040 - 0.031)	0.0028 (* - 0.0059)
Lu	0.0014 (* - 0.0025)	0.0029 (0.0014 - 0.0060)	0.00038 (* - 0.0013)
Actinides			
Th	0.059 (* - 0.13)	0.042 (0.016 - 0.085)	0.0065 (* - 0.018)
U	0.019 (* - 0.052)	0.035 (* - 0.055)	0.0057 (* - 0.019)

* = below detection limit

particles averaged 0.19 ng m^{-3}, for example.

Chapter 7

Conclusions

7.1 Summary of Results

To meet the objective of acquiring field experimental data to document particle chemical evolution over time within individual air parcels, several field studies were designed and conducted. Continuous measurements of single-particle size and chemical composition in the atmosphere were made using aerosol time-of-flight mass spectrometry (ATOFMS) instruments operated alongside more conventional reference air sampling instruments at Southern California urban air monitoring sites. Electrical aerosol analyzers and optical particle counters were employed to acquire continuous particle size distribution data, and inertial impactor and bulk filter samples with 4-h time resolution were collected for determination of particle size and chemical composition.

One such experiment was conducted in late summer and early autumn of 1996, with sampling sites at Long Beach, Fullerton, and Riverside, California. Filter and impactor samples were also collected upwind of the air basin at Santa Catalina Island in order to characterize background air quality. The airborne particle size and composition distribution as measured by the cascade impactors at inland sites differed from that over the ocean principally due to depletion of sea salt particles accompanied by addition of fine carbon-containing particles and secondary aerosol nitrate. Particle size distribution and size-resolved mass and

chemical distribution measurements show that the characteristic peak in the Los Angeles area aerosol mass distribution in the 0.2–0.3 μm size range observed during the 1987 SCAQS experiments has been reduced, consistent with reductions in diesel soot and elemental carbon emissions since that time. Data from the ATOFMS systems create a continuous time series of sodium, ammonium, nitrate and carbon-containing particle counts that provide a high resolution view of differences in particle composition as a function of location in the air basin. Many more sodium-containing particles were detected by the ATOFMS instrument at coastal Long Beach than at the two inland sites. Conversion of sea salt particles to sodium nitrate is evident over time. Time series of counted submicrometer diameter ammonium-containing particles and nitrate-containing particles at a site generally follow each other very closely.

Trajectory analysis shows that the air masses arriving at Riverside on the afternoons of September 24 and 25, 1996, previously passed near air monitoring sites at Santa Catalina Island, Long Beach, and Fullerton in succession. The size distribution data, inertial impactor and bulk filter sampler data, and aerosol time-of-flight mass spectrometry instrument single-particle data acquired at these sites permit particle evolution to be studied within single air masses as they sequentially pass several monitoring sites over a two-day period.

Air parcels associated with both of the trajectories studied show mineral dust, organic carbon, particulate nitrate and ammonium, and total suspended particulate matter concentrations that increase as transport occurs across the air basin. Large increases in particulate ammonium and nitrate concentrations occur between Fullerton and Riverside due to overnight air stagnation in an area with high gaseous ammonia emissions. NO and NO_2 concentrations increase during overnight stagnation in Long Beach, and NO oxidation to NO_2 can be seen between Long Beach and Fullerton.

The aerosol time-of-flight mass spectrometry data show how the externally mixed population of individual particles is modified chemically during transport from Long Beach to Riverside. The coastal aerosol at Long Beach containing sea

salt particles and primary carbon particles is changed substantially as these particles individually accumulate secondary ammonium nitrate and organics during travel across the air basin.

In the summer and fall of 1997, the Aerosol Project of the 1997 Southern California Ozone Study–North American Research Strategy for Tropospheric Ozone (SCOS97) experiments took place in California's South Coast Air Basin. A program of airborne particle research took place as part of those experiments which included the Vehicle- and Nitrate-Oriented Trajectory Studies. The trajectory studies were carried out with instrumentation similar to the 1996 trajectory experiment, and were designed to observe aerosol evolution in an urban atmosphere that is influenced by source emissions and physical and chemical transformation processes. The specific objective of the Vehicle-Oriented Trajectory Study was to observe the influence of vehicle emissions on aerosol evolution. In the Nitrate-Oriented Trajectory Study, the objective was to observe the formation of nitrogen-containing aerosols, including ammonium nitrate, at sites located upwind, inside, and downwind of the Chino dairy area, a large source of ammonia.

In each of these studies, aerosol samples were collected using filter samplers, cascade impactors, and electronic particle size distribution monitors. Two sets of filter samples were collected, one for particles smaller than 1.9 μm aerodynamic diameter ($PM_{1.9}$) and another for particles smaller than 10 μm aerodynamic diameter (PM_{10}). The filter and impactor samples were analyzed for aerosol mass and for the major aerosol chemical components including organic carbon, elemental carbon, sulfate, nitrate, ammonium, and 36 trace elements. Single-particle size and chemical composition data were simultaneously collected at each site with an ATOFMS instrument.

The Vehicle-Oriented Trajectory Study was conducted in August of 1997 at three sites in Southern California. The monitoring sites were located at Central Los Angeles, near the highest density of vehicle traffic in the Los Angeles area, at Azusa, which is often downwind of Central Los Angeles, and at Riverside. The objective of the experiment was to use trajectory-oriented sampling to observe

single air parcels that are heavily influenced by primary particle emissions from motor vehicles at several locations along an air parcel trajectory and by comparison to document the effects of emissions, chemical reactions, deposition, and other processes on the particle population.

Fine particle mass, ammonium ion, organic carbon, and elemental carbon concentrations at Central Los Angeles generally exhibited diurnal cycles with concentration peaks during or soon after the period of the morning traffic peak and concentration minima overnight. Fine particle mass and elemental carbon concentrations at Azusa exhibited a similar diurnal pattern. $PM_{1.9}$ mass balances were generally dominated by organic compounds and elemental carbon at both Central Los Angeles and Azusa.

During these experiments, two air parcels were identified that passed near both the Central Los Angeles and Azusa monitoring sites in succession. The compositions of aerosols in these single air parcels at the upwind and downwind sites were compared in order to assess the extent of aerosol transformation in the presence of continuing emissions, atmospheric reactions and deposition. Both of the air parcels passed near Central Los Angeles in the afternoon and progressed to the Azusa area where they stagnated overnight. Along these trajectories, the particle chemical composition and concentration changed very little between Central Los Angeles and Azusa. Less than 1.5% of the nitrogen in the air parcels stagnating in Azusa was in the form of HNO_3, and there was little particulate ammonium nitrate formation, which together indicate that nitric acid production was effectively balanced by dry deposition within the air parcels studied. With the onset of the morning traffic peak in Azusa, fine particle elemental and organic carbon concentrations within these air parcels increased by factors of 1.6–3.6 and 1.2–2.5 respectively, and NO and NO_2 concentrations increased by factors of 2.3–3.6 and 1.4–1.8, respectively.

In September and October of 1997, the Nitrate-Oriented Trajectory Study was conducted at three Southern California sites. These air monitoring stations were located in Diamond Bar, Mira Loma, and Riverside, sites which were upwind of,

within, and downwind of the Chino dairy area, a large source of gas-phase ammonia. This was the first time that air monitoring stations have been placed to observe the effects of a major source of ammonia emissions at close range.

Ammonium nitrate was the largest component of fine particle mass at all three sites. Nitrogen species balances show that NO and NO_2 concentrations were generally very high in comparison to the other nitrogen species. Together they almost always contained at least half, and sometimes as much as 87%, of the total nitrogen present. Alternatively, very little of the nitrogen, generally less than 5%, was present in the form of HNO_3. Nitric acid was produced by NO_2 oxidation, but because gas-phase ammonia was available in large concentrations, the nitric acid was quickly converted to particulate ammonium nitrate.

Air parcel trajectories were identified that passed successively over two air monitoring sites while sampling was taking place. The composition of aerosols within these air parcels at the upwind and downwind sites were compared in order to monitor aerosol transformation due to continuing emissions, atmospheric reactions and deposition. One of these air parcel trajectories passed the Diamond Bar air monitoring site in the morning, and stagnated near Mira Loma in the evening of the same day. Between Diamond Bar and Mira Loma, NO was oxidized to NO_2, and the ammonia concentration increased by a factor of 5. A second air parcel trajectory which stagnated near the Mira Loma site during the early morning hours and passed near the Riverside site approximately 24 hours later showed a decrease in ammonia concentration over time that is consistent with dilution as the air mass moves downwind from the virtual point source of ammonia in the dairy area. The particulate ammonium nitrate concentration in that air parcel remained approximately constant over time, consistent with a continued excess of NH_3 relative to HNO_3 and a widespread mass of air containing inorganic nitrate downwind of the dairy area.

A major factor in the recent establishment of federal ambient air quality standards for fine particulate matter and, by extension, the sampling and chemical analysis of these particles, has been the epidemiological evidence that the pres-

ence of such particles in large concentrations has an adverse effect on public health. Laboratory research by inhalation toxicologists suggests that ultrafine particles may also pose a threat to public health. Little is known thus far about the chemical composition of ultrafine particles in the atmosphere of cities. For this reason, the number concentration, size distribution and chemical composition of atmospheric ultrafine particles were determined under wintertime conditions at Pasadena, California. These experiments were conducted using a scanning differential mobility analyzer, laser optical counter, and two micro-orifice impactors. Samples were analyzed to create a material balance on the chemical composition of the ultrafine particles. Though the mass of ultrafine particles was found to be very small, in the range 0.88–1.58 $\mu g\ m^{-3}$, the number concentration was large; the number concentration of ultrafine particles in the size range $0.017 < D_p < 0.1\ \mu m$, averaged over 24-h sampling periods, was found to be consistently in the range $1.3 \times 10^4 \pm 8.9 \times 10^3$ particles cm^{-3} air. Organic compounds were the largest contributors to the ultrafine particle mass concentration. A small amount of sulfate was present in these particles, at concentrations too low to tell whether or not it existed as unneutralized sulfuric acid. Iron was the most prominent transition metal found in the ultrafine particles. These data may assist the health effects research community in constructing realistic animal or human exposure studies involving ultrafine particles.

7.2 Recommendations for Future Work

The trajectory-based field studies described in this work were designed to provide data for use in evaluating the accuracy of aerosol processes models which can represent the atmospheric aerosol population as a set of externally mixed single particles. Data from the September 24–25, 1996, Long Beach to Riverside trajectory (Trajectory 2 described in Chapter 3) have already been utilized in this capacity [89]. Model predictions of size-segregated particle chemical composition were compared to size-segregated particle chemical composition data

taken by cascade impactors at Long Beach, Fullerton, and Riverside. In general, model predictions matched the field experimental data well. In addition, the model is able to determine the contributions of various types of primary particle sources to the observed aerosol species concentrations. Non-sea-salt sulfate-containing background particles advected into the area from over the ocean acquired added mass in transit across the basin in the form of ammonium and nitrate from gas-to-particle conversion processes, becoming the largest contributors to fine particle mass at Riverside. Particles which originally came from diesel engine sources accounted for most of the $PM_{2.5}$ elemental carbon seen in Riverside, and these particles had also acquired ammonium and nitrate coatings. Particles from noncatalyst-equipped gasoline-powered vehicles were calculated to have contributed over six times more organic compound mass to the fine particle mass balance at Riverside than catalyst-equipped vehicles. Results such as these can guide the development of emissions control strategies so that controls can be directed toward those sources which contribute most to the air quality problem. The results of the Vehicle- and Nitrate-Oriented Trajectory Studies should be used in the future in much the same way to evaluate model performance in an urban environment dominated by motor vehicle sources and in an environment having substantial ammonium nitrate formation due to the presence of large local ammonia sources, respectively.

Kleeman et al. [89] used the size-segregated chemical composition data taken by cascade impactors during the 1996 trajectory study for comparison against model predictions. However, their model is able to make predictions at the externally-mixed single particle level. It is not yet possible to compare these model results directly against single particle data collected during the field studies reported here; the ATOFMS instruments have a particle counting efficiency that depends upon particle size and a detection sensitivity that varies by ion and by particle composition. Simultaneous operation of the ATOFMS instruments and impactors at monitoring sites during the trajectory-based field studies allows comparison of conventionally-obtained size-segregated mass and compo-

sition data with single particle data, allowing the counting efficiencies and sensitivity factors of the ATOFMS instruments to be examined. Such a comparison has yielded a simple exponential relationship between particle size and ATOFMS particle counting efficiency [58]. Preliminary work has been done comparing nitrate and ammonium concentration data from cascade impactors with collocated ATOFMS nitrate and ammonium ion mass spectrum peak areas, to determine the detection sensitivity of the ATOFMS instruments for those ions [136]. Laboratory experiments and further study of the entire database from these field experiments should be undertaken to determine detection sensitivities of the ATOFMS instruments for other chemical species. In particular, matrix effects, the dependence of ATOFMS instrument sensitivity to a given ion on particle composition and size should also be studied.

While at the time of these field studies the ATOFMS instruments were able to reliably detect only particles larger than a diameter of about 0.3 μm, modifications should be sought which allow them to sample particles in the ultrafine particle size range. There are currently plans for a field study in which ATOFMS instruments operating in the ultrafine particle range will be operated alongside ultrafine particle-measuring instruments analogous to those used in Chapter 6. Such a data set can offer insight into the character of ultrafine particles and thereby aid toxicologists in producing ultrafine particles in the laboratory which approximate those found in the ambient atmosphere. This would further the investigation of whether or not ultrafine particles should be a public health concern and by which pathways they may cause harm in people.

Bibliography

[1] Pope, C. A., D. W. Dockery, and J. Schwartz. Review of epidemiological evidence of health effects of particulate air pollution. Inhalation Toxicol., 7:1-18, 1995.

[2] Dockery, D. W., C. A. Pope, X. Xu, J. D. Spengler, J. H. Ware, M. E. Fay, B. G. Ferris, and F. E. Speizer. An association between air pollution and mortality in six US cities. New England Journal of Medicine, 329:1753-1759, 1993.

[3] Oberdorster, G., J. Ferin, R. Gelein, S. C. Soderholm, and J. Finkelstein. Role of the alveolar macrophage in lung injury, studies with ultrafine particles. Environ. Health Perspect., 97:193-199, 1992.

[4] Oberdorster, G. Lung dosimetry: Pulmonary clearance of inhaled particles. Aerosol Sci. Technol., 18:279-289, 1993.

[5] Oberdorster, G., J. Ferin, and B. E. Lehnert. Correlation between particle size, in-vivo particle persistence, and lung injury. Environ. Health Perspect., 102:173-179, 1994.

[6] Oberdorster, G., R. M. Gelein, J. Ferin, and B. Weiss. Association of particulate air pollution and acute mortality, involvement of ultrafine particles? Inhalation Toxicol., 7:111-124, 1995.

[7] Oberdorster, G. Significance of particle parameters in the evaluation of exposure-dose-relationships of inhaled particles. Particulate Science and Technology, 14:135-151, 1996.

[8] Christoforou, C. S., L. G. Salmon, M. P. Hannigan, P. A. Solomon, and G. R. Cass. Trends in fine particle concentration and chemical composition in Southern California. J. Air and Waste Management Assoc., 50:43-53, 2000.

[9] Dolislager, L. J. and N. Motallebi. Characterization of particulate matter in California. J. Air and Waste Management Assoc., 49:45-59 Sp. Iss., 1999.

[10] Kleeman, M. J. and G. R. Cass. Source contributions to the size and composition distribution of urban particulate air-pollution. Atmos. Environ., 32:2803-2816, 1998.

[11] Hidy, G. M., P. K. Mueller, D. Grosjean, B. R. Appel, and J. J. Wesolowski, eds. *Advances in Environmental Science and Technology, Vol. 9: The Character and Origins of Smog Aerosols, A Digest of Results from the California Aerosol Characterization Experiment (ACHEX).* John Wiley & Sons, Inc., New York, 1980.

[12] Lawson, D. R. The Southern California Air Quality Study. J. Air and Waste Management Assoc., 40:156-165, 1990.

[13] Russell, A. G. and G. R. Cass. Acquisition of regional air quality model validation data for nitrate, sulfate, ammonium ion and their precursors. Atmos. Environ., 18:1815-1827, 1984.

[14] Fraser, M. P., D. Grosjean, E. Grosjean, R. A. Rasmussen, and G. R. Cass. Air quality model evaluation data for organics 1. Bulk chemical composition and gas/particle distribution factors. Environ. Sci. Technol., 30:1731-1743, 1996.

[15] Kleeman, M. J., G. R. Cass, and A. Eldering. Modeling the airborne particle complex as a source-oriented external mixture. J. Geophys. Res., 102:21355-21372, 1997.

[16] Calvert, J. G., F. Su, J. W. Bottenheim, and O. P. Strausz. Mechanism of

the homogeneous oxidation of sulfur dioxide in the troposphere. Atmos. Environ., 12:197-226, 1978.

[17] Pandis, S. N., R. A. Harley, G. R. Cass, and J. H. Seinfeld. Secondary organic aerosol formation and transport. Atmos. Environ., 26A:2269-2282, 1992.

[18] Stelson, A. W., S. K. Friedlander, and J. H. Seinfeld. A note on the equilibrium relationship between ammonia and nitric acid and particulate ammonium nitrate. Atmos. Environ., 13:369-371, 1979.

[19] Stelson, A. W. and J. H. Seinfeld. Thermodynamic prediction of the water activity, NH_4NO_3 dissociation constant, density and refractive index for the NH_4NO_3-NH_4<$2SO_4$-H_2O system at 25 degrees C. Atmos. Environ., 16:2507-2514, 1982.

[20] Russell, A. G., G. J. McRae, and G. R. Cass. Mathematical modeling of the formation and transport of ammonium nitrate aerosol. Atmos. Environ., 17:949-964, 1983.

[21] Russell, A. G. and G. R. Cass. Verification of a mathematical model for aerosol nitrate and nitric acid formulation and its use for control measure evaluation. Atmos. Environ., 20:2011-2025, 1986.

[22] Gard, E. E., M. J. Kleeman, D. S. Gross, L. S. Hughes, J. O. Allen, B. D. Morrical, D. P. Fergenson, T. Dienes, M. E. Gaelli, R. J. Johnson, G. R. Cass, and K. A. Prather. Direct observation of heterogeneous chemistry in the atmosphere. Science, 279:1184-1187, 1998.

[23] Larson, S. M., G. R. Cass, and H. A. Gray. Atmospheric carbon particles and the Los Angeles visibility problem. Aerosol Sci. Technol., 10:118-130, 1989.

[24] Zhang, X. Q., P. H. McMurry, S. V. Hering, and G. S. Casuccio. Mixing characteristics and water content of submicron aerosols measured in Los Angeles and at the Grand Canyon. Atmos. Environ., 27A:1593-1607, 1993.

[25] Eldering, A., G. R. Cass, and K. C. Moon. An air monitoring network using continuous particle size distribution monitors connecting pollutant properties to visibility via mie scattering calculations. Atmos. Environ., 28:2733-2749, 1994.

[26] Phalen, R. F., R. G. Cuddihy, G. L. Fisher, O. R. Moss, R. B. Schlessinger, D. L. Swift, and H. C. Yeh. Main features of the proposed NCRP respiratory tract model. Radiat. Protect. Dosimetry, 38:179-184, 1991.

[27] Noble, C. A. and K. A. Prather. Profiles of individual atmospheric aerosol particles. Environ. Sci. Technol., 30:2667-2680, 1996.

[28] Gard, E. E., J. E. Mayer, B. D. Morrical, T. Dienes, D. P. Fergenson, and K. A. Prather. Real-time analysis of individual atmospheric aerosol-particles - design and performance of a portable ATOFMS. Anal. Chem., 69:4083-4091, 1997.

[29] Carson, P. G., K. R. Neubauer, M. V. Johnston, and A. S. Wexler. Online chemical analysis of aerosols by rapid singe particle mass spectrometry. J. Aerosol Sci., 26:535-545, 1995.

[30] Murphy, D. M. and D. S. Thomson. Laser ionization mass spectroscopy of single aerosol particles. Aerosol Sci. Technol., 22:237-249, 1995.

[31] Hinz, K. P., R. Kaufmann, and B. Spengler. Simultaneous detection of positive and negative ions from single airborne particles by real-time laser mass spectrometry. Aerosol Sci. Technol., 24:233-242, 1996.

[32] Hinz, K. P., R. Kaufmann, and B. Spengler. Laser induced mass analysis of single particles in the airborne state. Anal. Chem., 66:2071-2076, 1994.

[33] Reents, W. D., S. W. Downey, A. B. Emerson, A. M. Mujsce, A. J. Muller, D. J. Siconolfi, J. D. Sinclair, and A. G. Swanson. Single particle characterization by time of flight mass spectrometry. Aerosol Sci. Technol., 23:263-270, 1995.

[34] Kievit, O., M. Weiss, P. J. T. Verheijen, J. C. M. Marijnissen, and B. Scarlett. The online chemical analysis of single particles using aerosol beams and time of flight mass spectrometry. Chem. Eng. Communications, 151:79-100, 1996.

[35] Prather, K. A., T. Nordmeyer, and K. Salt. Real time characterization of individual aerosol particles using time of flight mass spectrometry. Anal. Chem., 66:1403-1407, 1994.

[36] Nordmeyer, T. and K. A. Prather. Real time measurement capabilities using aerosol time of flight mass spectrometry. Anal. Chem., 66:3540-3542, 1994.

[37] Carson, P. G., M. V. Johnston, and A. S. Wexler. Real time monitoring of the surface and total composition of aerosol particles. Aerosol Sci. Technol., 26:291-300, 1997.

[38] Russell, A. G., K. F. McCue, and G. R. Cass. Mathematical modeling of the formation of nitrogen-containing pollutants 1. Evaluation of an Eularian photochemical model. Environ. Sci. Technol., 22:263-270, 1988.

[39] Russell, A. G., K. F. McCue, and G. R. Cass. Mathematical modeling of the formation of nitrogen-containing pollutants 2. Evaluation of the effect of emission controls. Environ. Sci. Technol., 22:1336-1347, 1988.

[40] Hildemann, L. M., A. G. Russell, and G. R. Cass. Ammonia and nitric acid concentrations in equilibrium with atmospheric aerosols - experiment vs. theory. Atmos. Environ., 18:1737-1750, 1984.

[41] Wall, S. M., W. John, and J. L. Ondo. Measurement of aerosol size distributions for nitrate and major ionic species. Atmos. Environ., 22:1649-1656, 1988.

[42] McMurry, P. H. Organic and elemental carbon size distribution of Los Angeles aerosol measurements during SCAQS: Final report to California Air Resources Board. Technical Report A732-075, University of Minnesota, 1989.

[43] McMurry, P. H. and X. Q. Zhang. Size distributions of ambient organic and elemental carbon. Aerosol Sci. Technol., 10:430–437, 1989.

[44] Cahill, T. H., R. F. Matsumura, M. Surovick, C. Unger, and K. Wilkenson. Size - time - compositional analysis of aerosols during SCAQS: Final report to California Air Resources Board. Technical Report A732-074, University of Califonia-Davis, 1990.

[45] Lurmann, F. W., A. S. Wexler, S. N. Pandis, S. Musarra, N. Kumar, and J. H. Seinfeld. Modeling urban and regional aerosols–II. Application to California's South Coast Air Basin. Atmos. Environ., 31:2695–2715, 1997.

[46] Lu, R., R. P. Turco, and M. Z. Jacobson. An integrated airpollution modeling system for urban and regional scales. 2. Simulations for SCAQS-1987. J. Geophys. Res. A, 102:6081–6098, 1997.

[47] Jacobson, M. Z. Development and application of a new air pollution modeling system. 3. Aerosol phase simulations. Atmos. Environ., 31:587–608, 1997.

[48] Winkler, S. L. and D. P. Chock. Air quality predictions of the urban airshed model containing improved advection and chemistry algorithms. Environ. Sci. Technol., 30:1163–1175, 1996.

[49] Cheng, M. D., N. Gao, and P. K. Hopke. Source apportionment study of nitrogen species measured in Southern California in 1987. J. Environ. Eng, 122:183–190, 1996.

[50] Watson, J. G., C. J. C., Z. Q. Lu, E. M. Fujita, D. M. Lowenthal, D. R. Lawson, and L. L. Ashbaugh. Chemical mass balance source apportionment of PM10

during the Southern California Air Quality Study. Aerosol Sci. Technol., 21:1-36, 1994.

[51] Gao, N., M. D. Cheng, and P. K. Hopke. Receptor modeling of airborne ionic species collected in SCAQS. Atmos. Environ., 28:1447-1470, 1994.

[52] Pandis, S. N., A. S. Wexler, and J. H. Seinfeld. Secondary organic aerosol formation and transport. 2. Predicting the ambient secondary organic aerosol size distribution. Atmos. Environ., 27:2403-2416, 1993.

[53] Eldering, A. and G. R. Cass. Source-oriented model for air pollutant effects on visibility. J. Geophys. Res. A, 101:19343-19369, 1996.

[54] Grosjean, E., D. Grosjean, M. P. Fraser, and G. R. Cass. Air quality model evaluation data for organics 3. Peroxyacetyl nitrate and peroxypropionyl nitrate in Los Angeles air. Environ. Sci. Technol., 30:2704-2714, 1996.

[55] Grosjean, E., D. Grosjean, M. P. Fraser, and G. R. Cass. Air quality model evaluation data for organics 2. C-1-C-14 carbonyls in Los Angeles air. Environ. Sci. Technol., 30:2687-2703, 1996.

[56] Fraser, M. P., G. R. Cass, B. R. T. Simoneit, and R. A. Rasmussen. Air quality model evaluation data for organics 4. C-2-C-36 non-aromatic hydrocarbons. Environ. Sci. Technol., 31:2356-2367, 1997.

[57] Hering, S. V. 1998. Aerosol Dynamics, Inc., Berkeley, CA. Personal communication.

[58] Allen, J. O., D. P. Fergenson, E. E. Gard, L. S. Hughes, B. D. Morrical, M. J. Kleeman, D. S. Gross, M. E. Gälli, K. A. Prather, and G. R. Cass. Particle detection efficiencies of aerosol time of flight mass spectrometers under ambient sampling conditions. Environ. Sci. Technol., 34:211-217, 2000.

[59] Marple, V. A., K. L. Rubow, and S. M. Behm. A microorifice uniform deposit impactor (MOUDI): Description, calibration and use. Aerosol Sci. Technol., 14:434-446, 1991.

[60] John, W. and G. Reischl. A cyclone for size-selective sampling of ambient air. J. Air Pollut. Control Assoc., 30:872–876, 1980.

[61] Huntzicker, J. J., R. L. Johnson, J. J. Shah, and R. A. Cary. In G. T. Wolff and R. L. Klimisch, eds., *Particulate Carbon, Atmospheric Life Cycle*, pages 79–88. Plenum, New York, 1982.

[62] Birch, M. E. and R. A. Cary. Elemental carbon-based method for monitoring occupational exposures to particulate diesel exhaust. Aerosol Sci. Technol., 25:221–241, 1996.

[63] Mulik, J., R. Puckett, D. Willims, and E. Sawicki. Ion chromatographic analysis of sulfate and nitrate in ambient aerosols. Anal. Letters, 9:653–663, 1976.

[64] Bolleter, W. T., C. T. Bushman, and P. W. Tidwell. Spectrophotometric determinations of ammonium as indophenol. Anal. Chem., 33:592–594, 1961.

[65] Olmez, I. Instrumental neutron activation analysis of atmospheric particulate matter. In J. J. P. Lodge, ed., *Methods of Air Sampling and Analysis, 3rd Edition*, pages 143–150. Lewis Publishers, Inc., Chelsea, MI, 1989.

[66] Solomon, P. A., L. G. Salmon, and G. R. Cass. Spatial and temporal distribution of atmospheric nitric acid and particulate nitrate concentrations in the Los Angeles area. Environ. Sci. Technol., 26:1594–1601, 1992.

[67] Method for the determination of non-methane organic compounds in ambient air using cryogenic preconcentration and direct flame ionization detection. Technical Report EPA-600/4-89-018, U. S. Environmental Protection Agency, Research Triangle Park, NC, 1988.

[68] Goodin, W. R., G. J. McRae, and J. H. Seinfeld. A comparison of interpolation methods for sparse data: Application to wind and concentration fields. J. Applied Meteor., 18:761–771, 1979.

[69] Agency, U. S. E. P. National ambient air quality standards for particulate matter. Federal Register, 40 CFR Part 50, 62(138):38857, 1997.

[70] Gray, H. A. and G. R. Cass. Source contributions to atmospheric fine carbon particle concentrations. Atmos. Environ., 32:3805-3825, 1998.

[71] Gray, H. A., G. R. Cass, J. J. Huntzicker, E. K. Heyerdahl, and J. A. Rau. Characteristics of atmospheric organic and elemental carbon particle concentrations in Los Angeles. Environ. Sci. Technol., 20:580-589, 1986.

[72] Solomon, P. A., T. Fall, L. Salmon, and G. R. Cass. Chemical characteristics of PM10 aerosols collected in the Los Angeles area. J. Air Pollut. Control Assoc., 39:154-163, 1989.

[73] Chow, J. C., J. G. Watson, and E. M. Fujita. Temporal and spatial variations of PM(2.5) and PM(10) aerosol in the South Coast Air Basin. Atmos. Environ., 28:2061-2080, 1994.

[74] Hughes, L. S., D. Y. Liu, J. O. Allen, D. P. Fergenson, M. J. Kleeman, B. D. Morrical, K. A. Prather, and G. R. Cass. Evolution of atmospheric particles along trajectories crossing the Los Angeles basin. Environ. Sci. Technol., 34:3058-3068, 2000.

[75] Noble, C. A. and K. A. Prather. Single particle characterization of albuterol metered dose inhaler aerosol in near-real time. Aerosol Sci. Technol., 29:294-306, 1998.

[76] Gross, D. S., M. E. Gälli, P. J. Silva, S. H. Wood, D. Y. Liu, and K. A. Prather. Single particle characterization of automobile and diesel truck emissions in the Caldecott Tunnel. Aerosol Sci. Technol., 32:152-163, 2000.

[77] Hughes, L. S., J. O. Allen, M. J. Kleeman, R. J. Johnson, G. R. Cass, D. S. Gross, E. E. Gard, M. E. Gälli, B. D. Morrical, D. P. Fergenson, T. Dienes, C. A. Noble, D. Y. Liu, P. J. Silva, and K. A. Prather. The size and composition

distribution of atmospheric particles in Southern California. Environ. Sci. Technol., 33:3506–3515, 1999.

[78] Roberts, P. T. *Gas-to-particle conversion: sulfur dioxide in a photochemically reactive system.* Ph.D. thesis, California Institute of Technology, 1975.

[79] Reynolds, R., G. Tsou, and J. Holmes. The influence of gas phase ammonia on the formation of aerosol. Technical report, California Air Resources Board, El Monte, CA, 1975.

[80] Pandis, S. N. and J. H. Seinfeld. Heterogeneous sulfate production in an urban fog. Atmos. Environ., 26A:2509–2522, 1992.

[81] Seigneur, C. and A. M. Wegrecki. Mathematical modeling of cloud chemistry in the Los Angeles basin. Atmos. Environ., 24A:989–1006, 1990.

[82] Richards, L. W., D. J. Anderson, J. A. Blumenthal, G. L. McDonald, and A. L. Kok. Hydrogen peroxide and sulfur (IV) in Los Angeles cloud water. Atmos. Environ., 17:911–914, 1983.

[83] Richards, L. W. Airborne chemical measurements in nighttime stratus clouds in the Los Angeles basin. Atmos. Environ., 29:27–46, 1995.

[84] Pilinis, C., J. H. Seinfeld, and C. Seigneur. Mathematical modeling of the dynamics of multicomponent atmospheric aerosols. Atmos. Environ., 21:943–955, 1987.

[85] Russell, A. G., G. J. McRae, and G. R. Cass. The dynamics of nitric acid production and the fate of nitrogen oxides. Atmos. Environ., 19:893–903, 1985.

[86] SCAQMD. Sulfur dioxide/sulfate control study - main text. Technical report, South Coast Air Quality Management District, El Monte, CA, 1978.

[87] Cass, G. R. Sulfate air quality control strategy design. Atmos. Environ., 15:1227–1249, 1981.

[88] Fraser, M. P. and G. R. Cass. Detection of excess ammonia emissions from in-use vehicles and the implications for fine particle control. Environ. Sci. Technol., 32:1053-1057, 1998.

[89] Kleeman, M. J., L. S. Hughes, J. O. Allen, and G. R. Cass. Source contributions to the size and composition distribution of atmospheric particles: Southern California in September 1996. Environ. Sci. Technol., 33:4331-4341, 1999.

[90] Eldering, A., P. A. Solomon, L. G. Salmon, T. Fall, and G. R. Cass. Hydrochloric acid - a regional perspective on concentrations and formation in the atmosphere of Southern California. Atmos. Environ., 25:2091-2102, 1991.

[91] Pio, A. C. and R. M. Harrison. Vapour pressure of ammonium chloride aerosol: Effect of temperature and humidity. Atmos. Environ., 21:2711-2715, 1987.

[92] Ravishankara, A. R. Heterogeneous and multiphase chemistry in the troposphere. Science, 276(5315):1058-1065, 1997.

[93] Langer, S., R. S. Pemberton, and B. J. Finlayson-Pitts. Diffuse reflectance infrared studies of the reaction of synthetic sea salt mixtures with no2: A key role for hydrates in the kinetics and mechanism. Journal of Physical Chemistry A, 101(7):1277-1286, 1997.

[94] Vogt, R., P. J. Crutzen, and R. Sander. A mechanism for halogen release from sea salt aerosol in the remote marine boundary layer. Nature, 383(6598):327-330, 1996.

[95] Pszenny, A. A. P., W. C. Keene, D. J. Jacob, S. Fan, J. R. Maben, M. P. Zetwo, M. Springeryoung, and J. N. Galloway. Evidence of inorganic chlorine gases other than hydrogen chloride in marine surface air. Geophysical Research Letters, 20(8):699-702, 1993.

[96] Fujita, E. M., G. Green, R. Keislar, D. Koracin, H. Moosmuller, and J. Watson. SCOS97-NARSTO 1997 Southern California Ozone Study and Aerosol Study, volume I: Operational program plan. Technical report, Air Resources Board, Sacramento, CA, 1999.

[97] Fujita, E. M., G. Green, R. Keislar, D. Koracin, H. Moosmuller, and J. Watson. SCOS97-NARSTO 1997 Southern California Ozone Study and Aerosol Study, volume II: Quality assurance plan. Technical report, Air Resources Board, Sacramento, CA, 1999.

[98] Fujita, E. M., G. Green, R. Keislar, D. Koracin, H. Moosmuller, and J. Watson. SCOS97-NARSTO 1997 Southern California Ozone Study and Aerosol Study, volume III: Summary of field study. Technical report, Air Resources Board, Sacramento, CA, 1999.

[99] Allen, J. O., P. R. Mayo, L. S. Hughes, L. G. Salmon, and G. R. Cass. Emissions of ammonia and size-segregated aerosols from on-road vehicles in the Caldecott Tunnel. 2000. Submitted to Environ. Sci. Technol.

[100] Fraser, M. P., G. R. Cass, and B. R. T. Simoneit. Gas-phase and particle-phase organic compounds emitted from motor vehicle traffic in a Los Angeles roadway tunnel. Environ. Sci. Technol., 32:2051–2060, 1998.

[101] Kleeman, M. J., J. J. Schauer, and G. R. Cass. Size and composition distribution of fine particulate matter emitted from motor vehicles. Environ. Sci. Technol., 34:1132–1142, 2000.

[102] Beichert, P. and B. J. Finlayson-Pitts. Knudsen cell studies of the uptake of gaseous HNO_3 and other oxides of nitrogen on solid NaCl: The role of surface-adsorbed water. J. Phys. Chem., 100(37):15218–15228, 1996.

[103] Leu, M. T., R. S. Timonen, L. F. Keyser, and Y. L. Yung. Heterogeneous reactions of HNO_3(g)+NaCl(s) -> HCl(g)+$NaNO_3$(s) and N_2O_5(g)+NaCl(s) -> $ClNO_2$(g)+$NaNO_3$(s). J. Phys. Chem., 99(35):13203–13212, 1995.

[104] Fenter, F. F., F. Caloz, and M. J. Rossi. Kinetics of nitric acid uptake by salt. J. Phys. Chem., 98(29):9801-9810, 1994.

[105] Laux, J. M., J. C. Hemminger, and B. J. Finlayson-Pitts. X-ray photoelectron spectroscopic studies of the heterogenous reaction of gaseous nitric acid with sodium chloride - kinetics and contribution to the chemistry of the marine troposphere. Geophys. Res. Letters, 21(15):1623-1626, 1994.

[106] Mamane, Y. and J. Gottlieb. Heterogeneous reaction of nitrogen oxides on sea salt and mineral particles - a single-particle approach. J. Aerosol Sci., 21:S225-S228, 1990.

[107] Schlesinger, R. B. Toxicological evidence for health effects from inhaled particulate pollution, does it support the human experience? Inhalation Toxicol., 7:99-109, 1995.

[108] Chen, L. C., S. M. Peoples, and M. O. Amdur. Pulmonary effects of sulfur-oxides on the surface of copper-oxide aerosol. American Industrial Hygiene Association Journal, 52:187-191, 1991.

[109] Schlesinger, R. B. Factors affecting the response of lung clearance systems to acid aersols - role of exposure concentration, exposure time, and relative acidity. Environ. Health Perspect., 79:121-126, 1989.

[110] Lippman, M., R. B. Schlesinger, G. Leikauf, D. Spektor, and R. E. Albert. Effects of sulfuric-acid aersols on respiratory-tract airways. Annals of Occupational Hygiene, 26:677-690, 1982.

[111] Ghio, A. J., J. Stonehuerner, R. J. Pritchard, C. A. Piantadosi, D. R. Quigley, K. L. Dreher, and D. L. Costa. Humic-like substances in air pollution particulates correlate with concentrations of transition metals and oxidant generation. Inhalation Toxicol., 8:479-494, 1996.

[112] Dreher, K. L., R. H. Jaskot, J. R. Lehmann, J. H. Richards, J. K. McGee, A. J. Ghio, and D. L. Costa. Soluble transition metals mediate residual oil fly

ash induced acute lung injury. Journal of Toxicology and Environmental Health, 50:285–305, 1997.

[113] Hildemann, L. M., G. R. Markowski, M. C. Jones, and G. R. Cass. Submicrometer aerosol mass distributions of emissions from boilers, fireplaces, automobiles, diesel trucks, and meat-cooking operations. Aerosol Sci. Technol., 14:138–152, 1991.

[114] Flagan, R. C. and J. H. Seinfeld. *Fundamentals of Air Pollution Engineering.* Prentice-Hall, Inc., Englewood Cliffs, NJ, 1988.

[115] Bagley, S. T., K. J. Baumgard, L. D. Gratz, J. H. Johnson, and D. G. Leddy. Characterization of fuel and aftertreatment device effects on diesel emissions. Technical Report 76, Health Effects Institute, Cambridge, MA, 1996.

[116] Baumgard, K. J. and J. H. Johnson. The effect of fuel and engine design on diesel exhaust particle size distributions. Technical Report 960131, Society of Automotive Engineers, 1996.

[117] Whitby, K. T., B. J. Liu, R. B. Husar, and N. J. Barsic. The Minnesota aerosol-analyzing system used in the Los Angeles smog project. J. Colloid and Interface Sci., 39:136–176, 1972a.

[118] Whitby, K. T., R. B. Husar, and B. Y. H. Liu. The aerosol size distribution of Los Angeles smog. J. Colloid and Interface Sci., 39:177–204, 1972b.

[119] Whitby, K. T. and W. E. Clark. Electric aerosol particle counting and size distribution measuring system for the 0.015 to 1 μm size range. Tellus, 18:573–586, 1966.

[120] Lundgren, D. A. An aerosol sampler for determination of particle concentration as a function of size and time. J. Air Pollut. Control Assoc., 17:225–228, 1967.

[121] Hering, S. V., R. C. Flagan, and S. K. Friedlander. Design and evaluation of a new low-pressure impactor. Environ. Sci. Technol., 12:667-673, 1978.

[122] Ouimette, J. R. and R. C. Flagan. The extinction coefficient of multicomponent aerosols. Atmos. Environ., 16:2405-2419, 1982.

[123] Wang, H. C. and W. John. Characteristics of the Berner impactor for sampling inorganic ions. Aerosol Sci. Technol., 8:157-172, 1988.

[124] Dodd, J. A., J. M. Ondov, G. Tucel, T. G. Dzubay, and K. R. Stevens. Multimodal size spectra of submicrometer particles bearing various elements in rural air. Environ. Sci. Technol., 25:890-903, 1991.

[125] Kuhlmey, G. A., B. Y. H. Liu, and V. A. Marple. A micro-orifice impactor for sub-micron aerosol size classification. American Industrial Hygiene Association Journal, 42:790-795, 1981.

[126] Pitchford, M. L. and P. H. McMurry. Relationship between measured water vapor growth and chemistry of atmospheric aerosol for Grand Canyon, Arizona, in winter 1990. Atmos. Environ., 28:827-839, 1994.

[127] Wang, S. C. and R. C. Flagan. Scanning electrical mobility spectrometer. Aerosol Sci. Technol., 13:230-240, 1990.

[128] Deposition and R. M. for Internal Dosimetry of the Human Respiratory Tract. Task group on lung dynamics. Health Phys., 12:173-207, 1966.

[129] Meng, Z. Y. and J. H. Seinfeld. On the source of the submicrometer droplet mode of urban and regional aerosols. Aerosol Sci. Technol., 20:253-265, 1994.

[130] McDow, S. R. and J. J. Huntzicker. Vapor adsorption artifact in the sampling of organic aerosol - face velocity effects. Atmos. Environ., 24A:2563-2571, 1990.

[131] Grosjean, D. and S. K. Friedlander. Gas-particle distribution factors for organic and other pollutants in the Los Angeles atmosphere. J. Air Pollut. Control Assoc., 25:1038-1044, 1975.

[132] Mazurek, M., M. C. Masonjones, H. D. Masonjones, L. G. Salmon, G. R. Cass, K. A. Hallock, and M. Leach. Visibility-reducing organic aerosols in the vicinity of Grand Canyon National Park: Properties observed by high resolution gas chromatography. J. Geophys. Res., 102:3779-3793, 1997.

[133] Chow, J. C., J. G. Watson, Z. Lu, D. H. Lowenthal, C. A. Frazier, P. A. Solomon, R. H. Thuillier, and K. Magliano. Descriptive analysis of $PM_2.5$ and PM_10 at regionally representative locations during SJVAQS/AUSPEX. Atmos. Environ., 30:2079-2112, 1996.

[134] Salmon, L. G., C. S. Christoforou, and G. R. Cass. Airborne pollutants in the Buddhist cave temples at the Yungang Grottoes, China. Environ. Sci. Technol., 28:805-811, 1994.

[135] Salmon, L. G., G. R. Cass, R. Kozlowski, A. Hedja, E. C. Spiker, and A. L. Bates. Air pollutant intrusion into the Wieliczka Salt Mine. Environ. Sci. Technol., 30:872-880, 1996.

[136] Morrical, B. D., D. P. Fergenson, E. E. Gard, J. O. Allen, L. S. Hughes, K. A. Prather, and G. R. Cass. The quantitation of ammonium and nitrate ions in airborne particles by the univariate calibration of aerosol time-of-flight mass spectrometry. est. In preparation.